

Copyright

by

John M. Curtis, Jr.

1999

**Experimental Verification for Microwave
Processing of Materials in a Single Mode
Rectangular Resonant Cavity**

by

John M. Curtis, Jr., B.S.

Thesis submitted to the Faculty of the
Virginia Polytechnic Institute and State University
in partial fulfillment of the requirements for the degree of

Master of Science

in

Mechanical Engineering

Curtis H. Stern, Chair
James R. Thomas
William A. Davis

August 1999

Blacksburg, Virginia

Experimental Verification for Microwave Processing of Materials in a Single Mode Rectangular Resonant Cavity

John M. Curtis, Jr., M.S.

Virginia Polytechnic Institute and State University, 1999

Advisor: Curtis H. Stern

ABSTRACT

The benefits of applying microwave energy to material processing techniques have been well documented and studied. The potential benefits over conventional oven heating include faster processing times, more uniform heating, more consistent product quality, and the possibility of precise control.

The actual implementation of microwave technology has been lacking and the benefits have gone largely unrealized. This is due in part to the temperature dependence of the dielectric loss of many industrial materials such as ceramics and polymers. These materials absorb more microwave energy as they heat, creating uncontrollable heating, often called 'thermal runaway'. The focus of this research is to address this challenge.

The work described here is an experimental program for the microwave processing of specific ceramic rods and polymer tows. The objective of the program is to study the thermal runaway effect, and to provide data which will be used to verify numerical models. Accurate test data are essential to the development of precise, comprehensive models that can be used in applicator design and heating control strategies for thermal runaway materials. The experimental program explores the difficulties of microwave heating and offers solutions to more efficient systems. Successful measurements of power loss and control of thermal runaway are detailed for mullite, alumina, and nylon.

**Experimental Verification for Microwave
Processing of Materials in a Single Mode
Rectangular Resonant Cavity**

**Approved by
Advising Committee:**

To my cat, Roger.

Named for Roger Clemens, the great pitcher never to be forgiven for becoming a
Yankee.

Acknowledgments

I would like to thank my sister, who taught me how to multiply before any of the other kids knew how. If it weren't for her, I could have become an art major. Thanks to the parents, who forced me to go to Virginia Tech eventhough I wanted to go to Boston College (who in their right mind wouldn't want to be within walking distance to Fenway Park).

I would like to thank my advisor Dr. Stern, for his guidance, his expertise, and his encouragement. Without him, I would never have been able to explore the world of microwaves. I would also like to thank Dr. Davis, without his technical expertise I would have been lost. I would also like to thank Dr. Thomas, who was a helping hand on many occasions and to Jim Dolan for his help in setting me up with L^AT_EX.

Thanks also to Jeffrey Schwartz and Mark McEver, fellow grad students who kept me sane despite the radiation. I'd also like to say a special thank you to my fiancée, Amy Revita, who has supported me the whole way.

JOHN M. CURTIS, JR.

Virginia Polytechnic Institute and State University

August 1999

Contents

Abstract	iii
Acknowledgments	vi
List of Tables	x
List of Figures	xi
Chapter 1 Introduction	1
1.1 Objective	2
1.2 History of Modeling at Virginia Tech	2
1.3 Literature Review	4
1.3.1 Microwave Processing of Polymers	5
1.3.2 Microwave Processing of Ceramics	6
Chapter 2 Microwave Heating of Materials	9
2.1 Advantages	9
2.2 Dipolar Loss Mechanism	10
2.3 Dielectric Properties	10
2.4 Runaway Effects	11
2.5 Electromagnetic Field Propagation	13
Chapter 3 Experimental Setup	16
3.1 Power Generation	17
3.2 Single Mode Resonant Cavity	19

3.3	Power Measurement	23
3.4	Temperature Measurement	24
3.5	Data Acquisition	25
Chapter 4 Experimental Results		26
4.1	Heating Control Strategies	26
4.2	Source Power	27
4.3	Characterization of the Cavity	27
4.4	Microwave Heating of Mullite	29
4.4.1	Constant Power Absorbed: Mullite	30
4.4.2	Constant Power to Cavity: Mullite	38
4.4.3	Constant Electric Field in Cavity: Mullite	41
4.4.4	Constant Cavity Length Effects	43
4.4.5	Effects of Smaller Diameter Rod	45
4.5	Discussion of Results for Mullite	48
4.6	Microwave Heating of Alumina	53
4.7	Heating Rate: Mullite vs. Alumina	54
4.8	Microwave Heating of Nylon 66 Fiber	60
4.9	Sources of Error	67
4.9.1	Temperature Measurement	67
4.9.2	Power Measurement	68
4.9.3	Electric Field Strength	69
Chapter 5 Conclusions		71
5.1	Recommendations	72
5.1.1	Temperature Measurement System	72
5.1.2	Power Measurement	72
5.1.3	Data Acquisition System	72
5.1.4	Tuning Devices	73
5.1.5	Additional Equipment	73

Bibliography	74
Appendix A Calibration of Coupler	77
Appendix B Calibration of the Cavity Probe	80
Appendix C Pyrometer Calibration	83
C.1 Calibration for Mullite Rod	85
C.2 Calibration for Alumina Rod	86
C.3 Calibration for Nylon 66 Fiber	87
Appendix D Individual Data Runs	88
Appendix E Data Acquisition Program	95
Appendix F Characterization of Cavity	104
Vita	106

List of Tables

3.1	Cavity characteristics for TE_{10n} mode	21
4.1	Comparison of steady-state data for various microwave heating scenarios	48

List of Figures

2.1	Propagation of a plane wave in a lossy medium (Metaxas and Meredith, 1983)	11
2.2	Characteristic dielectric loss factor for a thermal runaway material . .	12
2.3	TE_{10} propagation fields (Roussy and Pearce, 1995)	14
3.1	Schematic of microwave heating system	16
3.2	Picture of microwave heating system	17
3.3	Picture of microwave power generator and remote launcher	18
3.4	Frequency performance of power generator	18
3.5	Picture of single mode resonant cavity	19
3.6	TE_{103} resonant cavity field pattern	22
3.7	TE_{105} resonant cavity field pattern	22
3.8	Attenuation of the signal by the reflected port	23
3.9	Picture of infrared pyrometer	24
4.1	Characterization of cavity at an incident power of 110 W	28
4.2	Dielectric properties of mullite (Thomas et al., 1998)	29
4.3	Heating of a 4.67 mm mullite rod to a steady-state temperature (a), where power absorbed by rod is increased to 5 W and held constant (b). (Average of 4 runs, individual runs shown in Appendix D; bars indicate measured range)	32

4.4	Heating of a 4.67 mm mullite rod to a steady-state temperature (a), where power absorbed by rod is increased to 7 W and held constant (b). (Average of 4 runs, individual runs shown in Appendix D; bars indicate measured range)	33
4.5	Heating of a 4.67 mm mullite rod to a steady-state temperature (a), where power absorbed by rod is increased to 9 W and held constant (b). (Average of 4 runs, individual runs shown in Appendix D; bars indicate measured range)	34
4.6	Comparison of temperature (a), and electric field strength (b), for the heating of a 4.67 mm mullite rod where power absorbed by rod is increased to and held constant at indicated level (bars on temperature plots indicate measured range).	36
4.7	Power loss to cavity walls for the heating of a 4.67 mm mullite rod	37
4.8	Comparison of temperature (a), and power absorbed by rod (b), for the heating of a 4.67 mm mullite rod where power to the cavity is increased to and held constant at indicated level (bars on temperature plots indicate measured range).	39
4.9	Comparison of electric field strength for the heating of a 4.67 mm mullite rod, where power to the cavity is increased to and held constant at indicated level (bars on temperature plots indicate measured range).	40
4.10	Comparison of temperature (a) and absorbed power by a 4.67 mm mullite rod, where electric field strength is held constant at 21 kV/m. (Average of 4 runs, individual runs shown in Appendix D; bars indicate measured range)	42
4.11	Heating of a 4.67 mm mullite rod, where cavity length is initially shorter (a) and equal to (b) the resonant cavity length	44
4.12	Heating of a 2.75 mm mullite rod to a steady-state temperature (a), where power absorbed by rod is increased to 3 W and held constant (b). (Average of 4 runs, individual runs shown in Appendix D; bars indicate measured range)	46

4.13 Heating of a 2.75 mm mullite rod to a steady-state temperature (a), where power absorbed by rod is increased to 5 W and held constant (b). (Average of 4 runs, individual runs shown in Appendix D; bars indicate measured range)	47
4.14 Comparison of dielectric loss factor values for 4.67 mm mullite rod (Literature data from Thomas et al. (1998))	49
4.15 Comparison of steady state electric field strength for 4.67 mm mullite rod	51
4.16 Comparison of steady-state absorbed power to 4.67 mm mullite rod	51
4.17 Dielectric properties of alumina (Cross, 1994)	53
4.18 Heating of a 4.75 mm alumina rod to a steady-state temperature (a), where power absorbed by rod is increased to 10 W and held constant (b). (Average of 4 runs; bars indicate measured range)	56
4.19 Heating of a 4.75 mm alumina rod to a steady-state temperature (a), where power absorbed by rod is increased to 15 W and held constant (b). (Average of 4 runs; bars indicate measured range)	57
4.20 Comparison of temperature (a) and electric field strength (b) for the heating of a 4.75 mm alumina rod where power absorbed by the rod is held constant at indicated level. (Average of 4 runs; bars indicate measured range)	58
4.21 Heating of ceramic rods alumina (a) and mullite (b) for a constant electric field of 50 kV/m	59
4.22 Dielectric properties of nylon 66 fiber (Huang, 1976)	60
4.23 Comparison of electric field (a) and power (b) for the heating of a 3 mm nylon 66 tow to a steady-state temperature of 120°C. (Average of 4 runs; bars indicate measured range)	63
4.24 Comparison of electric field (a) and power (b) for the heating of a 3 mm nylon 66 tow to a steady-state temperature of 160°C. (Average of 4 runs; bars indicate measured range)	64

4.25	Comparison of temperature (a) and electric field (b) for the heating of a 3 mm nylon 66 tow to steady-state. For run 1, the power absorbed by the tow ~ 0.5 W; for run 2, the power absorbed by the tow is ~ 0.4 W.	65
4.26	Comparison of temperature (a) and absorbed power (b) for the stepped heating of a 3 mm nylon 66 tow	66
A.1	Setup for calibration of coupler	78
A.2	Characterization of coupler	79
A.3	Measurement error for an uncorrected coupler	79
B.1	Equipment setup for electric field calibration	80
B.2	Coupler / Probe relationship	81
B.3	Total power vs. electric field	82
B.4	Power measured by probe vs. electric field	82
C.1	Fraction of emissive power vs λT for blackbody (Incropera and Dewitt, 1996)	84
C.2	Emissivity data for mullite (Bauer and Steinhardt, 1990)	85
C.3	Temperature calibration of pyrometer for mullite rod	85
C.4	Emissivity data for alumina rod (Touloukian, 1972)	86
C.5	Temperature calibration of pyrometer for alumina rod	86
C.6	Emissivity data for nylon 66	87
C.7	Temperature calibration of pyrometer for nylon 66	87
D.1	Individual runs for heating of a 4.67 mm mullite rod, where power absorbed by rod is increased to 5 W and held constant (see Figure 4.3)	89
D.2	Individual runs for heating of a 4.67 mm mullite rod, where power absorbed by rod is increased to 7 W and held constant (see Figure 4.4)	90
D.3	Individual runs for heating of a 4.67 mm mullite rod, where power absorbed by rod is increased to 9 W and held constant (see Figure 4.5)	91

D.4	Individual runs for heating of a 4.67 mm mullite rod, where electric field is held constant at 21 kV/m (see Figure 4.10)	92
D.5	Individual runs for heating of a 2.75 mm mullite rod, where power absorbed by rod is increased to 3 W and held constant (see Figure 4.12)	93
D.6	Individual runs for heating of a 2.75 mm mullite rod, where power absorbed by rod is increased to 5 W and held constant (see Figure 4.13)	94
F.1	Characterization of cavity at an incident power of 65 W	105
F.2	Characterization of cavity at an incident power of 135 W	105

Chapter 1

Introduction

The need for better ways to process materials has led to the development of microwave processing, which has been applied to numerous materials. Researchers have been exploring new applications where microwave energy can have a serious impact. This interest is primarily due to the improved performance characteristics of the processed material and possible economic savings that can be achieved with microwave processing. The potential advantages of microwave heating over conventional heating include uniform volumetric heating, reduced overheating at the surface, instant control, energy savings, and reduced operating costs. These benefits have led researchers to design and implement new processes that take advantage of the characteristics of microwaves.

One significant obstacle to widespread use of microwave heating is the temperature dependence of the dielectric properties of the material being heated. If the dielectric loss factor (a measure of the material's ability to absorb microwave energy) increases with temperature, there is a possibility that the heating will rapidly accelerate. This effect is called thermal runaway. Many industrial materials such as ceramics and polymers are thermal runaway materials. Usually, these materials require precise processing temperatures for complete heating. Overheating can lead to cracking in ceramics, and melting in polymers. Underheating can lead to uneven material composition and quality. The instability of thermal runaway materials at high temperatures is a major limitation to full scale industrial microwave heating.

The goal of the research program at Virginia Tech is to use a combination of modeling and experimentation to develop new applicator designs and heating control strategies to successfully process thermal runaway materials using microwave energy. It is hoped that this research will lead to industrial applications for microwave heating.

1.1 Objective

The objective of the research presented in this thesis is to provide experimental data for selected thermal runaway materials through controlled heating in a resonant rectangular applicator. These data will provide an essential element in the study of thermal runaway and may also point toward strategies for control of thermal runaway.

This research involves the development and operation of an experimental apparatus for the microwave heating of two metal-oxide ceramic fibers, mullite, and alumina. One polymer yarn, nylon 66, will also be tested. This research will address the problem of batch processing, or stationary heating. The basic apparatus will include an applicator and aperture, a short, a microwave power source at 2.45 GHz, microwave power measuring devices, and a pyrometer for temperature measurement.

1.2 History of Modeling at Virginia Tech

The past few years have seen an increasing amount of research devoted to microwave applications at Virginia Tech. The first mathematical model to determine the temperature profile of a stationary or moving cylindrical rod through a rectangular microwave cavity was completed by Duchez (1996). He used a 1-dimensional model to simulate the behavior of cylindrical ceramic fibers heated in a rectangular cavity. He examined the role of electric field profiles along the length of the cavity in the microwave heating of alumina and zirconia fibers. Assuming specific electric field profiles, temperature distributions along the length of the fiber for each material were predicted. Duchez was able to specify electric field profiles that would achieve a more

constant temperature along the length of the fiber as it was heated in the cavity. He concluded that temperature control of thermal runaway materials is possible by using specific electric field distributions. However, the limitations of the model include its one dimensional simplification, which is increasingly more susceptible to error as the thermal conductivity of the material decreases or the diameter of the fiber increases. Another limitation of his model is the assumption that the electric field distribution can be accurately controlled. The model also does not take into account the influence of the temperature of the material on the electric field. This model was groundwork for further study.

The research completed by Goodson (1997) was a continuation of that by Duchez. Goodson's objective was to improve the thermal model and verify it by accurately reproducing known experimental results. Goodson's improvement to the model included a 2-dimensional simulation and the addition of another ceramic material, mullite. A 2-dimensional model was implemented to account for radial temperature variation for thicker rods. Goodson computed temperature profiles of a mullite rod at various absorbed power levels. The experimental data used to validate his model for mullite rods were collected at the Los Alamos National Laboratory (LANL). The simulation results for temperature distributions along the mullite rods at specific absorbed powers were higher than the temperature distributions of the experimental results. Goodson concluded that the power loss to the walls of the cavity could explain the higher simulation temperatures. The data trends compared relatively well to the simulation and Goodson suggested that thermal runaway can be avoided by controlling the power absorbed in the material while varying the electric field strength.

Another important step was the development of an electromagnetic field simulation for microwave heating of cylindrical loads inside a rectangular cavity (Terril, 1998). Terril determined that the electric field distribution along the length of the cavity transverse to the load was fairly constant with a slight peak at the fiber. The electromagnetic field simulation takes into account the shape of the aperture and the complex relationship between the material being heated and the electric field dis-

tribution. The field simulation computes electric field shapes, but does not predict temperature distributions.

The next logical step in the evolution of the simulation is to combine the electromagnetic field simulation developed by Terril and the heat transfer model developed by Goodson. In addition, the model will incorporate power losses to the cavity walls. Most importantly, this new model is needed to accurately simulate the complex interactions between the dielectric material and the electromagnetic field. The electric field profile is dependent on the source, cavity dimensions, and dielectric properties of the load material. The dielectric properties for thermal runaway materials are temperature dependent which means the electric field is dependent on the temperature of the material. Therefore, the electric field in the cavity and the temperature profile of the material are interdependent. This complex relationship must be taken into account to accurately predict temperature profiles for thermal runaway materials heated in a microwave cavity.

The work presented in this document is the first step in developing an experimental apparatus at Virginia Tech for microwave heating in a resonant rectangular cavity. The data are essential for verification of the next generation simulation discussed above and for understanding the hardware issues relevant to successful processing.

The ultimate objective of the combined research is to build an applicator that will be used to controllably heat thermal runaway materials using microwave energy.

1.3 Literature Review

The heating of materials is an important step used in many processes including curing, cooking, thawing, sintering, and drying. The first microwave ovens emerged in the 1940's and were put to use mostly in the food industry. These multimode ovens were not sufficient for bulk heating or batch processing of industrial materials.

The first use of a resonant microwave cavity for the specific heating of a moving dielectric was in the late 1960's. Lewis (1971) patented a method of operation of a

microwave resonant cavity system in a pre-selected, under-coupled or over-coupled mode. The system offered stable heating of a dielectric material advancing through a cavity for the purposes of moisture removal or heating. The system included a three-port circulator coupled between a microwave power source, a resonant cavity and a water load. Researchers have since expanded this basic system to experimentally heat many materials including ceramics and polymers.

1.3.1 Microwave Processing of Polymers

The first industrial application of microwave energy for the processing of polymeric materials occurred in the late 1960's with the vulcanization of rubber. The technology was limited due to the non-uniformity of the field in the ovens and thermal runaway of the rubber.

It was clear that for microwave processing of polymeric materials to be successful, thermal runaway must be overcome. Huang (1969) was the first to use a resonant cavity system for the microwave heating of polymeric yarns and filaments. The keys to the design were the selection of an efficient applicator, and a means for tuning the resonant frequency. He developed a cylindrical microwave resonant cavity heater design based on the design by Lewis for the rapid heating of polymer yarns. A few years later, he used the same cavity to heat nylon fibers. Huang successfully attenuated the nylon filament temperature fluctuation by impedance mismatching and frequency offset between the power source and the applicator. Using the inherent characteristics of the resonant cavity, Huang (1976) was able to heat nylon monofilament to near melt temperatures and avoid thermal runaway. Large exit temperature fluctuations limited the design to laboratory scale heating.

Other researchers have experimented with combining microwave processing with conventional drying techniques. Holme and Metaxas (1979) experimentally used a twin cavity microwave applicator as part of a conventional system for the final drying of nylon tufted carpets. They concluded that microwave drying of nylon carpet would substantially increase throughput. They also concluded that as the moisture level of the carpet decreased, the power loss to the cavity walls rose substantially.

Kumar (1982) conducted experiments on the drying of polyester fibers in a multimode microwave oven. Drying times were reduced in proportion to the source power.

The most comprehensive study of microwave processing of polymers was done by Chen et al. (1993). They examined the relationship between the chemical structure and the microwave absorptivity of the polymer. They tested ethylene/vinyl acetate copolymers and nitrile rubbers in a cylindrical microwave resonant cavity, and found that small variations in composition of the polymer created large variations in temperature profiles and heating rates.

The vulcanization of rubber was improved in the late 1980's for the extrusion of rubber in weather stripping applications (Krieger, 1992). Other recent advances in the microwave processing of polymers can be found in Iskander et al. (1996). There have been no recent, published attempts to improve the microwave heating of nylon fiber.

1.3.2 Microwave Processing of Ceramics

Since the 1970's, microwave processing of ceramics has been the subject of a large amount of exploratory research. Bertaud and Badot (1976) examined the sintering of alumina and zirconia, as well as the melting of silica in a rectangular single mode cavity. Colomban and Badot (1979) investigated the sintering of alumina in a single mode cavity. Microwave sintering of ceramics was determined to be successful and there were many attempts to apply these techniques to industrial processes. These attempts were unsuccessful mostly because of the inefficient microwave equipment available at that time. A more in-depth history of the sintering of ceramics using microwave energy can be found in Stein (1994).

Researchers at Virginia Tech have been working closely with those from Los Alamos National Laboratory (LANL) in the experimental heating of ceramic fibers. The most recent research at LANL involved the stationary and continuous heating of mullite. These data, as stated earlier, were compared to Goodson's simulation. The simulation overestimated sample temperature for a given power. Thomas et al.

(1998) suggested that there were significant losses in the cavity walls.

Attempts to minimize the thermal runaway effect in alumina based filaments included carbon coating the tow (Vogt and Unruh, 1993). This new method is used to counteract the insufficient heating of the alumina tow at low temperatures (less than 700°C). At low temperatures, the carbon couples well to the microwave energy and heat is conducted into the ceramic rod. As the entire tow heats up, the coating burns off and the ceramic is indirectly heated to a sufficient temperature such that it absorbs the microwave energy. This is called hybrid heating. There was evidence, however, that the filaments did not heat up to the desired temperature of 1300°C. Vogt explained this by the phase transition of amorphous silica to mullite at high temperatures. Vogt asserted that the mullite phase must not be sufficiently lossy to absorb the microwave energy. He further asserts that the resulting reduction in dielectric loss caused by the mullite phase offers an internal mechanism to control thermal runaway (Vogt et al., 1994).

Another important discovery during this research was the observance of thermal spikes or large temperature increases over a short span of time. The temperature spikes occurred at temperatures above 900°C and were caused by small increases in microwave power (less than 15%). It was observed that the temperature after the spike was much lower than the temperature before the spike, despite the increase in microwave power. This surprising phenomenon is also attributable to the mullite phase transition. The rapid thermal gradient causes a phase change from amorphous silica to mullite, thus rapidly lowering the dielectric loss (its ability to absorb microwave energy).

An improvement on the ability to control the sintering temperature of ceramic tows, rods, and tubes was achieved through the combination of the design of a rapid feedback control system and a traveling wave tube source (Vogt et al., 1996). The control system was able to regulate the power absorbed by the rod by varying the frequency of the source in maintaining sample temperature. Temperature control was obtained for stationary and slow moving rods, but not for faster moving samples. They documented the difficulties in measuring temperature due to the small target

view of the temperature sensor used.

Temperature control was not achieved for faster moving NICALON tows (Vogt et al., 1995). No publications have been found that describe a model based on experimental work that can predict the temperature profiles of ceramic and polymer tows in a microwave cavity.

Chapter 2

Microwave Heating of Materials

2.1 Advantages

Conventional heating relies on conduction to transport energy to the interior of the material. The heat incident on the surface of the material must be conducted to the core of the material to heat the entire specimen. The temperature gradient between the surface and the core can be large for bulky or low thermal conductivity materials, such as polymers and ceramics. Large temperature gradients create uneven heating, burnt surfaces, thermal stresses, etc. Relying on conduction as a means of heating also has the disadvantage of relatively long processing times.

Microwave heating has several advantages over conventional heating. Microwave energy, when directly coupled to a material, can provide volumetric and accelerated heating, high energy concentration, and more control. Volumetric heating can reduce surface temperatures, reverse thermal gradients, and reduce thermal stresses. This is because the heat is generated within the material and is conducted to the cooler surface. Volumetric heating can often improve product quality and uniformity.

2.2 Dipolar Loss Mechanism

The heating of a material with microwave power is the result of the complex interaction between the electromagnetic field and the dielectric. Particles within the dielectric are displaced from their equilibrium positions due to the alternating electromagnetic field. This is mainly the result of induced polarization and orientation polarization. Induced polarization occurs when electrons are displaced about their nuclei (electronic polarization), or when atomic nuclei themselves are displaced due to an unequal distribution of charge in the molecule formation (atomic polarization). Orientation polarization occurs in dielectrics that have permanent dipoles, such as water, which tend to reorient due to a changing electric field. Since these loss mechanisms are frequency dependent, the relative importance of each mechanism can be weighed for certain frequencies. At high frequencies used in industrial microwave applications, reorientation polarization is the most important loss mechanism.

Dipole rotation in solids is hindered by strong interatomic bonds. The dipoles cannot follow the rapidly alternating electric field. The maximum rate of microwave heating in solids is achieved when the period of the applied electric field equals the relaxation time of the polarization.

2.3 Dielectric Properties

The amount of attenuation of the electromagnetic field is dependent on the absorptivity of the dielectric, which can be described in terms of the complex dielectric constant of the material. The complex dielectric constant first appears in the determination of the total equivalent current density of the applied field (Metaxas and Meredith, 1983)

$$\overline{J}_{TOT} = j\omega\epsilon_o\epsilon^*\overline{E} \quad (2.1)$$

where ϵ_o is the permittivity of free space, \overline{E} is the electric field vector, ω is the frequency, and ϵ^* is the complex dielectric constant. The complex dielectric constant

attains a complex form and is given by

$$\epsilon^* = \epsilon' - j\epsilon''_{eff} \quad (2.2)$$

and

$$\epsilon''_{eff} = \left(\frac{\sigma}{\omega\epsilon_0} \right) \quad (2.3)$$

where ϵ' is the relative dielectric constant, ϵ''_{eff} is the effective loss factor, and σ is the effective conductivity of the dielectric.

The relative dielectric constant (real part) describes how well the material can store electromagnetic energy and the dielectric loss factor (imaginary part) represents the material's ability to absorb this energy as heat.

As the electromagnetic field passes through the dielectric, a portion of the electrical energy is absorbed by the material, thus reducing the strength of the electromagnetic field. Figure 2.1 is a graphical representation of an electromagnetic wave being attenuated as it passes through a dielectric.

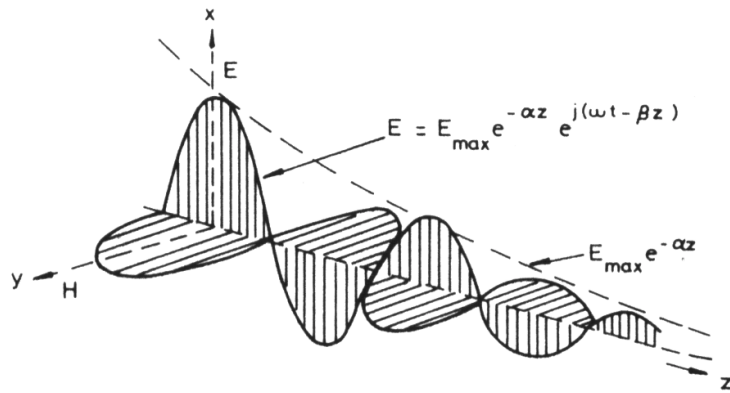


Figure 2.1: Propagation of a plane wave in a lossy medium (Metaxas and Meredith, 1983)

2.4 Runaway Effects

Thermal runaway occurs in materials that become more lossy with an increase in temperature. This uncontrolled rise in temperature occurs because of a positive slope

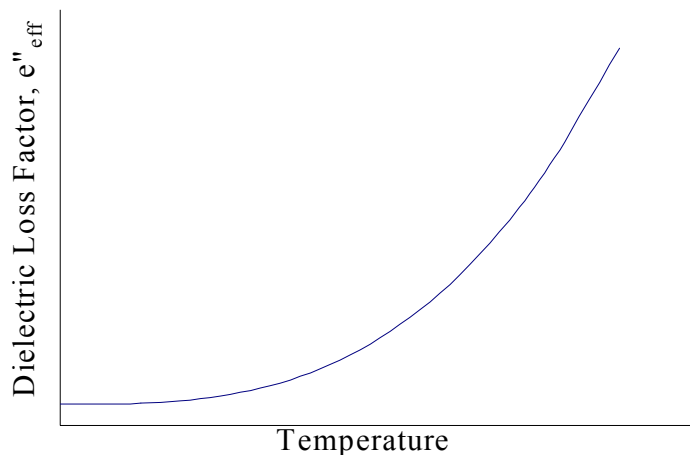


Figure 2.2: Characteristic dielectric loss factor for a thermal runaway material

of the dielectric loss factor, $d\epsilon''_{eff}/dT$. A typical dielectric loss factor as a function of temperature for a thermal runaway material is plotted in Figure 2.2.

Thermal runaway occurs when the material absorbs more energy than it can remove. Thus, the heat input, $\epsilon''_{eff}\omega E^2$, must be greater than the heat conducted away, $\alpha_T \nabla^2 T$, where α_T represents the thermal diffusivity of the material. To avoid thermal runaway, the microwave energy must be altered or the material must be removed from the heated zone. Removing the material from the heated zone is usually not an option, so an applicator that can adjust the electromagnetic field must be designed. Knowledge of the dielectric properties of the material to be heated is crucial in the proper design of microwave applicators.

It is important to understand how the dielectric properties influence the electromagnetic field and the absorbed power. The average power of the electromagnetic field is given by (Metaxas and Meredith, 1983)

$$P_{AV} = \omega\epsilon_o\epsilon''_{eff}E_{RMS}^2V \quad (2.4)$$

where V is the volume of the material. From a heat transfer point of view, the relationship between an internal power source and the temperature of that material

is given by

$$P = mC_p \frac{dT}{dt} \quad (2.5)$$

where m is the mass of the material, and C_p is the specific heat of the material. Combining these equations, the heating rate of the material is

$$\frac{dT}{dt} = \frac{\omega \epsilon_o \epsilon''_{eff} E_{RMS}^2}{\rho C_p} - losses \quad (2.6)$$

where ρ is the density of the material, and *losses* represent heat transfer from the material. There are only two user inputs in the determination of the heating rate; the strength of the electric field, and the frequency of the applied field. Use of a constant frequency source limits the user to just one means to control the heating rate of the dielectric, the applied electric field. Therefore, the electric field is of primary importance in microwave heating, and it is the control of this field that will make heating thermal runaway materials possible.

2.5 Electromagnetic Field Propagation

The most common ways of transmitting high frequency electromagnetic waves (microwaves) to a load are through co-axial cables, waveguides, or micro strip lines. Waveguides, which are essentially hollow tubes of constant cross section, are widely used because of their low attenuation and high power handling capability. The rectangular waveguide designated WR-284 (inner dimensions: $a = 7.02$ cm, $b = 3.40$ cm) was used in this research to match the operating frequency of the source. There are many possible electromagnetic field patterns (called modes) that can exist in the waveguide. TE_{lm} propagation occurs when the electric field is normal to the waveguide axis, where l and m are integers that specify the mode of propagation. TE_{10} mode is the most fundamental mode that can propagate in a rectangular waveguide. Figure 2.3 shows the transverse electric and magnetic field lines in the TE_{10} mode. It should be noted that the electric field is a maximum at the centerline of the waveguide (Figure 2.3 a). To take advantage of this fact, the single mode cavity is fabricated

with opposing circular ports for sample feed through the centerline of the waveguide. The relationship between the electric field and the total power in the waveguide is

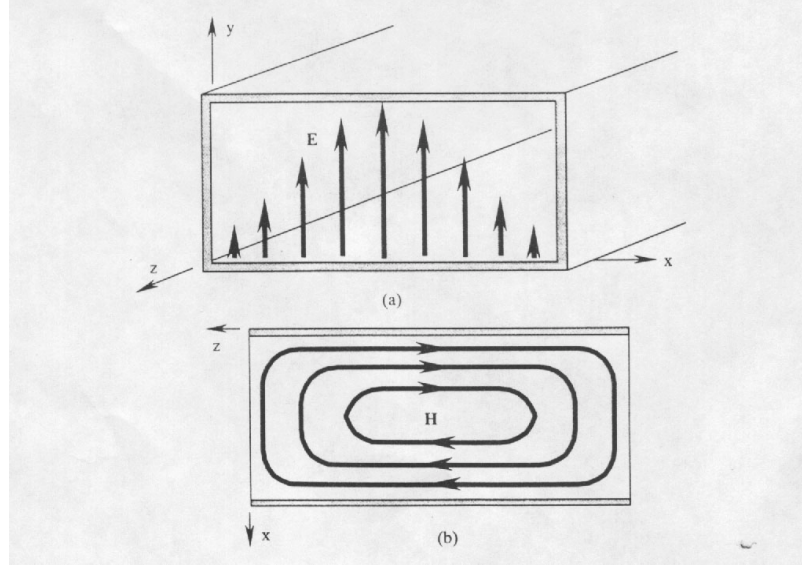


Figure 2.3: TE_{10} propagation fields (Roussy and Pearce, 1995)

important in measuring electric field strength in the cavity. The total power in the waveguide is given by (Roussy and Pearce, 1995)

$$P = \int_{a,b} |\overline{E}_t|^2 \frac{1}{Z_{TE_{10}}} ds = \frac{ab}{2} \frac{E_{RMS}^2}{Z_{TE_{10}}} \quad (2.7)$$

where a is the width of the waveguide, b is the height of the waveguide, E_{RMS} is the RMS value of the electric field ($\frac{V}{m}$), and $Z_{TE_{10}}$ is the impedance (Ω) of the waveguide. Impedance is defined as the ratio of the electric field to the magnetic field. The impedance of a waveguide is given by (Roussy and Pearce, 1995)

$$Z_{TE_{10}} = \frac{\omega\mu}{k_{Z_{TE_{10}}}} \quad (2.8)$$

$$k_{Z_{TE_{10}}} = \sqrt{\omega^2\mu\epsilon_o - \left(\frac{\pi}{a}\right)^2} \quad (2.9)$$

where $k_{Z_{TE_{10}}}$ is the propagation phase constant ($\frac{1}{m}$), ω is the angular frequency $2\pi f$ (rad/s), μ is a constant, $4\pi * 10^{-7}$ ($\frac{H}{m}$), and ϵ_o is the permittivity of free space,

$8.85 * 10^{-12} \left(\frac{F}{m}\right)$. In this document, the electric field strength is always the root-mean-square (RMS) value. A more detailed analysis of electromagnetic field patterns can be found in Roussy and Pearce (1995), Chapter 2.

Chapter 3

Experimental Setup

The apparatus used for the experiments includes a switching power supply, remote microwave launcher (magnetron), circulator, water load, dual directional couplers, WR-284 copper waveguide cavity with coupling iris, waveguide, adjustable short, and power and temperature measurement equipment. The layout of the experimental components is shown in Figure 3.1. The microwave generator includes both the power supply and the remote launcher. The microwave heating system is pictured in Figure 3.2.

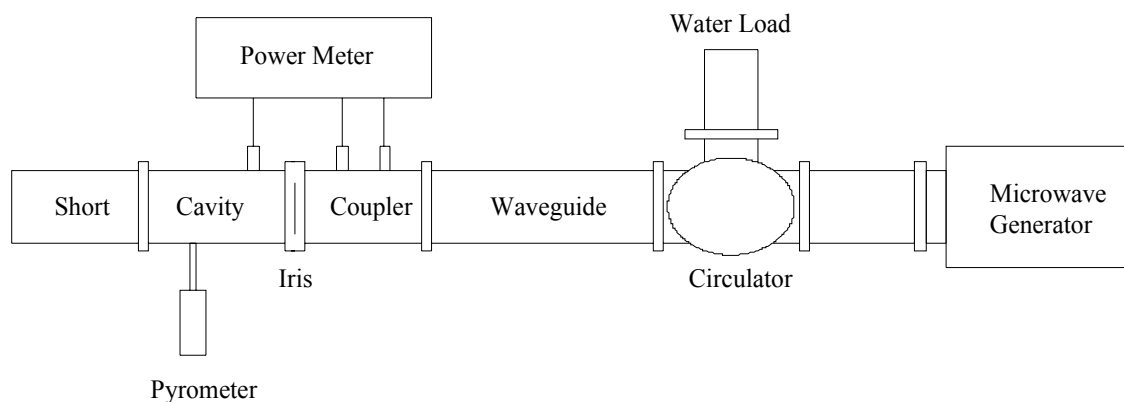


Figure 3.1: Schematic of microwave heating system

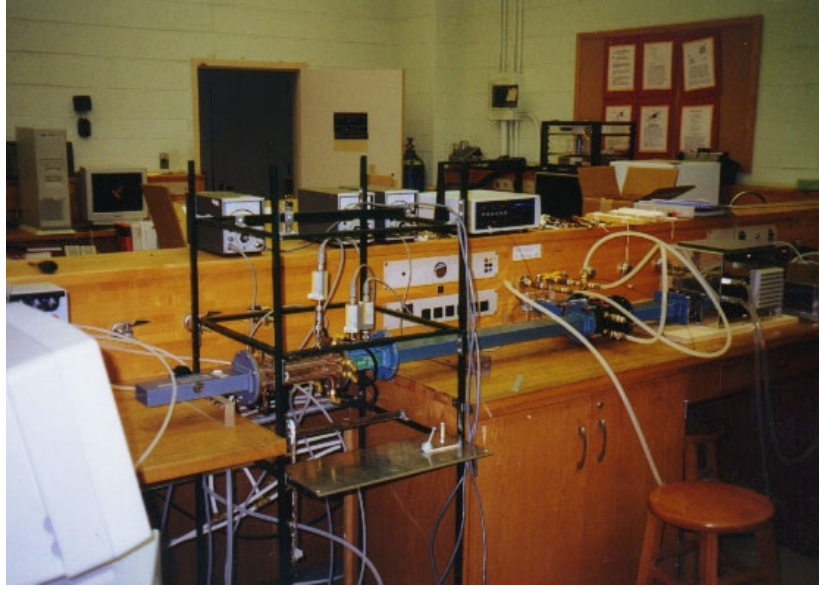


Figure 3.2: Picture of microwave heating system

3.1 Power Generation

The microwave system is powered by a Cober SM 1545D power generator. The power generator can supply up to 3 kW to the CWM-4-S magnetron from a remote location. The power generator and remote launching section is pictured in Figure 3.3. The magnetron is water cooled and launches the microwaves into a tapered WR-340 to WR-284 waveguide section. Although the technical manual states that the microwave output is set at a frequency of 2.45 GHz, the actual frequency varies with power output. Using a PRD LS-518 frequency meter, the performance of the power generator was measured up to 1 kW and plotted in Figure 3.4.

The power that is not absorbed by the system and the load is reflected back toward the source. To protect the power generator from reflected power, the system is equipped with a circulator and dummy load. This is important because high reflected power into the source increases the chance of arcing, decreases the life of the magnetron, and lowers the efficiency of the microwave generator. The circulator employs two large ferrite magnets at the center of the component. The circulator has little effect on the forward power. The circulator redirects the reflected power into a water load, which couples well in the frequency range of the power generator.



Figure 3.3: Picture of microwave power generator and remote launcher

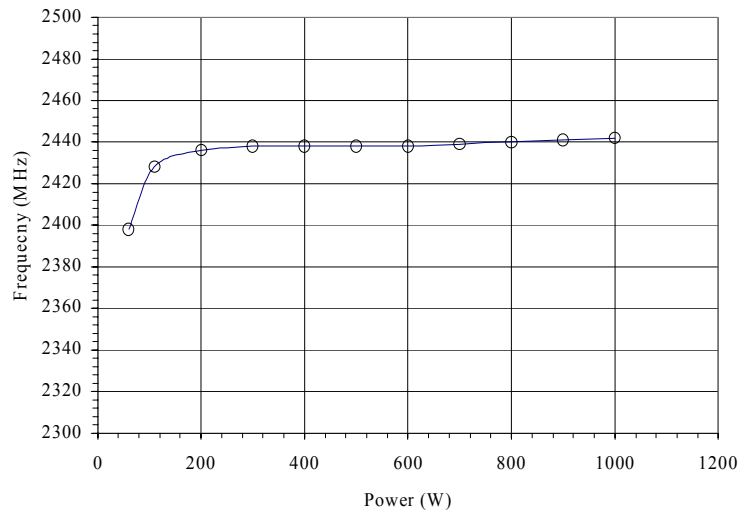


Figure 3.4: Frequency performance of power generator

3.2 Single Mode Resonant Cavity

A resonant cavity is an enclosure that is fed a radio frequency signal such that the absorption of the power by the cavity is at a maximum. A resonant cavity may have a number of different resonant frequencies.

The copper WR-284 single mode resonant cavity used in these experiments is pictured in Figure 3.5. This copper cavity was designed and used during the LANL experiments (described in section 1.3.2). The walls are water cooled to maintain a constant temperature.

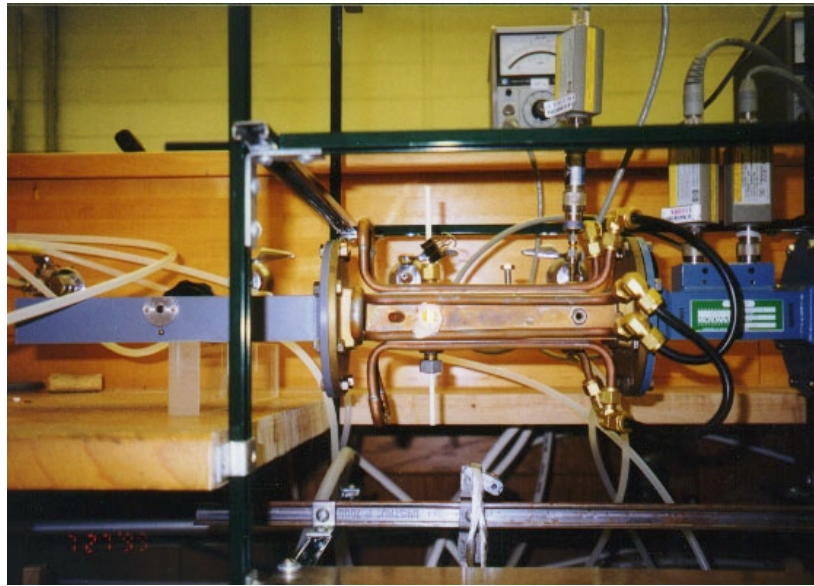


Figure 3.5: Picture of single mode resonant cavity

For the same applied power, the single mode resonant cavity establishes much higher electric field strengths than a multimode or a traveling wave applicator. The single mode resonant cavity is therefore the natural choice for the heating of low loss dielectrics.

The single mode resonant cavity causes the electromagnetic field waves to experience multiple reflections, giving rise to a standing wave pattern. The cavity is short-circuited at both ends with a moving short at the back and an iris (aperture) at the front. The cavity impedance, or the resistance at resonance, does not equal the impedance of the waveguide. Adding an aperture allows coupling of the energy

from the connecting waveguide. The aperture used in the experimental program was borrowed from LANL. The power absorbed by the cavity peaks at 2.93 GHz. Coupling efficiency decreases at the frequencies of the power generator in use for this experimental program.

The adjustable short consists of a plunger mechanism to vary the cavity length. Adjusting the cavity length allows the user to tune the cavity to the highest possible electric field strength. This is because the resonant frequency of the cavity occurs when the length of the cavity (d_c) is equal to an integer multiple of half the guide wavelength (λ_g).

For a rectangular single mode resonant cavity, the electromagnetic field is well defined. Knowledge of the electromagnetic field configuration allows precise placement of the dielectric at an electric field maximum for optimum efficiency. Given the frequency, dimensions of waveguide, and length of cavity, the field pattern can be derived. The cutoff and waveguide wavelengths are related by the equation (Metaxas and Meredith, 1983)

$$\lambda_g = \frac{2d_c}{n} = \frac{\lambda_o}{\sqrt{1 - \left(\frac{\lambda_o}{\lambda_c}\right)^2}} \quad (3.1)$$

where n is the number of nodes in the axial direction, λ_o is the wavelength at a frequency f , and λ_c is the cutoff wavelength of the waveguide. Wavelength is related to frequency by the equation (Metaxas and Meredith, 1983)

$$\lambda_o = \frac{c}{f} \quad (3.2)$$

The cutoff wavelength is a function of the waveguide dimensions and the waveguide mode. They are related by the equation (Metaxas and Meredith, 1983)

$$\lambda_c = \frac{2}{\sqrt{\left(\frac{l}{a}\right)^2 + \left(\frac{m}{b}\right)^2}} \quad (3.3)$$

The TE_{10n} mode is $l = 1$ and $m = 0$. Using these equations, the number of modes and the location of the electric field peaks can be easily determined for a given frequency and cavity length. Table 3.1 lists the field parameters at typical resonant frequencies

Cavity Characteristics	P = 60 W	P = 110 W	LANL Data
Frequency (MHz)	2398	2428	2930
Cavity Length, d_c (mm)	378.6	359.2	363.3
Guide Wavelength, λ_g (mm)	252.4	239.4	145.3
Number of nodes, n	3	3	5
1 st peak (mm from iris)	63.1	59.9	36.1
2 nd peak (mm)	189.3	179.6	108.3
3 rd peak (mm)	315.5	299.3	180.4
4 th peak (mm)	--	--	252.6
5 th peak (mm)	--	--	324.8

Table 3.1: Cavity characteristics for TE_{10n} mode

that the cavity underwent during the experimental program at Virginia Tech and at LANL. The location of the electric field peaks are given as distance from the iris.

The placement of the dielectric within the cavity changes the resonant frequency of the cavity. Therefore, the length of the cavity must be adjusted (decreased) to tune the cavity at the source frequency. By changing the length of the cavity, the user is adjusting the resonant frequency back to the value it was prior to introduction of the dielectric. This change in length has little effect on the location of the peaks in the waveguide.

The location of the introduced dielectric in the experiments is 175 mm from the aperture. In all three cases in Table 3.1, the dielectric is within 15 mm of an electric field peak. However, the location of the first peak for $n = 5$ is much different than for $n = 3$. This is important for the electric field measurement.

The cavity is equipped with two locations where a probe can be placed to measure electric field strength. Probe slots are located 53 mm and 106 mm from the aperture. It is important to move the probe to the optimum location to ensure that the largest electric field strength will be measured. Figures 3.6 and 3.7 give simple schematics of the cavity for two different electric field patterns. If the probe had been placed 106 mm from the aperture for the wave pattern in Figure 3.6, the measured electric field would have been closer to a minimum rather than a maximum. To accurately determine the electric field at the dielectric (rod), both the dielectric and the probe need to be placed at electric field peaks.

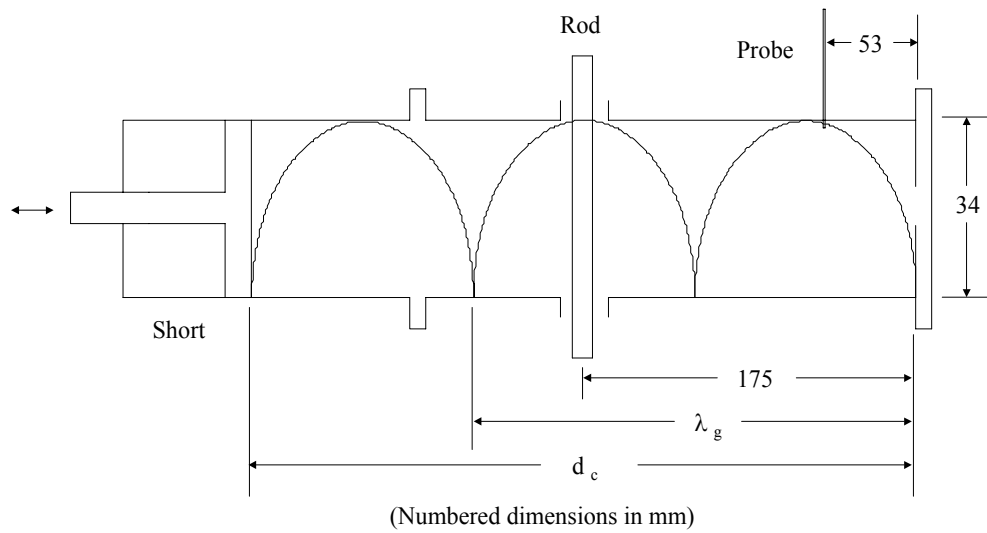


Figure 3.6: TE_{103} resonant cavity field pattern

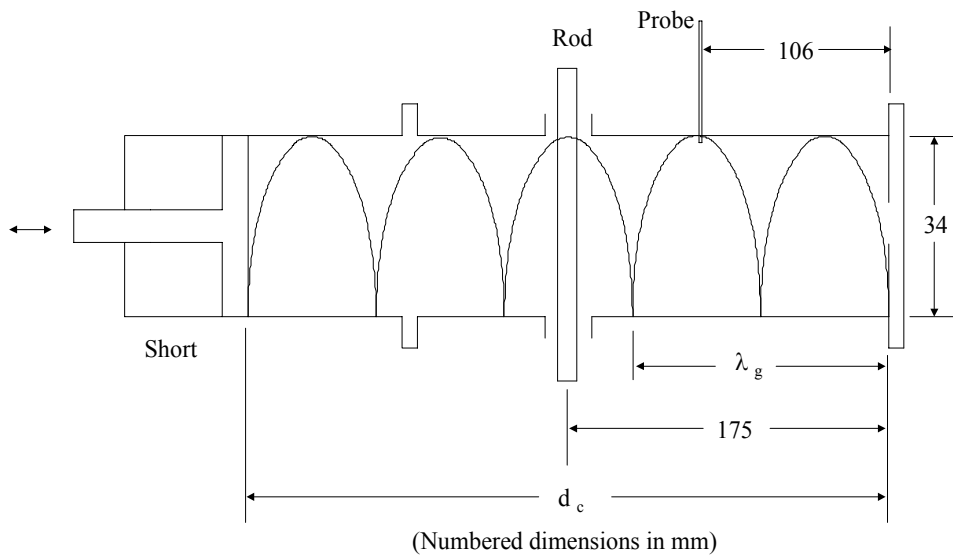


Figure 3.7: TE_{105} resonant cavity field pattern

3.3 Power Measurement

Accurate microwave power measurement is essential in the determination of the power absorbed by the dielectric. The power measurement system used in these experiments included a Cober dual directional coupler, HP 8481A power sensors, and HP 435B power meters. The dual directional coupler transfers power in two directions to two specified ports, a reflected port and a forward port. For an ideal coupler, the power measured at the forward port is not affected by the reflected power. Likewise, the power measured at the reflected port should not be affected by the incident power. However, the coupler is not ideal, and there is some interference between ports. This was impossible to eliminate in this work.

The coupling value of the forward port is factory rated at 60.3 db, while the reflected port is rated at 59.6 dB. The coupling value is the attenuation between the signal and the port, where it is read by a sensor. The power sensors are rated to a maximum power of 300 mW. Figure 3.8 shows that a reflected power of 100 W is

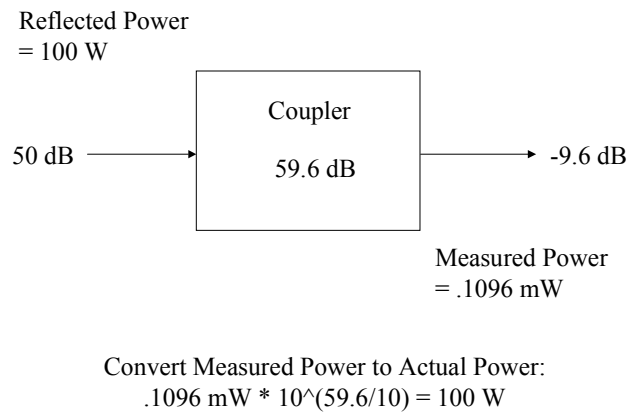


Figure 3.8: Attenuation of the signal by the reflected port

attenuated to about 0.1 mW. Precise knowledge of the coupling value is important in converting the measured value to the actual power. The correction procedure for accurately measuring these values is described in Appendix A.

The electric field strength in the cavity is also measured using the power sensor

and power meter. The power sensor is coupled to the electric field probe on the cavity. As stated earlier, there are two possible probe locations. The measured electric field strength is converted to power in watts by the power meter. Thus, to determine the electric field strength, the power meter reading must be converted back into V/m. This conversion procedure is described in Appendix B.

3.4 Temperature Measurement

To precisely monitor the microwave heating process, an Heitronics KT 15D infrared radiation pyrometer (Figure 3.9) was chosen. A radiation pyrometer measures the infrared radiation emitted by a surface. Given the emissivity ϵ of the surface being measured, the temperature of the surface can be determined. The emissivity is the ratio of the emission of a real body to the emission of a black body. This value is set by the user. The spectral sensitivity for the pyrometer is factory set between 8 and 14 μm (which is the atmospheric window where carbon dioxide particles and water vapor have high transmissivity).

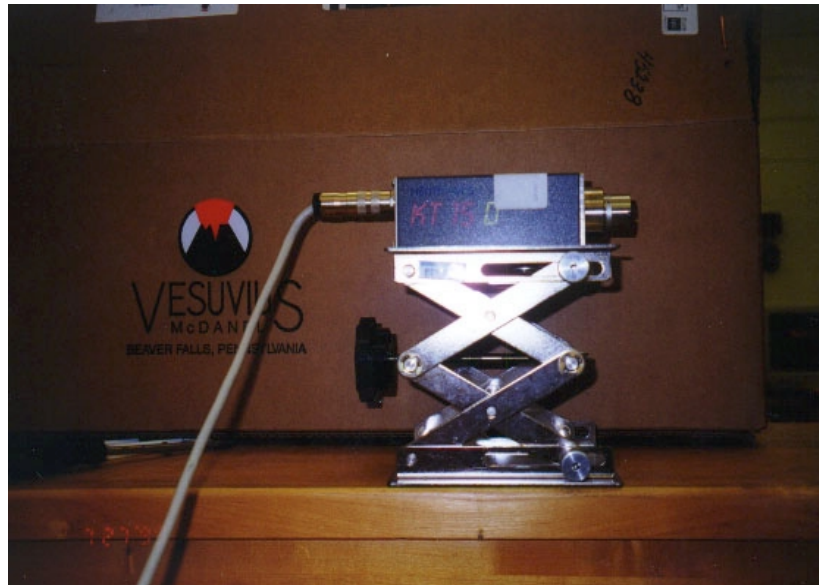


Figure 3.9: Picture of infrared pyrometer

The radiation pyrometer has several advantages including non-contact temperature measurement, no distortion of the temperature field due to dissipation (as with

a contact probe), long term stability, and a measuring field of view as small as 1 mm in diameter. One disadvantage is that the temperature range at an emissivity of 1.00 is limited to 0 to 500°C.

The materials to be tested in this experimental program have emissivities that change significantly as a function of temperature. Varying the emissivity used by the pyrometer during an experiment is not practical since it must be done manually. Instead, the emissivity is set at 1.00 for the duration of the experiment. The actual temperature is then determined from the measured temperature knowing the emissivity as a function of temperature for the material heated. For the ceramic materials mullite and alumina, the emissivity is less than 1.00 and temperatures up to 700°C can be measured. This is because the pyrometer, at an emissivity setting of 1.00, underestimates the temperature for non-black body objects. The temperature correction procedure is documented in Appendix C.

3.5 Data Acquisition

The data acquisition system (National Instruments, Model AT-MIO-16F data acquisition board with National Instruments Labwindows software) was used to record data output from the instrumentation used with the microwave heating system. This system was integrated into a 486DX-33MHz computer.

The instrumentation provides a voltage signal that is read by the data acquisition board through a terminal block. Voltage readings were recorded from the Heitronics infrared pyrometer (1 channel), and the power meters (3 channels). Data were acquired at 0.2 second intervals. The typical data acquisition program, mullite.c, is listed in Appendix E.

Chapter 4

Experimental Results

The goal of the experimental program was to accurately measure the important parameters of the microwave heating system for various heating control strategies. These parameters include the temperature of the dielectric, the power absorbed by the dielectric, the electric field strength in the cavity, and the frequency of the applied field. The three dielectric materials chosen were mullite, alumina, and nylon 66. All three materials exhibit thermal runaway and have known dielectric properties, making them ideal for this research.

4.1 Heating Control Strategies

There are three heating control strategies that guided the experimental program. Depending on the desired heating rate and steady-state sample temperature, the electric field can be varied for three basic conditions that can be maintained in the cavity: constant electric field strength, constant power to the cavity, and constant power to the dielectric. For each condition, the parameter is held constant for the duration of the test run. The test run ends when the sample reaches steady-state temperature.

The limitations of the physical process that can make these conditions difficult to meet include

1. Precision of the power measuring instrumentation (for low power applications

such as heating nylon 66)

2. Extremely low dielectric loss factor of the material to be heated (alumina)
3. Temperature range of the pyrometer (limited to 700°C)
4. Thermal runaway
5. Manual control

Despite these limitations, there were many successful heating experiments for all three materials.

4.2 Source Power

The incident power that is measured at the forward port of the directional coupler is the power from the microwave source. Higher electric field strengths in the cavity can be achieved by increasing incident power. A suitable incident power from the source must be chosen based on the desired heating rate, as well as the size and properties of the material to be heated. The power output from the source should be the minimum power sufficient to heat the material to the highest temperature to be measured during the experimental program. It is beneficial to be at the minimum power output because as power is increased, the resolution of the power meters decreases.

All experiments involving mullite were run at an incident power of 110 W. Alumina required higher field strengths and thus a higher source power setting of 135 W was used. The heating of nylon 66 required an incident power of only 65 W.

4.3 Characterization of the Cavity

The power absorbed by the dielectric cannot be measured directly. The directional coupler indirectly measures the power that is absorbed by the cavity walls and the dielectric. Therefore, it was necessary to quantify the power loss to the cavity walls in order to quantify the power absorbed by the dielectric.

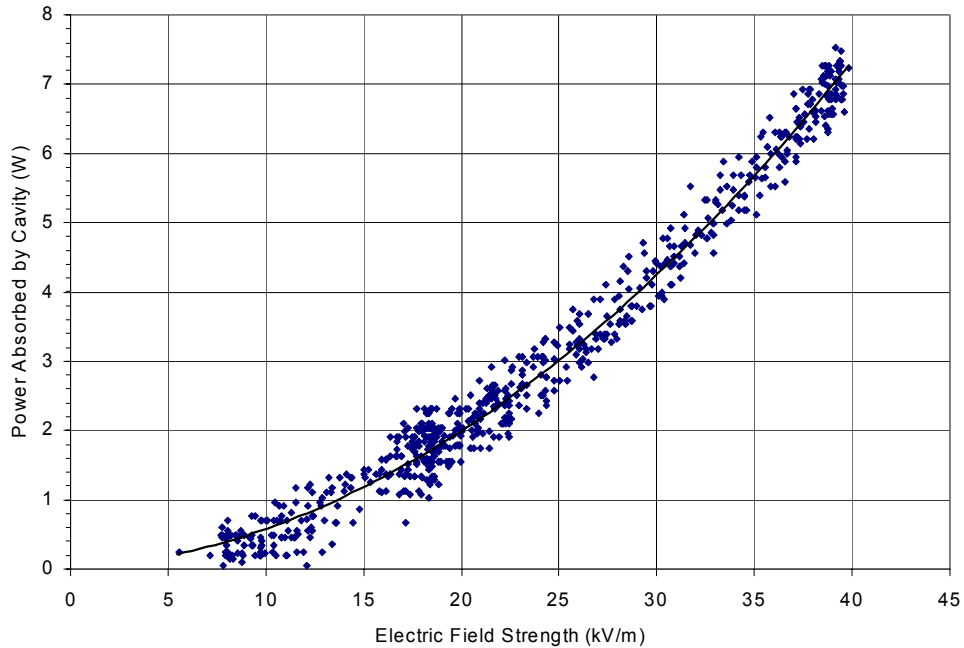


Figure 4.1: Characterization of cavity at an incident power of 110 W

Characterization of the cavity is an experimental procedure to estimate the power absorbed by the cavity walls. As stated earlier, the dual directional coupler measures the forward and reflected power at the entrance to the cavity. When the cavity is tuned without a dielectric, the difference between forward and reflected power can be entirely attributed to the power absorbed by the cavity walls. The cavity walls include the adjustable short inner walls, the copper cavity walls, and the iris.

The cavity needs to be characterized at each of the three incident power settings, 65 W, 110 W, and 135 W because of the frequency dependence of the source at this low power range (see Figure 3.4). The short was adjusted to span the range of electric field strengths expected to occur during the actual heating of the dielectric.

The amount of loss to the inner walls of the cavity is a function of the magnitude of the electric field strength, as measured by the probe in the cavity. Figure 4.1 shows the power loss to the cavity walls as a function of electric field strength at an incident power of 110 W. For each loss curve produced (See Appendix F for loss curves at 65

W and 135 W), a second order polynomial was fit to the data. This curve fit was then incorporated into the data acquisition program.

4.4 Microwave Heating of Mullite

Mullite is a white ceramic consisting of aluminum oxide Al_2O_3 , and silica glass SiO_2 , which has been sintered at temperatures greater than 1550°C to form fine crystals. Mullite is used for its strength, refractoriness, good chemical resistance, consistent chemical properties, absence of contaminants, stability at high temperatures, and low thermal conductivity.

The dielectric properties of mullite are shown in Figure 4.2. The dielectric loss factor does not increase significantly until the rod temperature reaches 800°C . Therefore, the thermal runaway effect is less significant at the temperature range for the experimental program (up to 700°C). There were two different size mullite rods used in the experimental program: 4.67 mm diameter and 2.75 mm diameter.

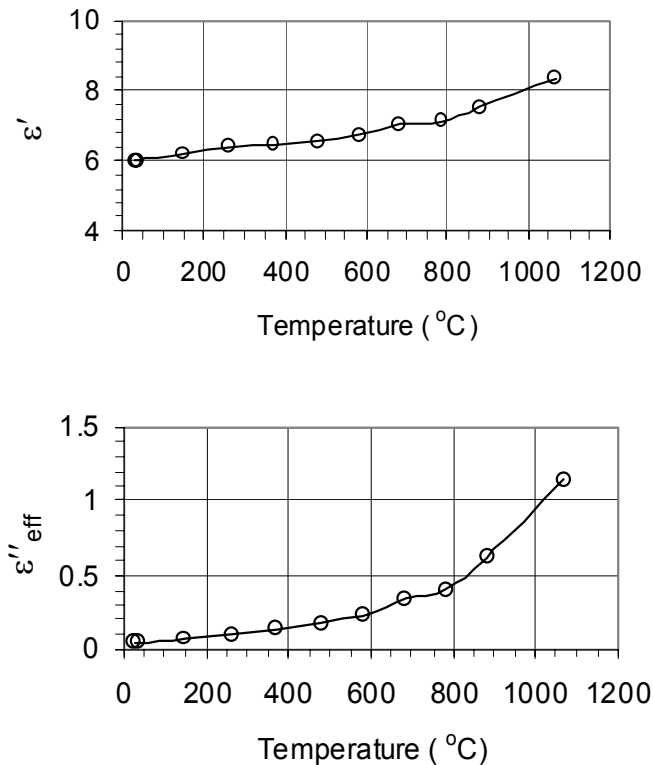


Figure 4.2: Dielectric properties of mullite (Thomas et al., 1998)

There were three basic heating strategies. The experimental results for the heating of mullite for each strategy are discussed next.

4.4.1 Constant Power Absorbed: Mullite

The temperature of a material will only reach steady-state when the heat loss matches the heat input. When a material is heated, the temperature of the sample initially increases. As temperature increases, losses due to conduction, radiation, and convection become more significant until the sample reaches equilibrium. The equilibrium temperature can be limited by controlling the power absorbed by the material. In this way, thermal runaway can be avoided.

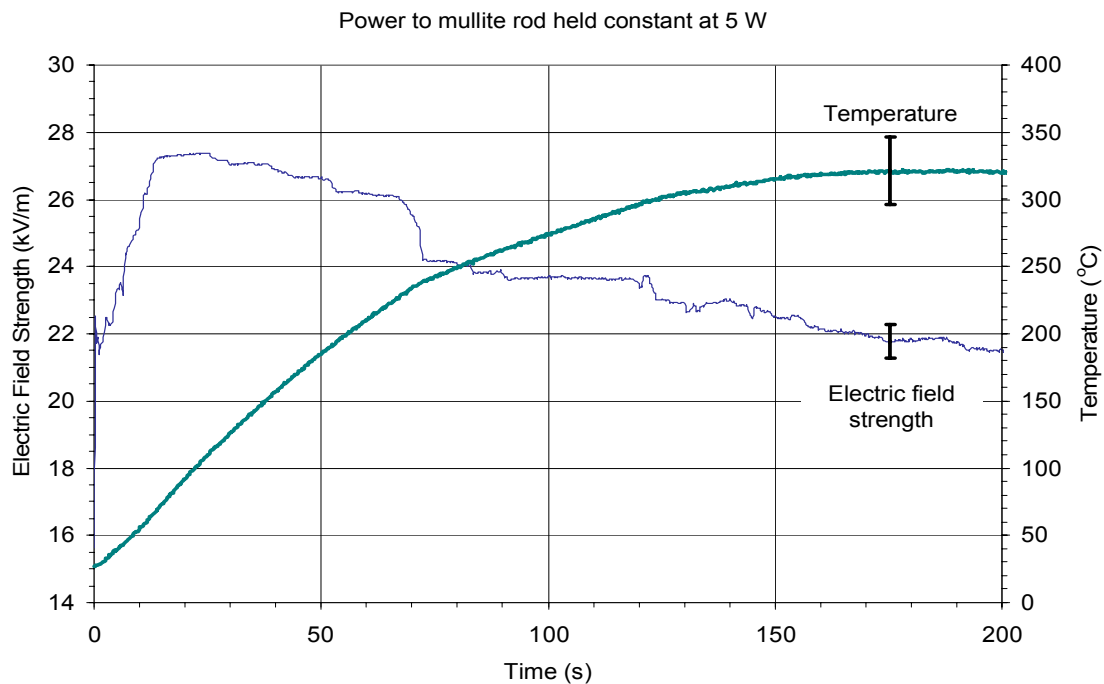
This strategy was explored in the heating of mullite. The power absorbed by the sample was set and the corresponding steady-state temperature measured. The power absorbed by the sample was held constant throughout these experiments by varying the electric field strength in the cavity. This was done by repeatedly adjusting the cavity length using the adjustable short. The heating continued until a steady-state electric field strength and sample temperature were reached.

This procedure was repeated four times at three different absorbed powers (5 W, 7 W, and 9 W). Figure 4.3 shows the average of four runs for a constant absorbed power of 5 W. Figures 4.4 and 4.5 show the average of four runs for a constant absorbed power of 7 W and 9 W, respectively. The general trends from these data include:

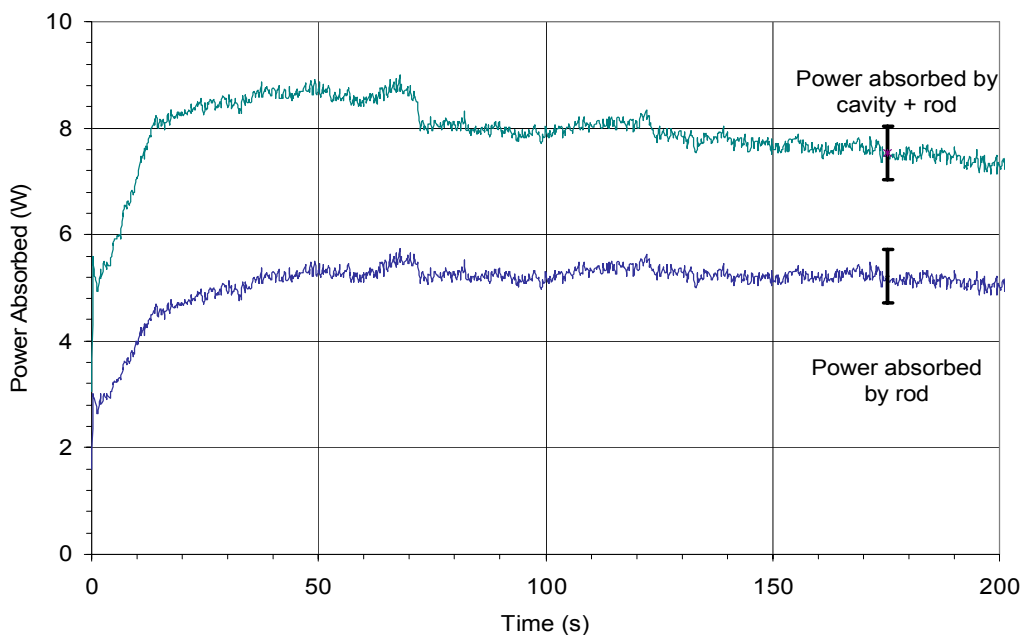
- Power loss to the cavity walls decreases as the electric field strength decreases and the rod temperature increases
- The required electric field strength decreases as the rod temperature increases (after nominal absorbed power has been reached)
- The electric field strength peaks initially and decreases to a lower, steady-state value

These results were expected because the electric field strength required to

maintain a constant absorbed power by the rod must decrease as the dielectric loss factor increases (assuming a constant frequency; see Eqn 2.4). Greater cavity wall losses at higher electric field strengths are also expected because cavity wall losses have been shown to increase exponentially with electric field strength (see Figure 4.1).

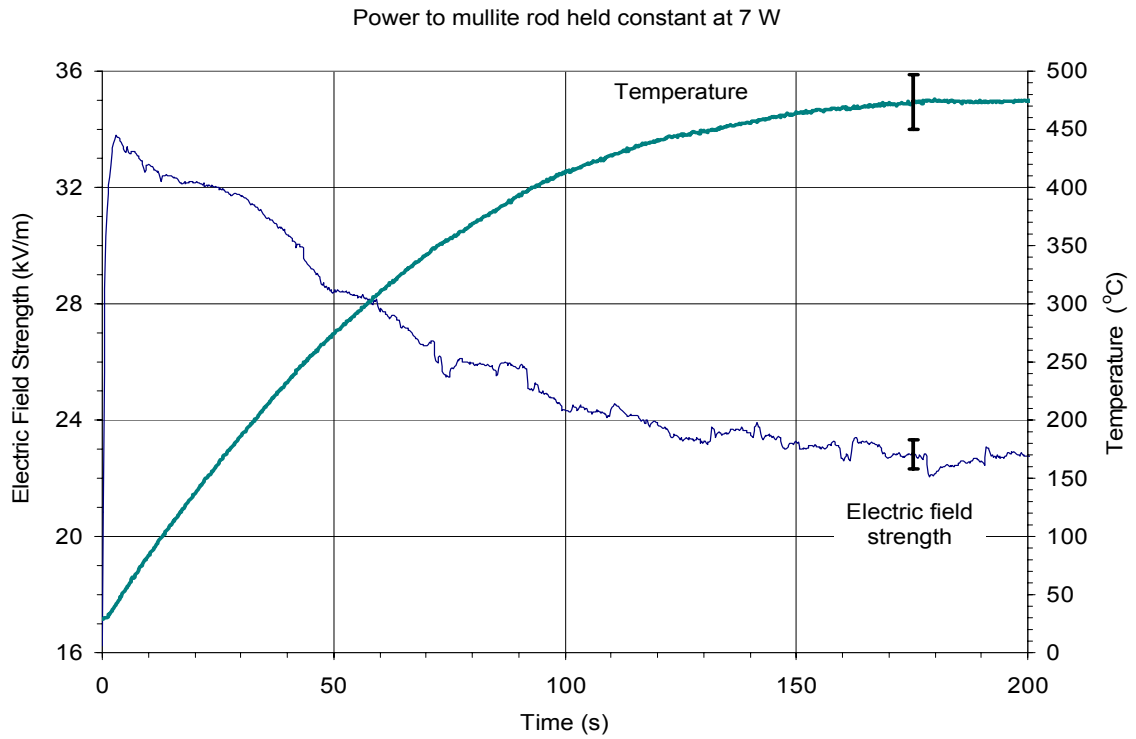


(a)

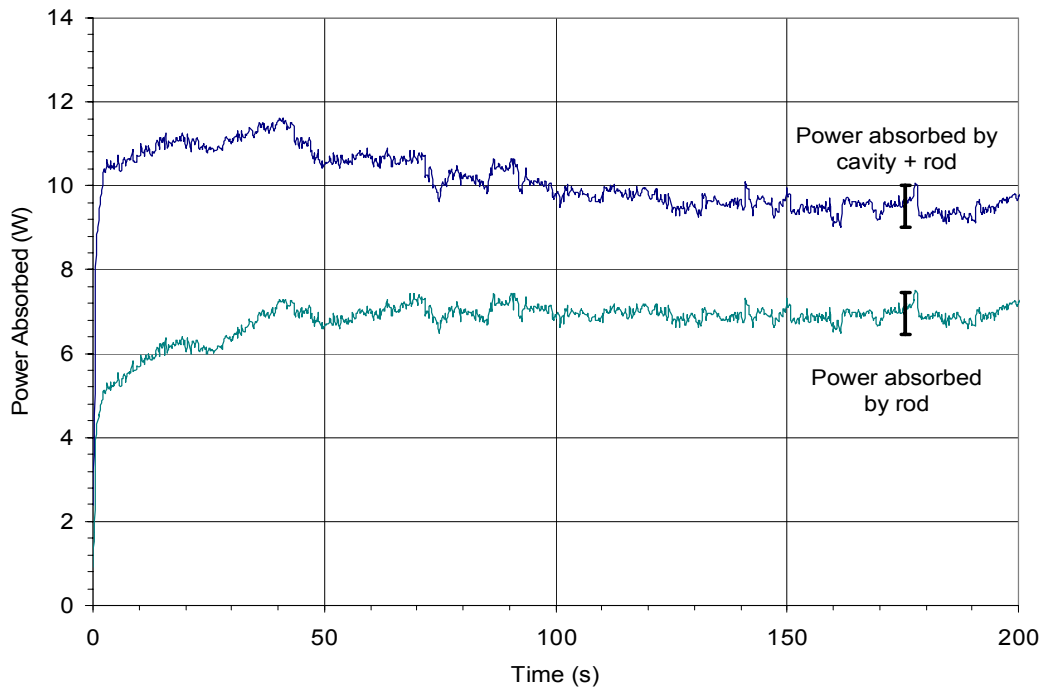


(b)

Figure 4.3: Heating of a 4.67 mm mullite rod to a steady-state temperature (a), where power absorbed by rod is increased to 5 W and held constant (b). (Average of 4 runs, individual runs shown in Appendix D; bars indicate measured range)



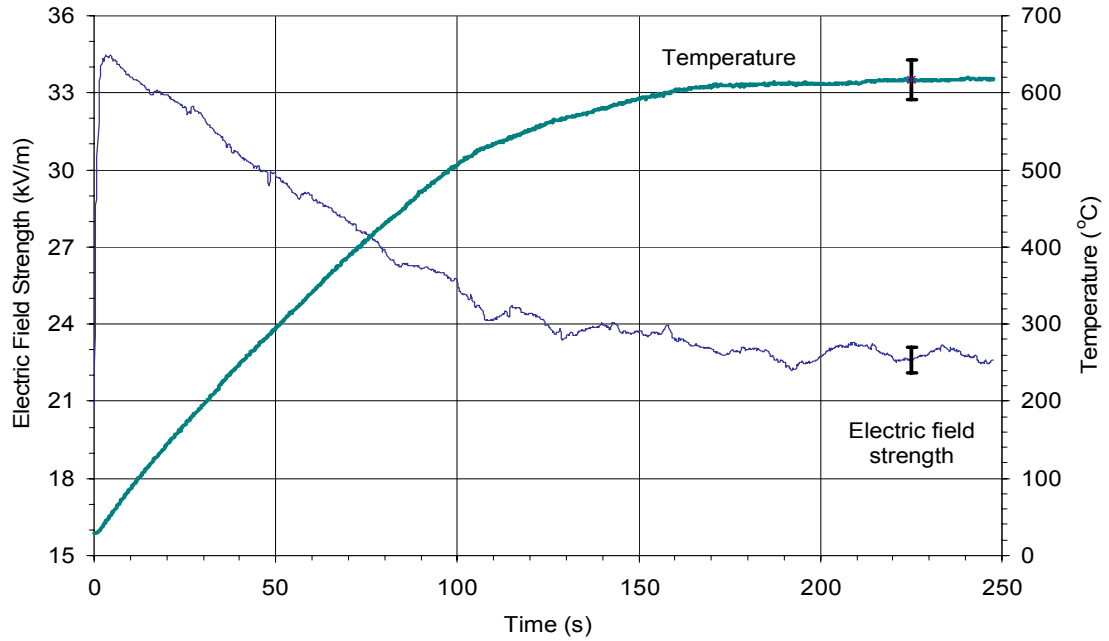
(a)



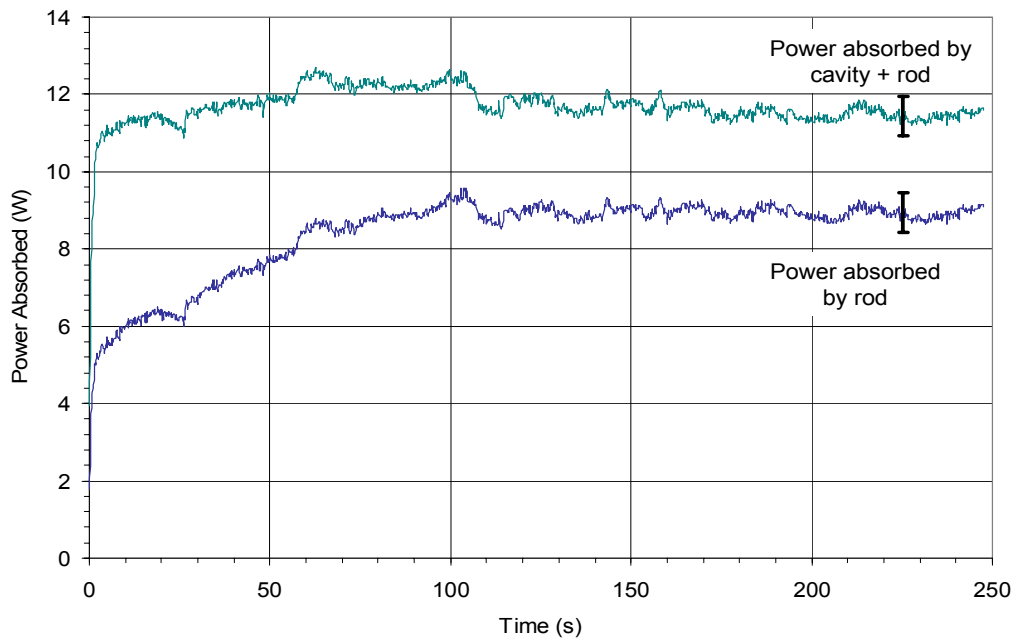
(b)

Figure 4.4: Heating of a 4.67 mm mullite rod to a steady-state temperature (a), where power absorbed by rod is increased to 7 W and held constant (b). (Average of 4 runs, individual runs shown in Appendix D; bars indicate measured range)

Power to mullite rod held constant at 9 W



(a)



(b)

Figure 4.5: Heating of a 4.67 mm mullite rod to a steady-state temperature (a), where power absorbed by rod is increased to 9 W and held constant (b). (Average of 4 runs, individual runs shown in Appendix D; bars indicate measured range)

The temperature and electric field strength plots are combined in Figure 4.6. There are several trends that are observed as the power absorbed by the rod is increased:

- Higher power input leads to higher steady-state rod temperatures
- Steady state electric field strengths are similar (~ 22 kV/m), but increases slightly with higher power input
- Times required to reach steady-state are similar (~ 200 s)
- Cavity efficiency increases (i.e., a higher percentage of the overall power to the cavity is absorbed by the rod)

Figure 4.7 shows that the loss to the cavity walls reaches a maximum as the rod initially heats up. This maximum power absorbed by the cavity walls increases for higher initial electric field strengths. However, at steady-state, the loss to the cavity walls becomes less significant. This is because a higher percentage of the total power in the cavity is absorbed by the rod itself. The projected trend for the heating of mullite at sintering temperatures is that the steady-state electric field strengths will continue to decline. Thus, power loss to the cavity walls becomes small for steady-state high temperature heating of mullite.

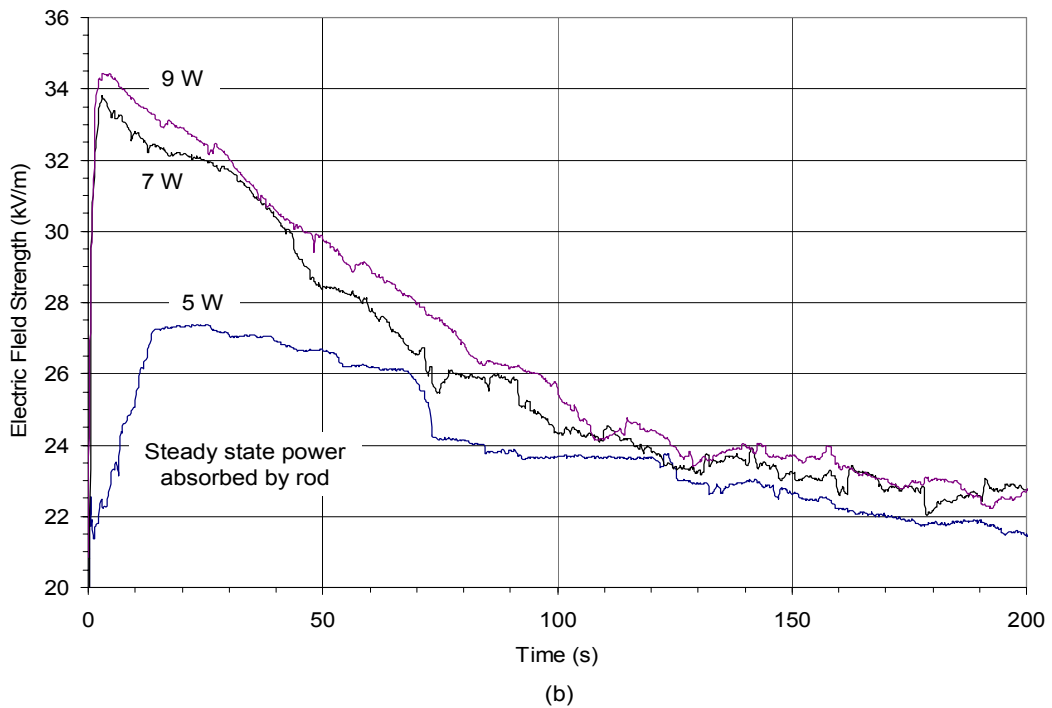
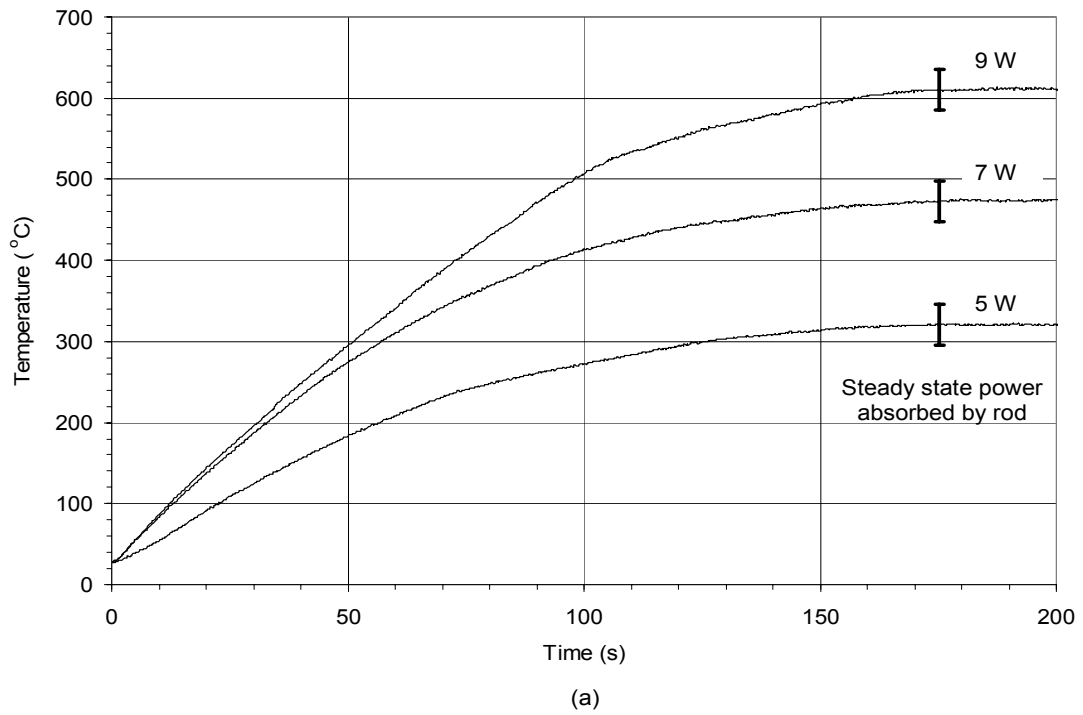


Figure 4.6: Comparison of temperature (a), and electric field strength (b), for the heating of a 4.67 mm mullite rod where power absorbed by rod is increased to and held constant at indicated level (bars on temperature plots indicate measured range).

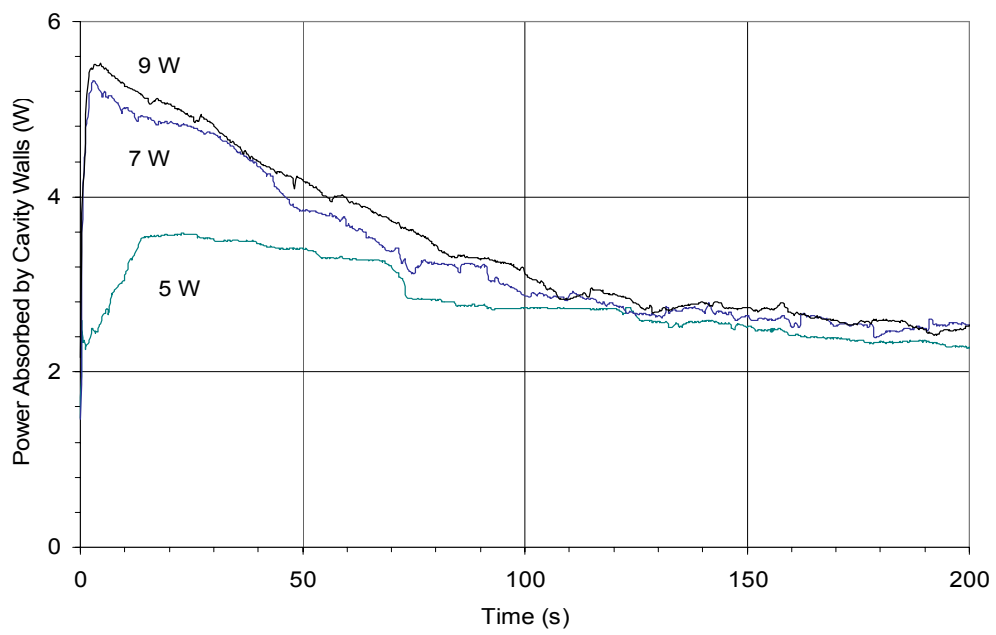


Figure 4.7: Power loss to cavity walls for the heating of a 4.67 mm mullite rod

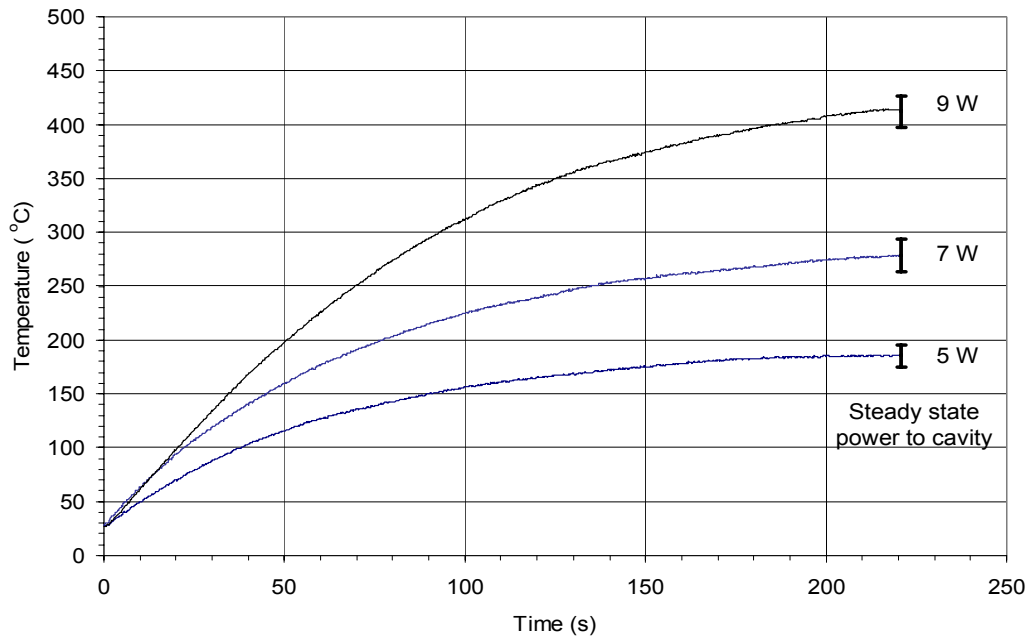
4.4.2 Constant Power to Cavity: Mullite

The next heating strategy was maintaining a constant power to the cavity. In this case, the power absorbed by the rod varies. If the power to the cavity is held constant long enough, the temperature and power absorbed by the rod will reach steady-state values. Therefore, the steady-state data can be directly compared to the data for constant power absorbed by the rod.

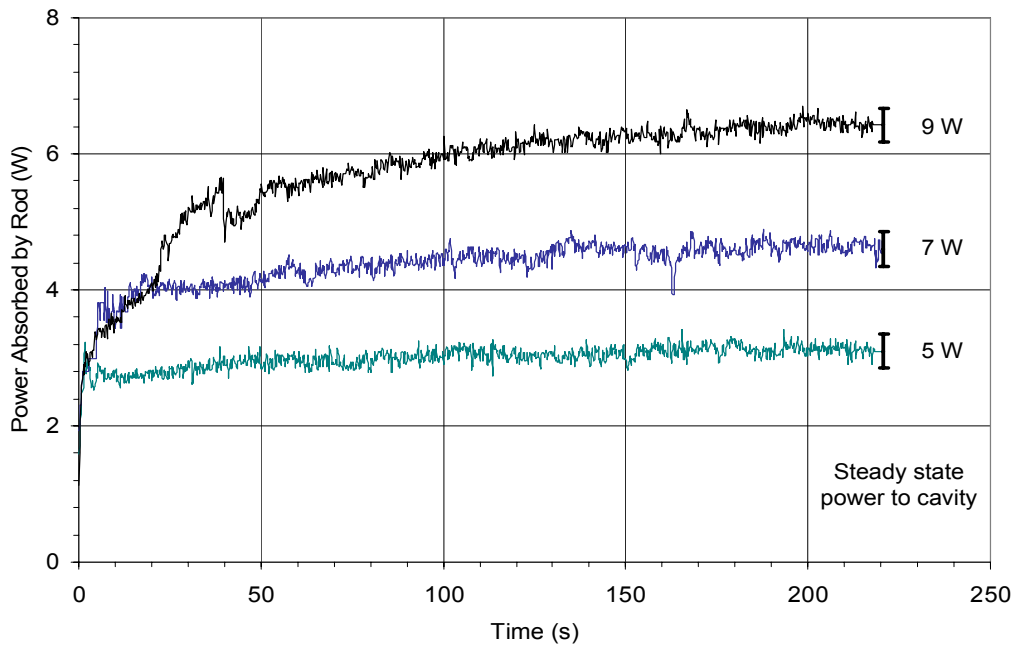
Figure 4.8 shows the temperature of the rod and power absorbed by the rod for three cavity powers (5 W, 7 W, and 9 W). Steady-state rod temperatures are lower for all three cases when compared to Figure 4.6. This is because less power is absorbed by the rod.

The power absorbed by the rod increases slightly over the duration of the experiment, until it reaches steady-state. By definition, the cavity efficiency increases as the power absorbed by the rod increases because the same amount of power is available in the cavity throughout the run. However, there is a maximum efficiency for the cavity which is limited by the amount of power the rod absorbs, which is based on its temperature.

The electric field strength is compared for each power setting in Figure 4.9. The steady-state electric field strength is clearly higher for higher power to the cavity.



(a)



(b)

Figure 4.8: Comparison of temperature (a), and power absorbed by rod (b), for the heating of a 4.67 mm mullite rod where power to the cavity is increased to and held constant at indicated level (bars on temperature plots indicate measured range).

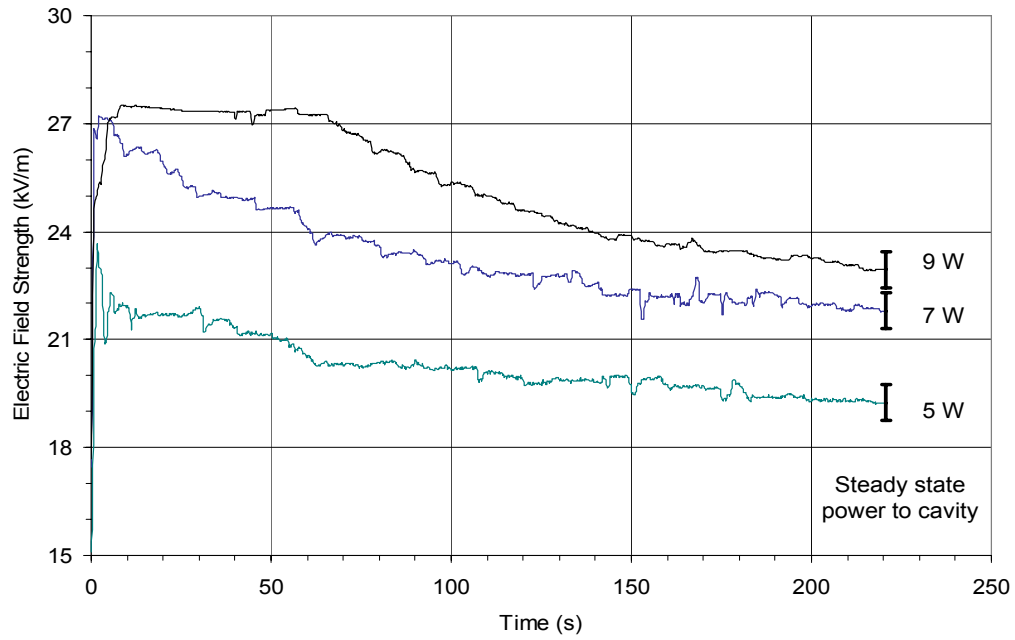


Figure 4.9: Comparison of electric field strength for the heating of a 4.67 mm mullite rod, where power to the cavity is increased to and held constant at indicated level (bars on temperature plots indicate measured range).

4.4.3 Constant Electric Field in Cavity: Mullite

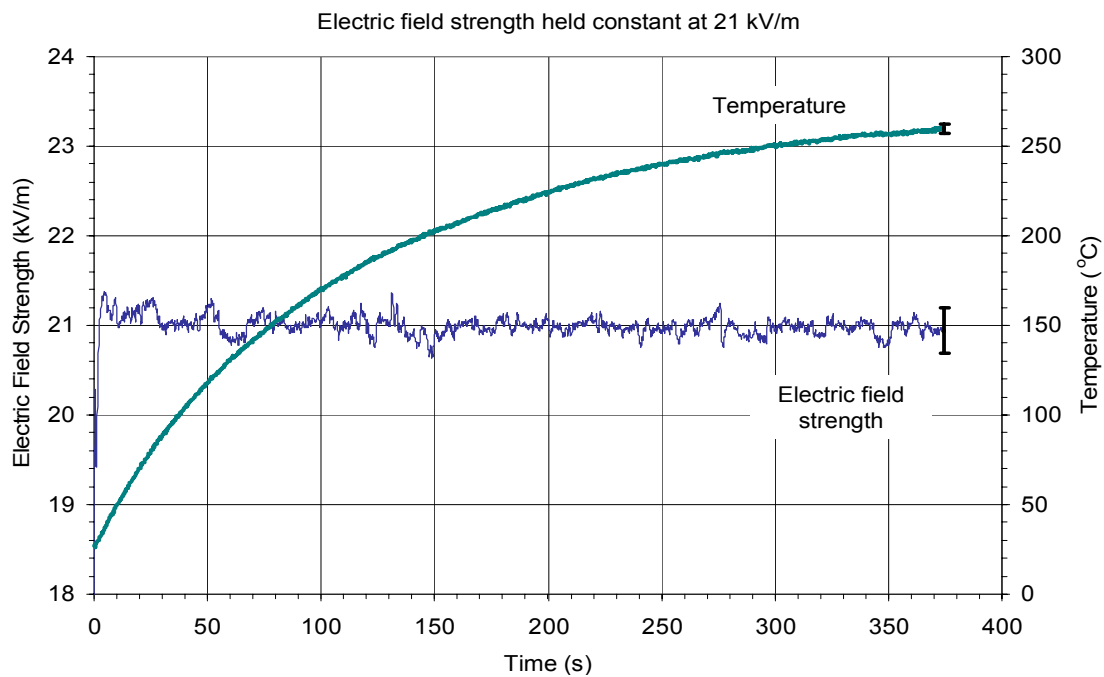
By maintaining a constant electric field strength as measured at the probe in the cavity (see Figure 3.6), the power absorbed by the dielectric rod must increase as the dielectric loss factor increases. The influence of the dielectric on the electric field in the single mode resonant cavity made it difficult to maintain a constant electric field throughout an individual run. At high temperatures, the electromagnetic field is substantially attenuated by the rod. Therefore to maintain a constant electric field strength, an increasing amount of electromagnetic energy must be dumped into the cavity. This introduces the possibility of thermal runaway.

Figure 4.10 shows the heating of a mullite rod at a constant electric field strength of 21 kV/m (which is comparable to the steady state values of 22 kV/m in Figure 4.6 b). The electric field strength was low enough not to induce thermal runaway.

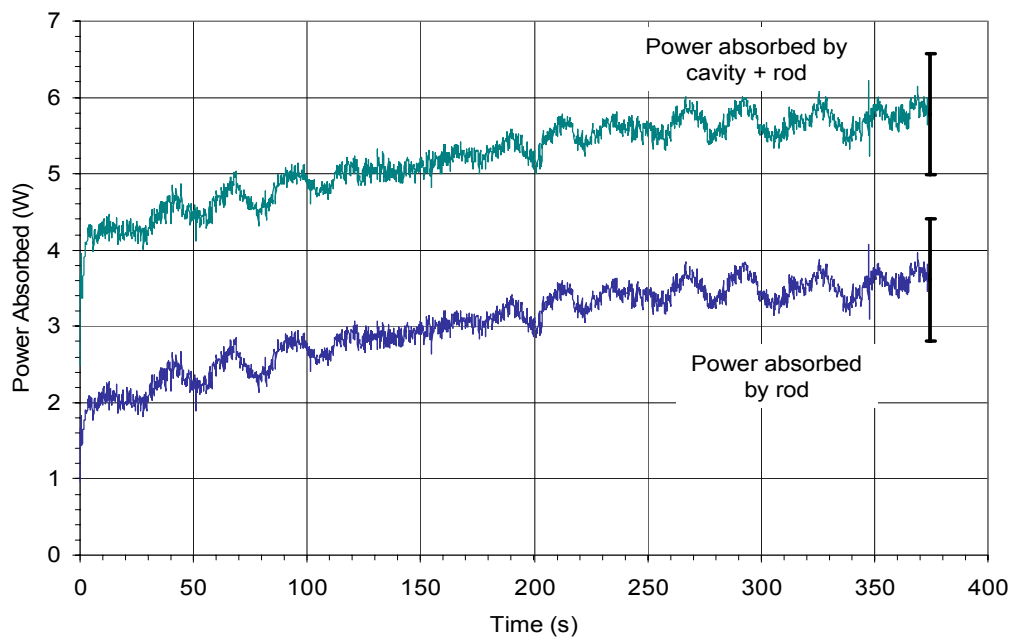
There are many important trends that occur for this heating strategy:

- Power to the cavity increases as the rod temperature increases (more energy must be dumped into the dielectric to maintain a constant electric field strength)
- Power absorbed by the rod increases as the rod temperature increases (the dielectric becomes more lossy)
- Power absorbed by the cavity walls remains constant at 2.2 W
- The heating rate is substantially lower than in Figure 4.6 a, leading to longer times to achieve steady-state temperatures (~ 370 s vs. ~ 200 s)

Since the electric field strength is held constant during the experiment, the power absorbed by the cavity walls is constant. All of the additional power that enters the cavity (once the electric field strength has been established) is absorbed by the rod.



(a)



(b)

Figure 4.10: Comparison of temperature (a) and absorbed power by a 4.67 mm mullite rod, where electric field strength is held constant at 21 kV/m. (Average of 4 runs, individual runs shown in Appendix D; bars indicate measured range)

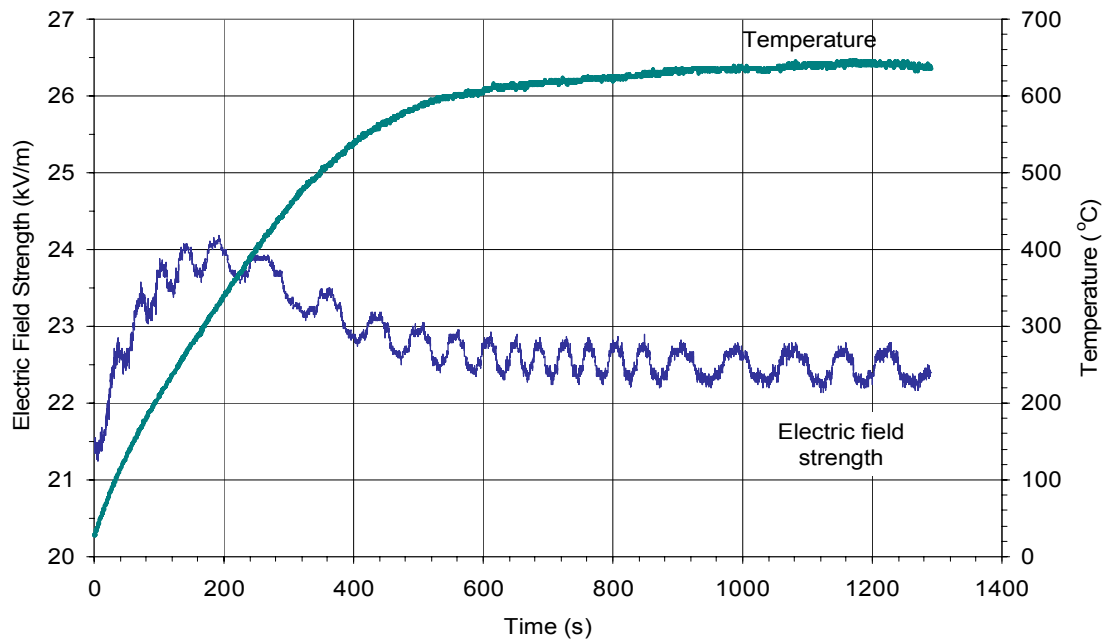
4.4.4 Constant Cavity Length Effects

Another method of heating is to tune the cavity once (i.e., adjust the cavity length), and let the system reach steady-state with no further user influence. As the rod heats, the effective cavity length increases because the dielectric constant of the rod increases. In Figure 4.11 a, the cavity length was initially adjusted to a position shorter than the resonant cavity length (the cavity length that excites the resonant frequency). As the rod heated, the effective cavity length increased and internally tuned the cavity to resonance. As the rod continued to heat and the effective cavity length became longer than the resonant cavity length, the cavity began to detune. The electric field increased to some maximum and then decreased to a new level, higher than the initial electric field strength.

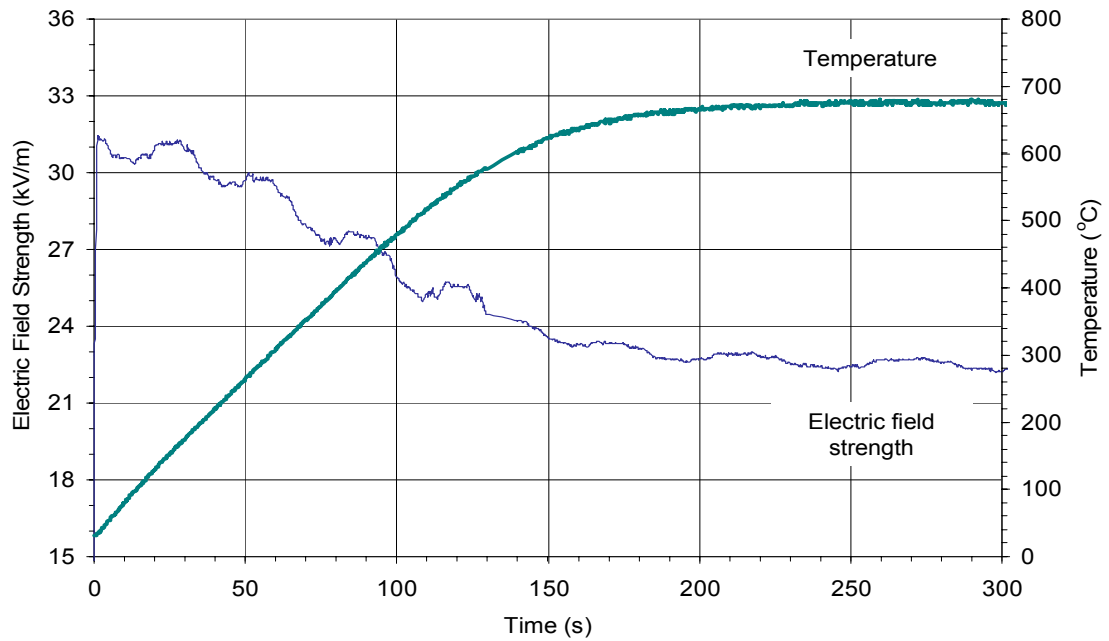
In a different run, the cavity was tuned to the resonant cavity length initially, such that the electric field strength was peaked. As the rod heated, the effective cavity length became longer than the resonant cavity length, thus detuning the cavity. This result is shown in (Figure 4.11 b). The resonant condition is not sustained because the effective cavity length increases while the actual cavity length is not changed.

The steady-state rod temperatures are similar for the two conditions, but the electric field strength profiles are much different. In the second case, the highest electric field strength in the cavity was ~ 31.5 kV/m. For the first case, the highest electric field strength was ~ 24 kV/m. Steady-state electric field strengths are similar for each case, ~ 22.5 kV/m.

Another scenario could be to tune the cavity such that the cavity length is initially larger than the resonant cavity length. As the effective cavity length increases, the cavity detunes. For this case, the cavity never tunes to resonance.



(a)



(b)

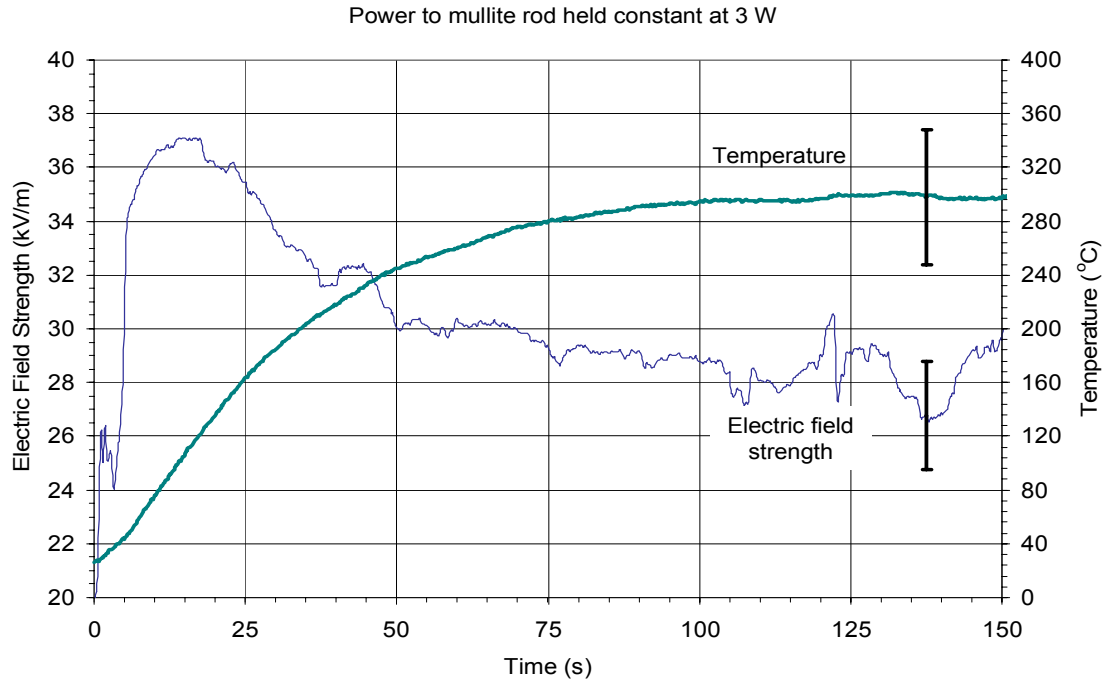
Figure 4.11: Heating of a 4.67 mm mullite rod, where cavity length is initially shorter (a) and equal to (b) the resonant cavity length

4.4.5 Effects of Smaller Diameter Rod

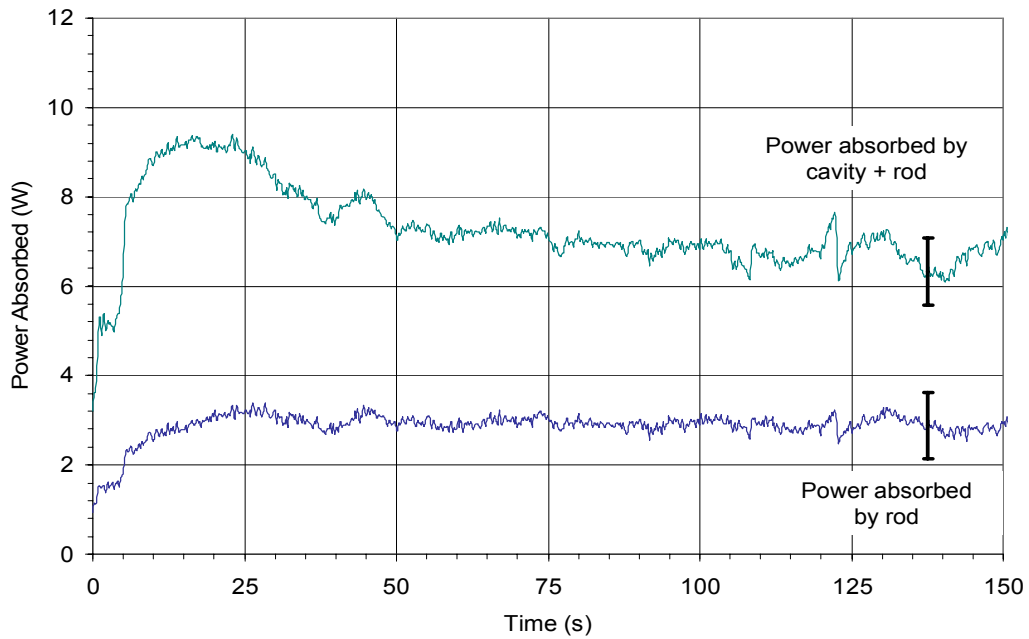
The effects of sample size were explored by heating a mullite rod of 2.75 mm diameter. The power absorbed by the rod was held constant at 3 W and 5 W (Figures 4.12 and 4.13). For an equivalent power absorbed by the rod, the general trends are (comparing Figures 4.3 and 4.13)

- The smaller rod achieves higher steady-state sample temperatures (At 5 W, 520°C for 2.75 mm rod vs. 320°C for 4.67 mm rod)
- Higher electric field strengths are needed to heat the smaller rod (At 5 W, 30 kV/m for 2.75 mm rod vs. 21.5 kV/m for 4.67 mm rod)
- Loss to the cavity walls is significantly higher for the smaller rod (At 5 W absorbed by rod, 4.2 W wall loss for 2.75 mm rod vs. 2.3 W wall loss for 4.67 mm rod)

The same power in a smaller volume results in higher power density and higher rod temperatures. Higher electric field strengths exist because there is less material to attenuate the field. Higher electric field strengths result in more loss to the cavity walls.



(a)



(b)

Figure 4.12: Heating of a 2.75 mm mullite rod to a steady-state temperature (a), where power absorbed by rod is increased to 3 W and held constant (b). (Average of 4 runs, individual runs shown in Appendix D; bars indicate measured range)

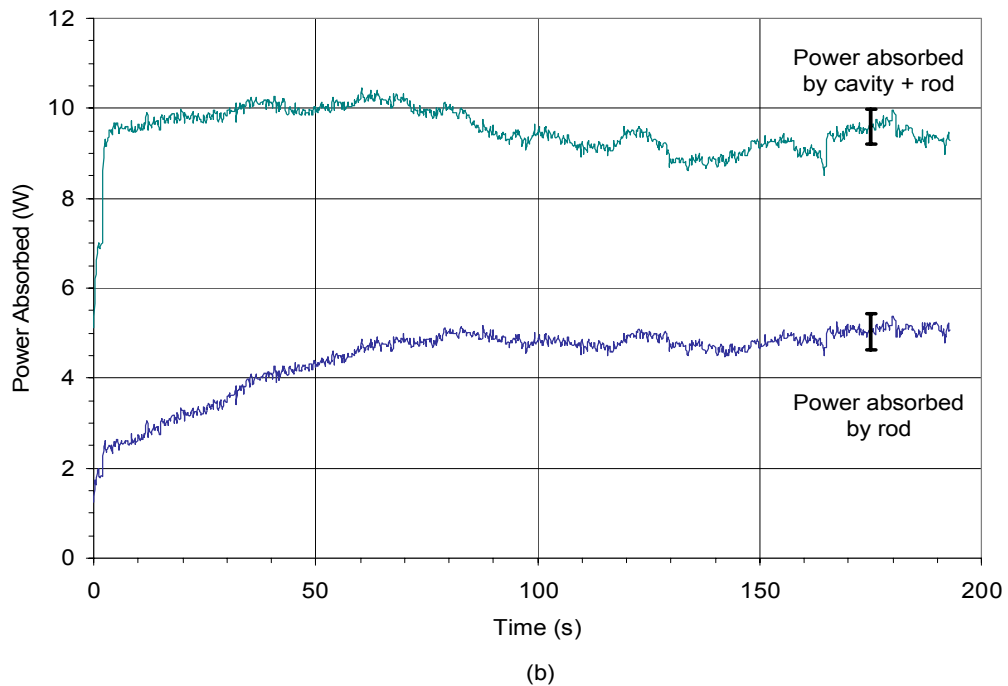
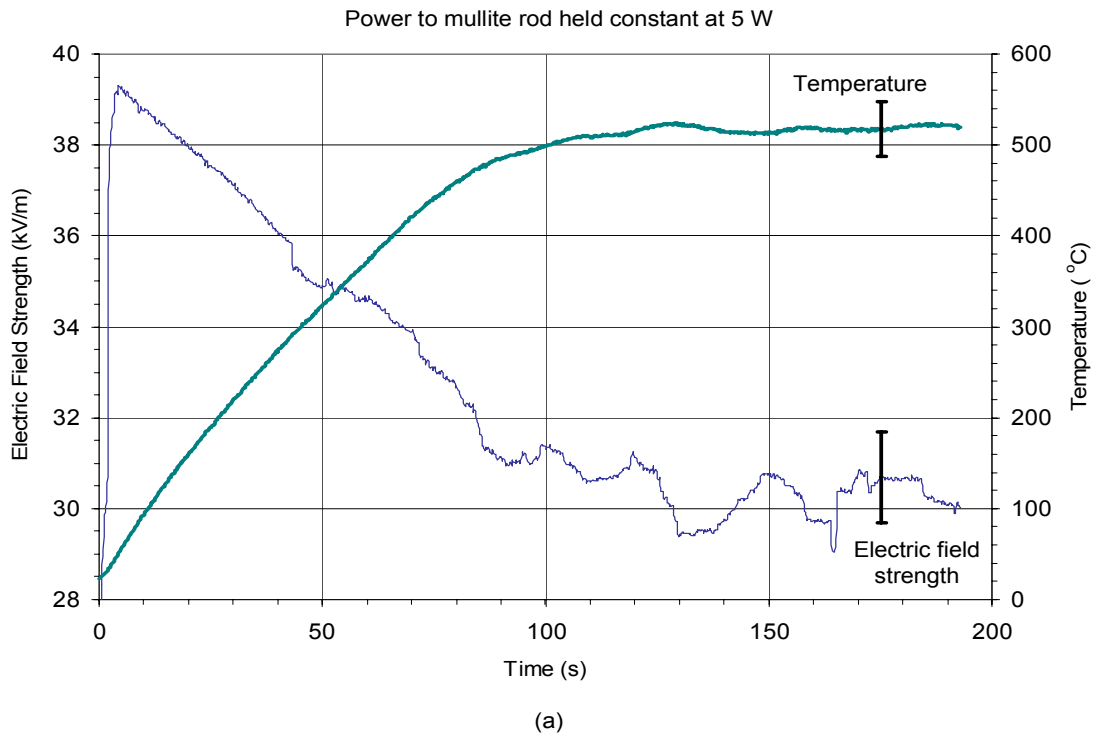


Figure 4.13: Heating of a 2.75 mm mullite rod to a steady-state temperature (a), where power absorbed by rod is increased to 5 W and held constant (b). (Average of 4 runs, individual runs shown in Appendix D; bars indicate measured range)

4.5 Discussion of Results for Mullite

The steady-state data for the heating of a 4.67 mm mullite rod are presented in Table 4.1.

CASE	Temperature of Mullite (°C)	E Field Strength (kV/m)	Power to Cavity (W)	Power to Rod (W)	Cavity Efficiency (%)
Fig 4.11 b	675	22.5	12.7	10.2	80
Fig 4.11 a	640	22.4	12.1	9.7	80
PROD = 9 W	619	22.5	11.6	9.1	81
PROD = 7 W	476	22.6	9.7	7.2	74
PCAV = 9 W	414	22.9	9.0	6.4	71
PROD = 5 W	320	21.5	7.4	5.1	69
PCAV = 7 W	279	21.8	7.0	4.6	66
PCAV = 5 W	185	19.2	5.0	3.1	62

Table 4.1: Comparison of steady-state data for various microwave heating scenarios

It is clear that the efficiency of the cavity increases significantly as the temperature and absorbed power of the rod increase. The steady-state electric field strength is similar for each case. Therefore, as the mullite rod is heated to sintering temperatures, the cavity efficiency will increase further and wall loss will become negligible.

It is also important to determine how well the measured data fits the simple theoretical model. The power absorbed by the rod is given by (Metaxas and Meredith, 1983)

$$P_{ROD} = \omega \epsilon_o \epsilon_{eff}'' E_{RMS}^2 V \quad (4.1)$$

where $\omega = 1.5256 * 10^{10} (\frac{cyc}{s})$, $V = 5.8237 * 10^{-7} m^3$ (for a 4.67 mm mullite rod), and $\epsilon_o = 8.85 * 10^{-12} \frac{F}{m}$.

For the calculations to be valid using the measured data, the RMS value of the electric field measured at the probe must be equal to the RMS value of the electric field at the rod. Also, the electric field is assumed to be constant over the length of the rod. The dielectric loss factor is assumed to be constant radially and axially along the rod.

At the frequency of 2428 MHz, the mullite rod is 4.6 mm from an electric field peak (see Table 3.1 and Figure 3.6). The probe is 6.9 mm from an electric field peak. Assuming the electromagnetic field pattern to be sinusoidal, the dielectric is located where the field is 99.3% of the electric field peak. The probe is measuring about 98.4% of the electric field peak. This small difference is about 180 V/m for a 20 kV/m signal. The measured electric field strength is therefore slightly less than the electric field strength at the rod. The measured electric field strength values are corrected for this slight error.

The electric field is not uniform across the length of the rod. It has been shown to decrease at the center of the rod where the dielectric loss factor of the rod is highest. The error of this assumption is highly dependent on the actual shape of the electric field and the variation in magnitude at the center of the rod.

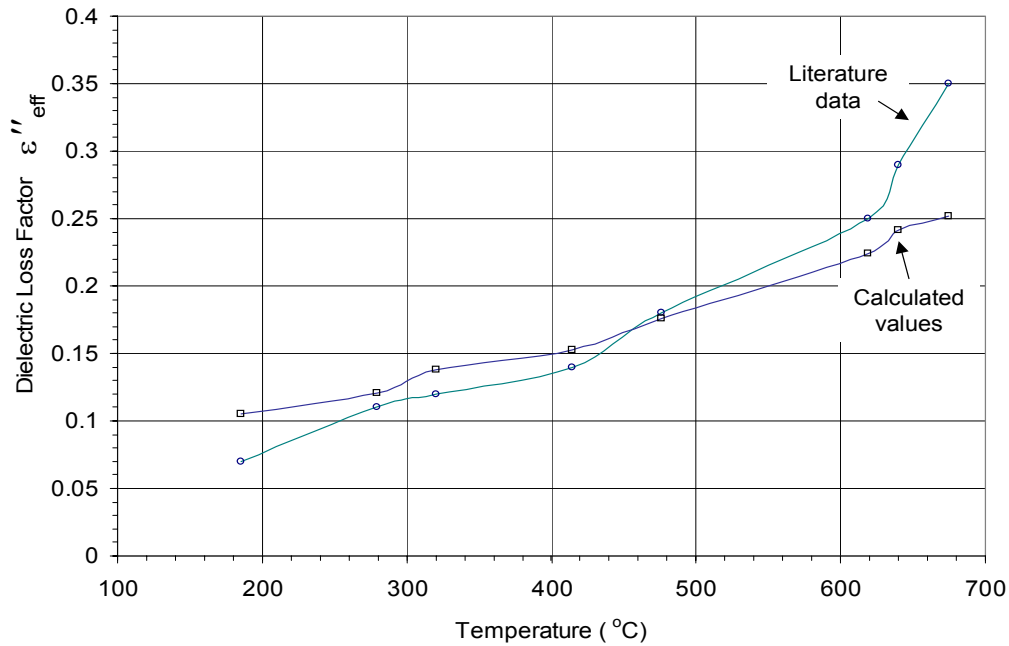


Figure 4.14: Comparison of dielectric loss factor values for 4.67 mm mullite rod (Literature data from Thomas et al. (1998))

For each measured steady-state electric field strength and absorbed power to

the rod, the dielectric loss factor can be computed using Equ. 4.1. The calculated values for the dielectric loss factor of mullite are shown in Figure 4.14. The graph also shows the literature data for the dielectric loss factor of mullite (Thomas et al., 1998). The results show there is good agreement between the calculated and measured dielectric loss factor data.

In the heating experiments, the dielectric loss factor of the rod is not constant because the temperature of the rod is not uniform radially or axially. It is assumed that the pyrometer measures temperature at the hottest part of the rod (center). The dielectric loss factor is largest here, and decreases towards the ends of the rod where it is cooler. Therefore, the calculated values for dielectric loss factor should be shifted to the left in Figure 4.14. For example, at a steady state temperature of 675°C measured by the pyrometer, the calculated dielectric loss factor is 0.36. Since 675°C is the highest temperature of the rod (assuming the pyrometer measures the hottest part of the rod), the average temperature of the entire rod is somewhat less. The ends of the rod can be estimated to be at 375°C (using Goodson's simulation), giving a mean rod temperature of 525°C. Therefore, the dielectric loss factor at a measured temperature of 675°C should be compared to the literature data at 525°C. The temperature shift makes the discrepancy larger at lower temperatures.

Given the power absorbed by the rod and the assumed dielectric loss factor data from the literature, the steady-state electric field strength can be calculated using Equ. 4.1. The calculated values are compared to the measured values in Figure 4.15. Both sets of data for the electric field strength are fairly constant as steady-state temperature increases.

Similarly, the absorbed power to the rod can be calculated using Equ 4.1 given the measured electric field strength and dielectric loss factor data from the literature. The calculated values are very similar to the measured values in Figure 4.16.

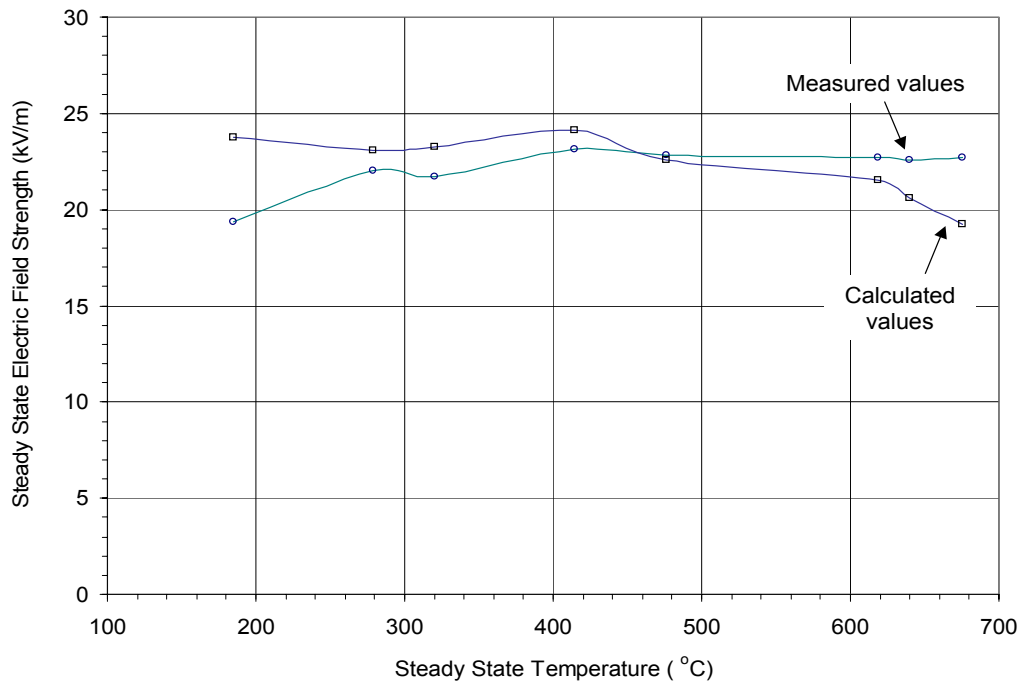


Figure 4.15: Comparison of steady state electric field strength for 4.67 mm mullite rod

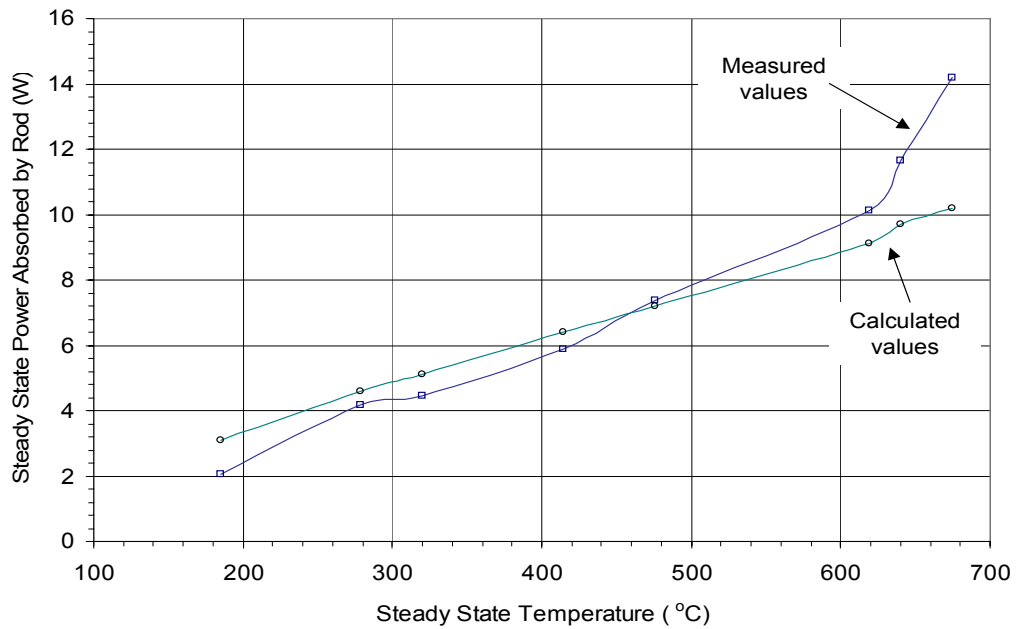


Figure 4.16: Comparison of steady-state absorbed power to 4.67 mm mullite rod

In interpreting the comparisons using Equ 4.1, (Figs 4.14 - 4.16), it is important to note the uncertainty of the measured power levels and the simplifications of the theoretical model. Given these issues, the agreement between calculated and measured values in Figures 4.14 - 4.16 is very encouraging.

The measured temperature ranges (bars on the temperature graphs which indicate the range of temperatures measured for all individual runs) for the mullite experiments are more indicative of the unsteadiness of the power measurement than of the pyrometer measurement. For the cases when the power absorbed by the rod is maintained constant, the noise in the power measurement makes it difficult to ensure this condition. The measured range for power absorbed by the 4.67 mm mullite rod averaged about ± 0.5 W. At lower powers absorbed by the rod, this fluctuation can cause large temperature changes. Consequently, the measured temperature range (i.e., variability) increases at lower absorbed powers. The measured temperature range for all mullite heating experiments averaged $\pm 8\%$ of the steady-state value. The range increases at lower temperatures to $\pm 10\%$. As the rod is heated to higher temperatures, the noise in the power measurement is less of a factor. Therefore, the experiments at higher temperatures had better repeatability.

For the case of a constant electric field, the temperature range was within 5°C of the steady state value of 260°C . This result implies that better repeatability was achieved when maintaining a constant electric field in the cavity than when maintaining a constant power absorbed by the rod.

The measured temperature and power ranges increase for the smaller 2.75 mm rod. This is because the slight power increases have more of an effect on the smaller rod. Therefore the repeatability for the smaller rod was substantially less than for the larger rod.

In conclusion, the more power absorbed by the rod, the less sensitive the rod is to small variations in power and the better the repeatability of the experiment. This result is encouraging for a future heating program to study the temperature of the rod at higher power levels.

4.6 Microwave Heating of Alumina

High purity alumina (99.8% Al_2O_3) is an ivory ceramic used in semiconductor and electronic applications. Alumina has excellent corrosion, wear, and thermal properties for use in harsh environments. The dielectric properties of alumina are shown in Figure 4.17. The dielectric loss factor increases substantially once the rod temperature exceeds about 700°C.

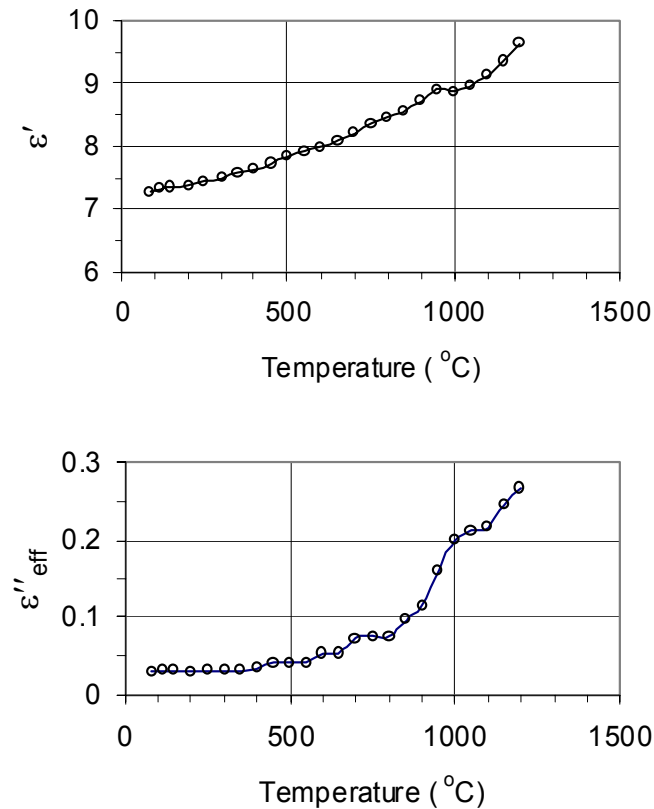


Figure 4.17: Dielectric properties of alumina (Cross, 1994)

The only successful strategy for the heating of alumina rods was maintaining a constant power absorbed by the rod. The alumina rods required very high field strengths to heat at ambient temperatures. Once the heating rate has been increased, the field strength must then be significantly reduced to avoid heating the rod to sintering temperatures.

The general trends for the heating of alumina were similar to mullite. However, there are some important differences. These include the high loss to the cavity walls

at low rod temperatures. For an equivalent power absorbed, the alumina rod heats to a lower steady-state temperature. The alumina rod was longer in length (200 mm for alumina vs. 95 mm for mullite). Since alumina is a much more conductive material than mullite, this can have a large effect. Figure 4.18 shows the heating of an alumina rod to a constant absorbed power of 10 W. Figure 4.19 shows the heating of an alumina rod to a constant absorbed power of 15 W. These data were combined to compare the steady-state electric field strengths and temperatures at both power levels (Figure 4.20).

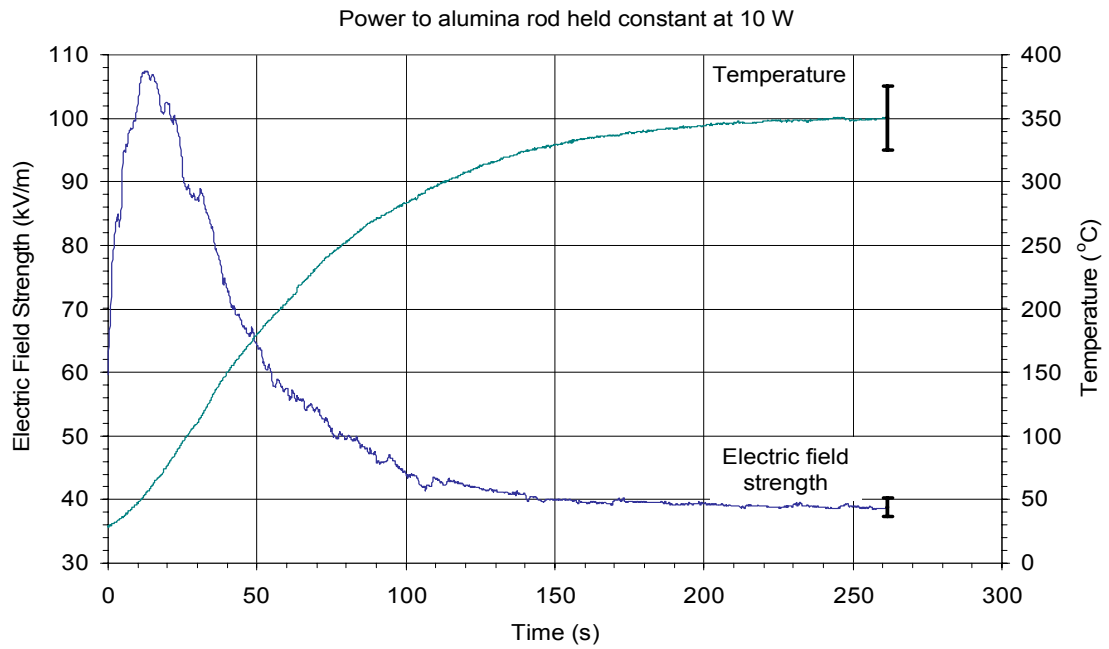
The measured range of the data was larger for alumina than for mullite. This is because of electric field strength fluctuations rather than noise in the power measurement data. At higher field strengths, there are larger fluctuations (see Figure 4.19 b). Since the power absorbed by the alumina rod is indirectly calculated using the electric field strength, larger fluctuations in electric field strength result in larger fluctuations in absorbed power. So it is difficult for the user to ensure that the power absorbed by the rod is maintained for the duration of the experiment. Most of this variation is averaged out, which can be seen in the stable steady-state power absorbed values in Figures 4.18 b and 4.19 b.

Using Eqn 4.1, the steady-state alumina data showed less agreement with the calculated values than the mullite data. The dielectric loss factor is calculated to be higher than the literature data (0.09 vs. 0.05 at 350°C and 0.11 vs. 0.06 at 590°C). Similarly, the power absorbed can be calculated (given measured electric field strength and literature data for the dielectric loss factor of alumina) and compared to the measured data. The measured power absorbed is higher than the calculated levels (10 W vs. 6 W at 350°C and 15 W vs. 8 W at 590°C). The data set is too small to make any significant conclusions.

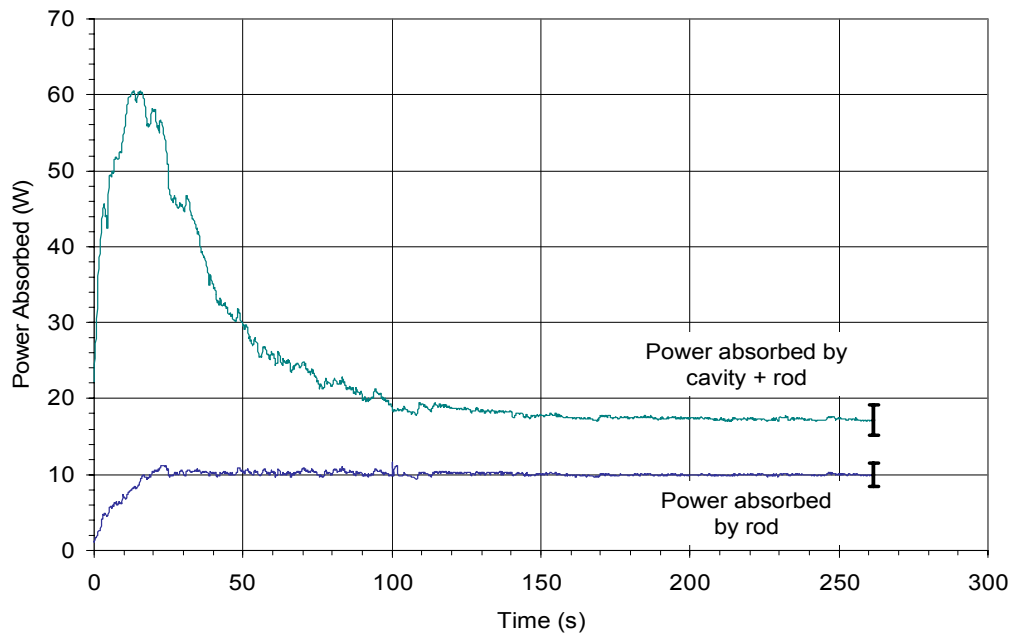
4.7 Heating Rate: Mullite vs. Alumina

The two aluminum oxide based ceramics were heated at a constant electric field strength of 50 kV/m as shown in Figure 4.21. The large difference in heating rates

(30 s for mullite to reach 600°C vs. 500 s) for alumina to reach 600°C can be attributed to the lower loss factor for alumina at low temperatures (compare Figures 4.2 and 4.17).

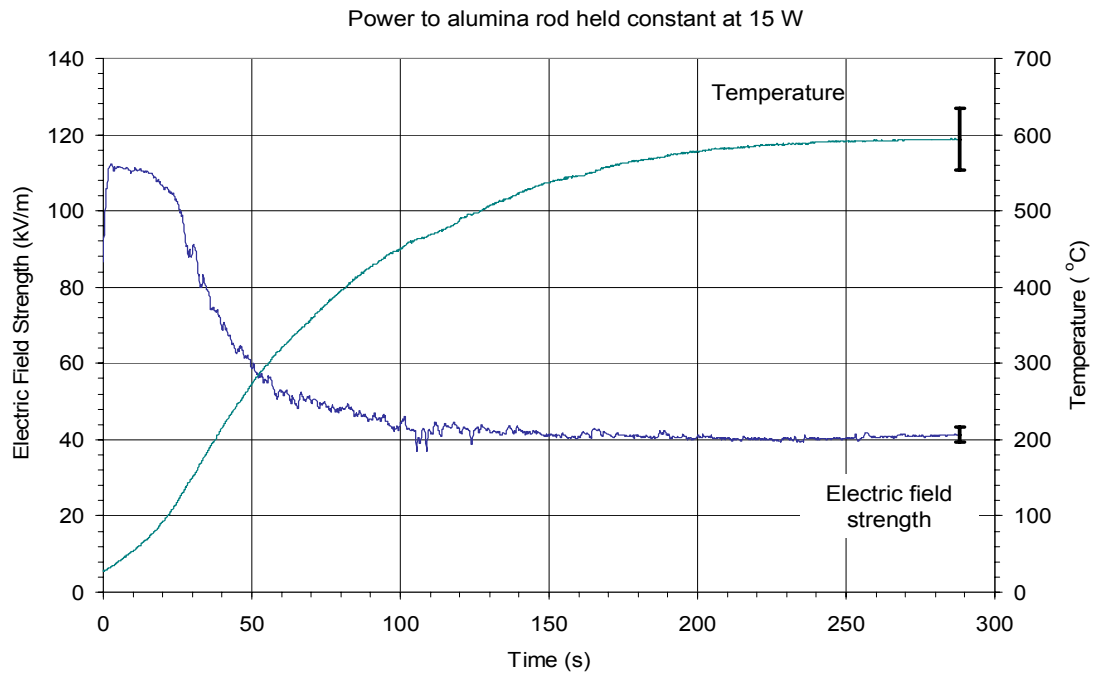


(a)

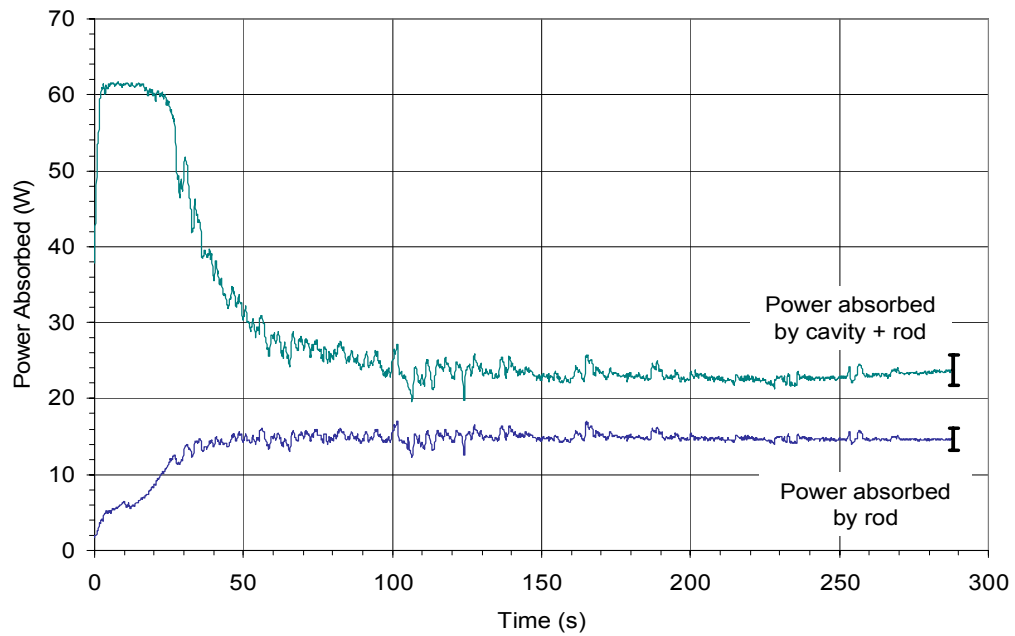


(b)

Figure 4.18: Heating of a 4.75 mm alumina rod to a steady-state temperature (a), where power absorbed by rod is increased to 10 W and held constant (b). (Average of 4 runs; bars indicate measured range)

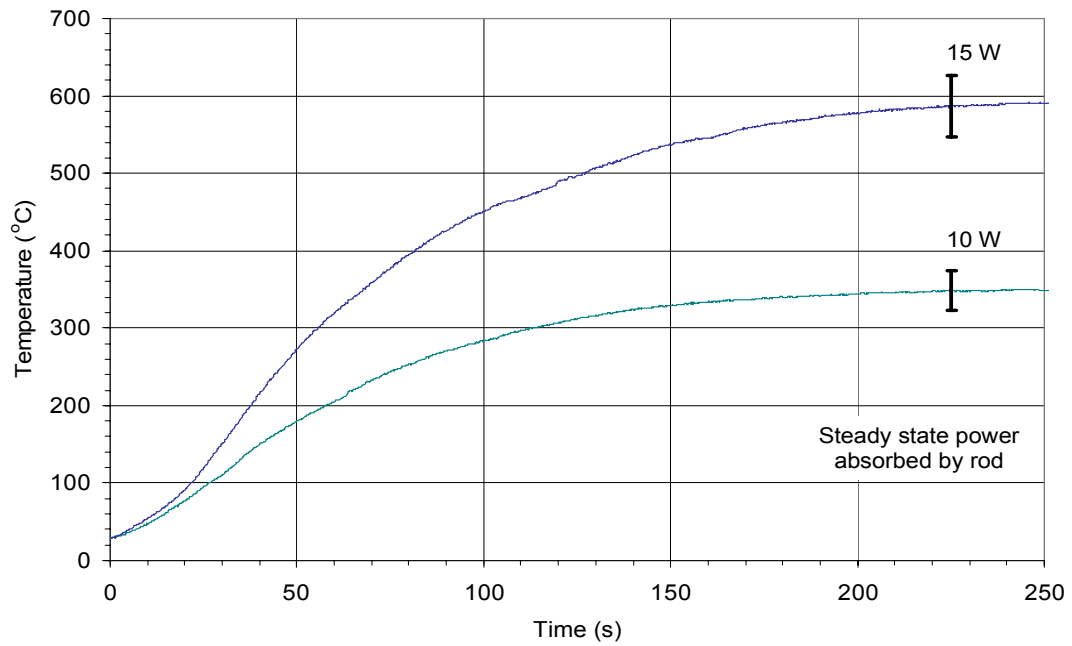


(a)

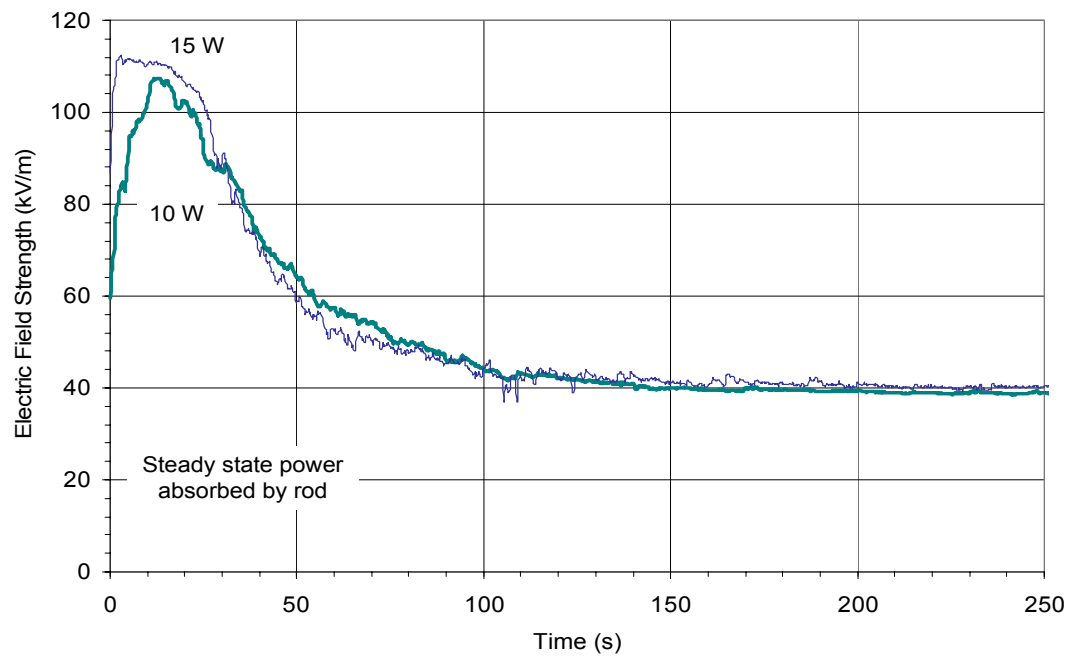


(b)

Figure 4.19: Heating of a 4.75 mm alumina rod to a steady-state temperature (a), where power absorbed by rod is increased to 15 W and held constant (b). (Average of 4 runs; bars indicate measured range)

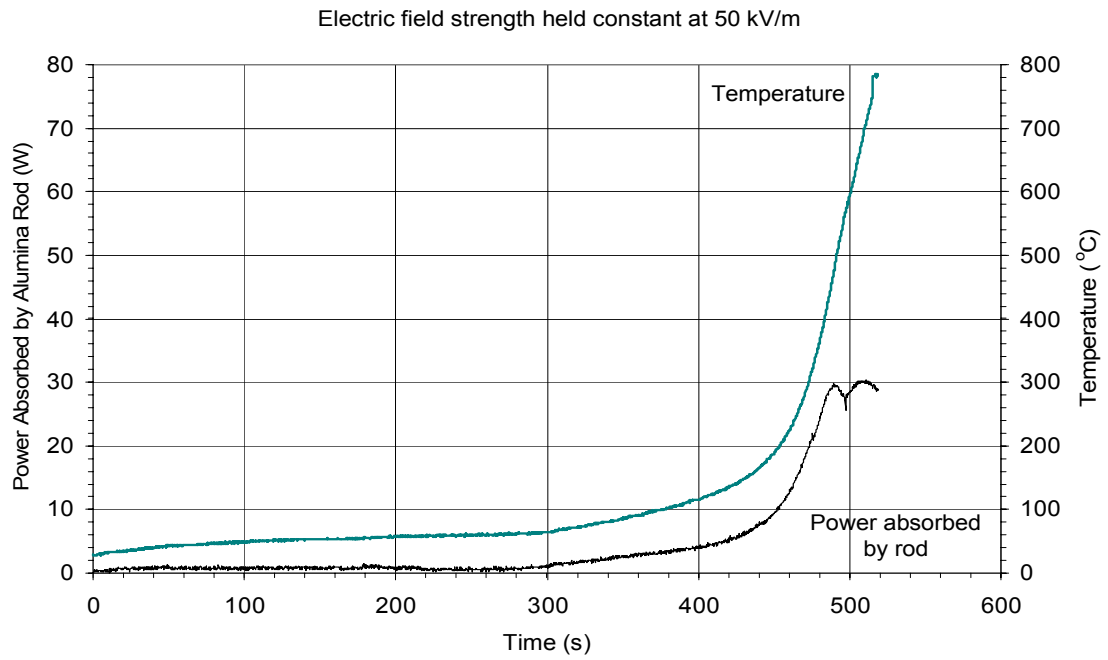


(a)

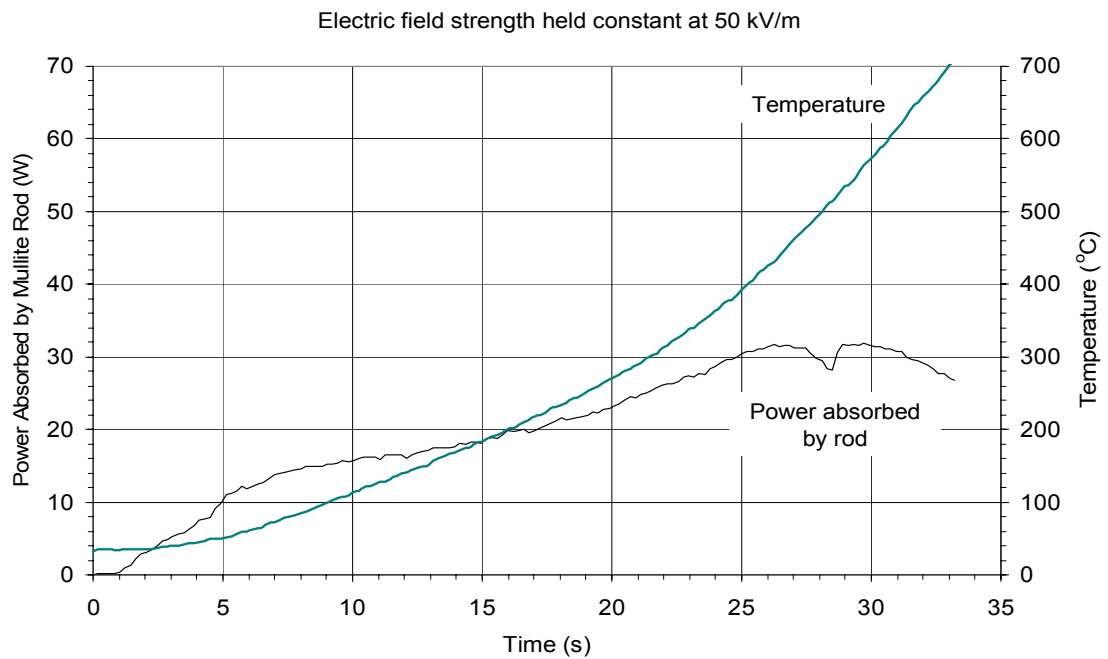


(b)

Figure 4.20: Comparison of temperature (a) and electric field strength (b) for the heating of a 4.75 mm alumina rod where power absorbed by the rod is held constant at indicated level. (Average of 4 runs; bars indicate measured range)



(a)



(b)

Figure 4.21: Heating of ceramic rods alumina (a) and mullite (b) for a constant electric field of 50 kV/m

4.8 Microwave Heating of Nylon 66 Fiber

Nylon 66 is a very strong polymer fiber, that offers toughness, thermal stability and non-corrosiveness. The 1680 denier Type 716 nylon 66 fiber used in this research was donated by Dupont. The fiber was much less than 1 mm in diameter. For all heating experiments, twenty fibers were wrapped together to form a continuous tow. This tow, when tightly wound, was ~ 3 mm in diameter. The melt temperature of nylon 66 is near 260°C . The dielectric properties of nylon 66 fiber are shown in Figure 4.22.

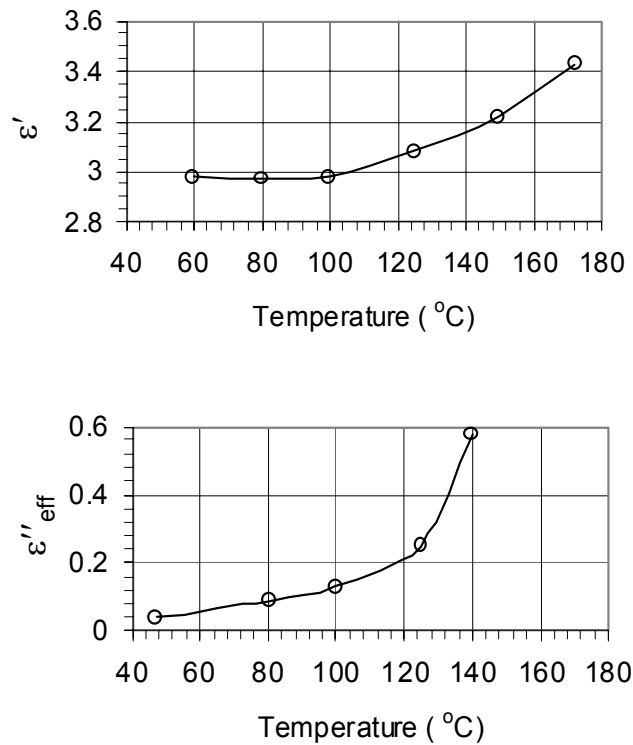


Figure 4.22: Dielectric properties of nylon 66 fiber (Huang, 1976)

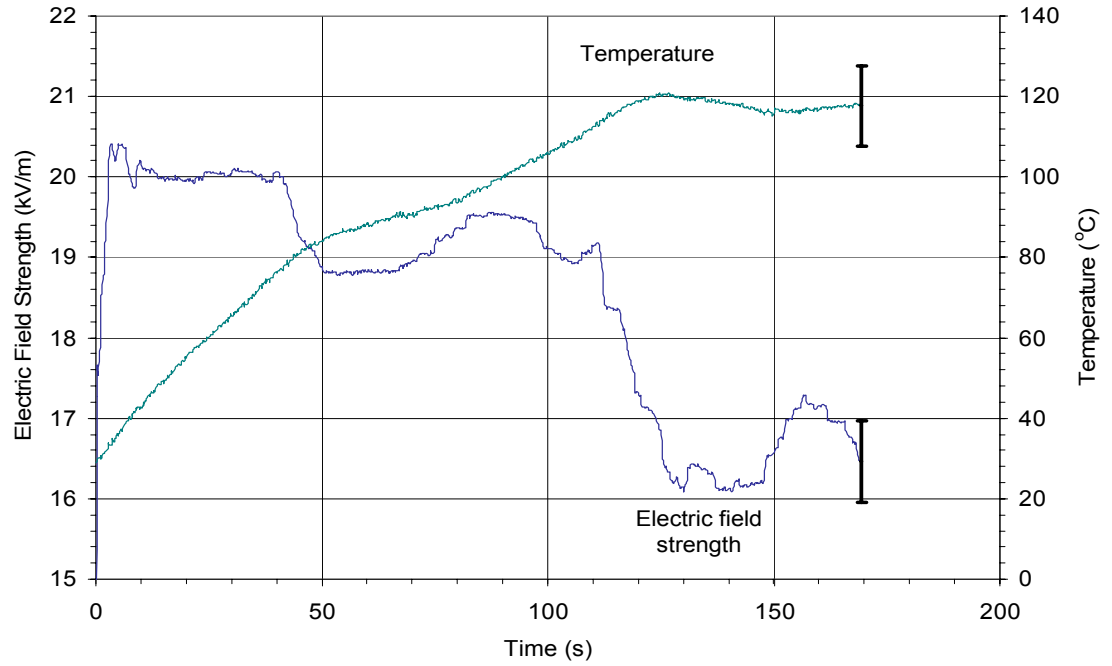
Because of the limited precision of the power measurement equipment, maintaining a constant absorbed power to the nylon tow was nearly impossible. This is because the tow absorbed less than 1 W. Precise control of the electric field to maintain a desired sample temperature was the most efficient way of avoiding thermal runaway. The goal for the heating of the nylon 66 tow was to achieve high steady-state temperatures. In Figure 4.23, the nylon 66 tow is heated to a steady-state temperature of 120°C . This temperature was maintained within 5°C . The electric

field strength was stepped down twice, once at 40 seconds and again at 110 s. The slight decline in temperature at 120 s coincides with the severe decrease in electric field strength. The electric field strength had to be increased at 147 s to raise the temperature back to the desired level. As can be seen in Figure 4.23 b, the power absorbed by the tow stays nearly constant throughout the duration of the run at about 0.4 W.

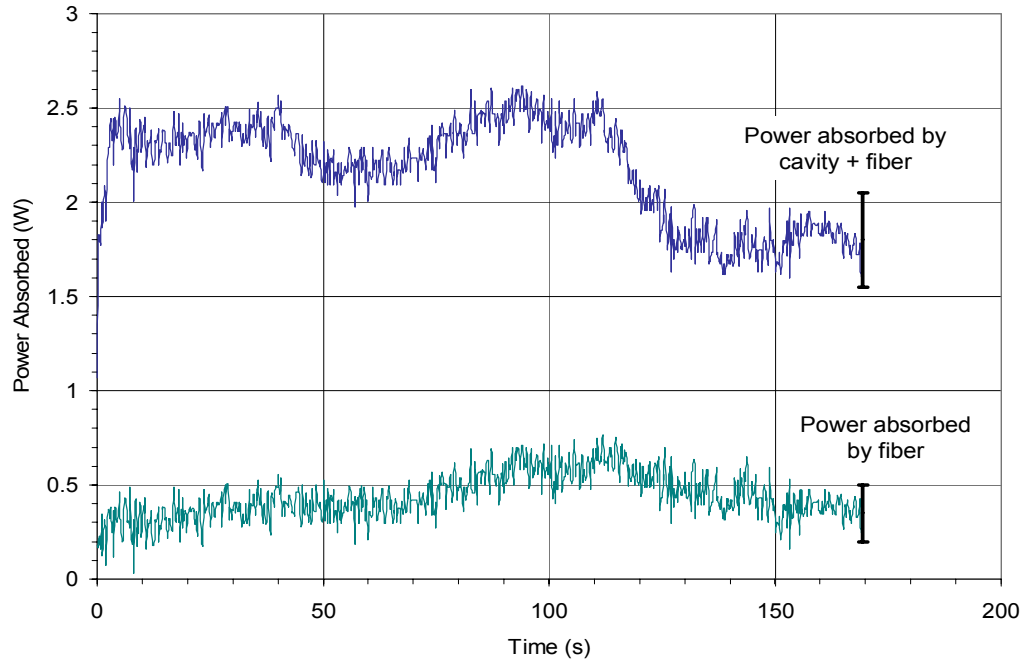
The goal for the second nylon heating schedule in Figure 4.24 was to maintain a steady-state temperature of 160°C. This again required a stepped approach to setting the electric field strength. The electric field strength was decreased from 25 kV/m to 20 kV/m when the tow reached a temperature of 80°C. It was then slowly stepped down as the tow temperature increased to 160°C. The average power to the tow was again fairly constant, this time at about 0.5 W. Power loss to the cavity walls was still significant at steady-state. The temperature and electric field histories for the two heating schedules are compared in Figure 4.25. It should be noted that for the heating of nylon, the electric field measurement error is greater because at the lower frequency, the nylon tow is 15 mm from the electric field peak (see Table 3.1). Once again assuming the electric field pattern is a sinusoidal wave, the tow is at a location where the electric field strength is 94% of its peak. The probe is 10 mm from an electric field peak (97%). Therefore, the probe is measuring an electric field strength 5% larger than the field strength at the tow.

The last objective for the heating of the nylon 66 tow in Figure 4.26 was to step the temperature at 10°C intervals to the highest possible setting without melting. The sequence of electric field spikes can be seen in Figure 4.26 a. These spikes were manually controlled to heat the tow to successively higher steady-state temperatures. The power absorbed by the tow is controlled to under 1 W for the entire duration of the experiment (Figure 4.26 b). As the tow heats to near melt temperatures, lower electric field strengths are needed to maintain steady-state. The spikes seen in Figure 4.26 b coincide with the increase in electric field strength. Wall losses decrease as the tow approaches melt temperatures. It is clear from the data that thermal runaway was controlled for the heating of nylon 66 tow by precisely controlling the electric

field strength in the cavity, which effectively limited the power absorbed by the fiber tow.

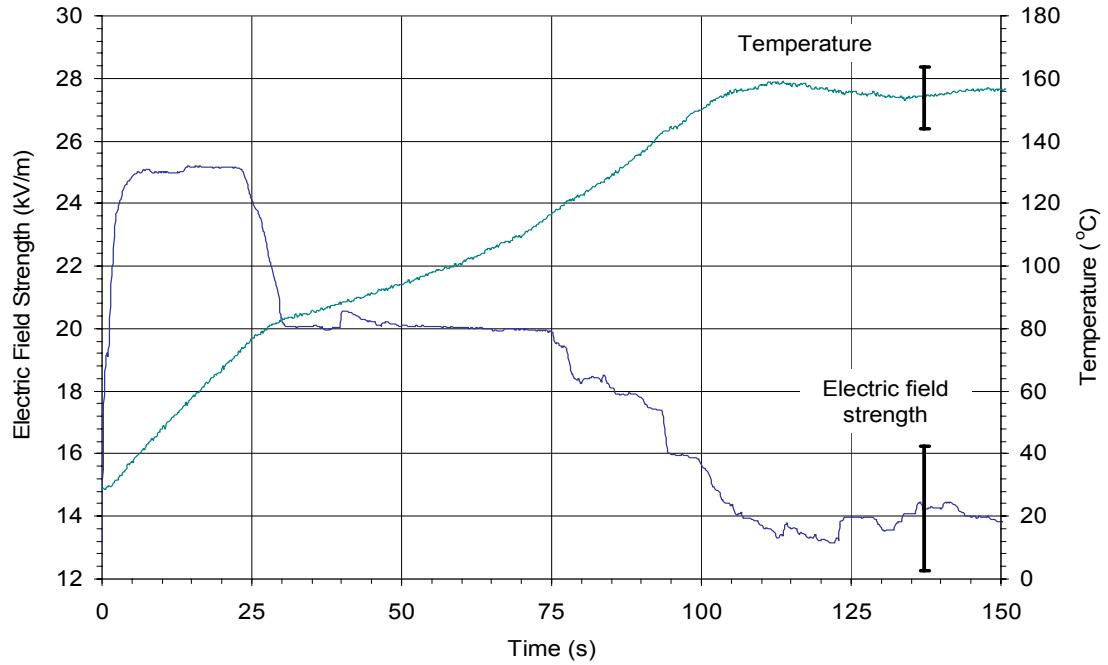


(a)

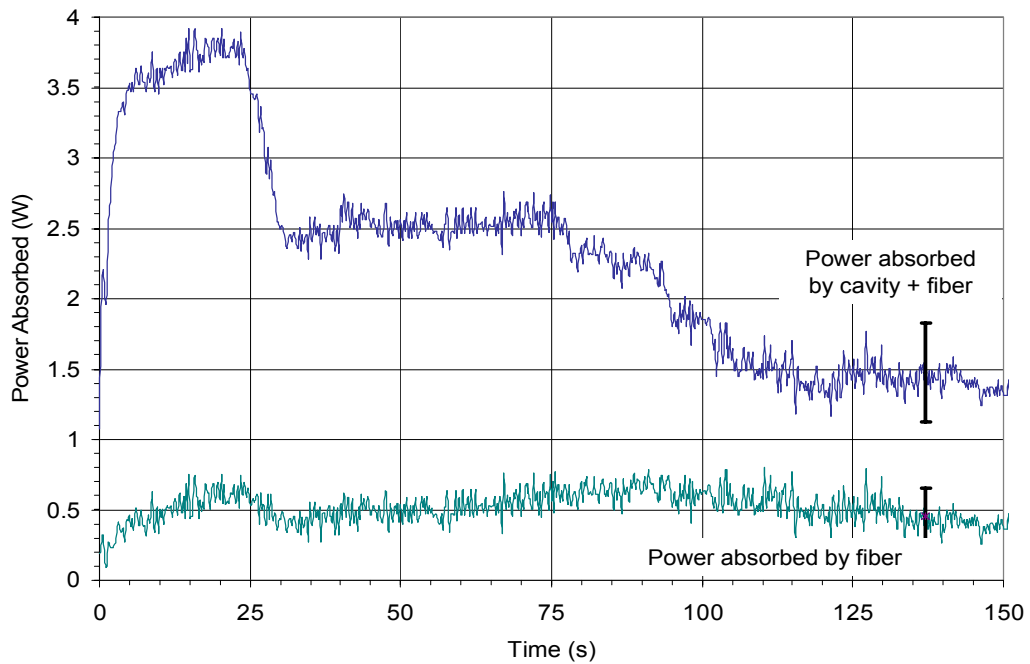


(b)

Figure 4.23: Comparison of electric field (a) and power (b) for the heating of a 3 mm nylon 66 tow to a steady-state temperature of 120°C. (Average of 4 runs; bars indicate measured range)

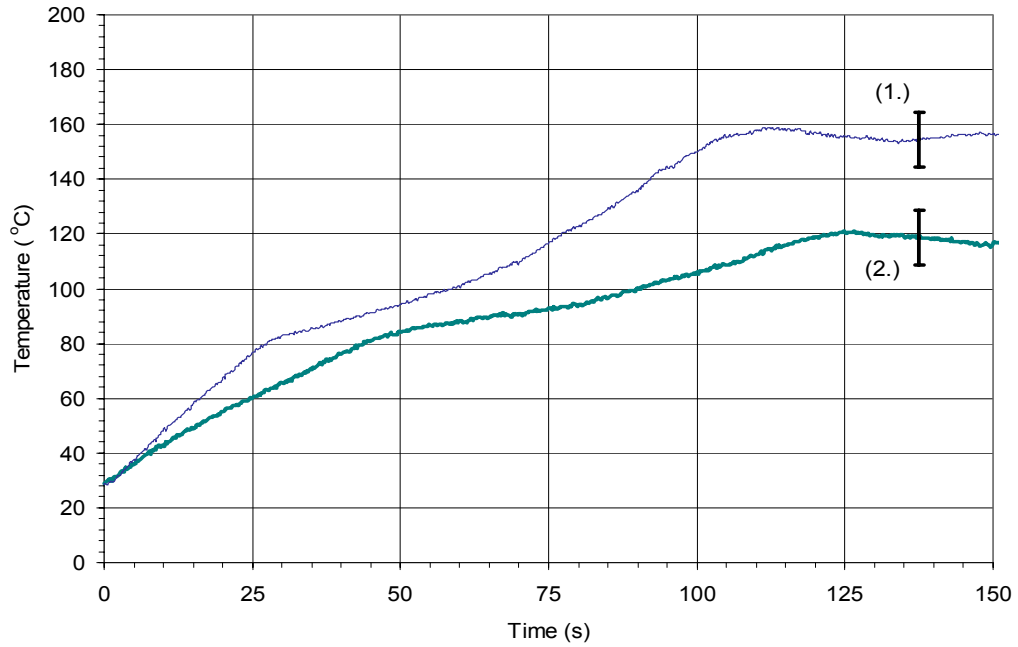


(a)

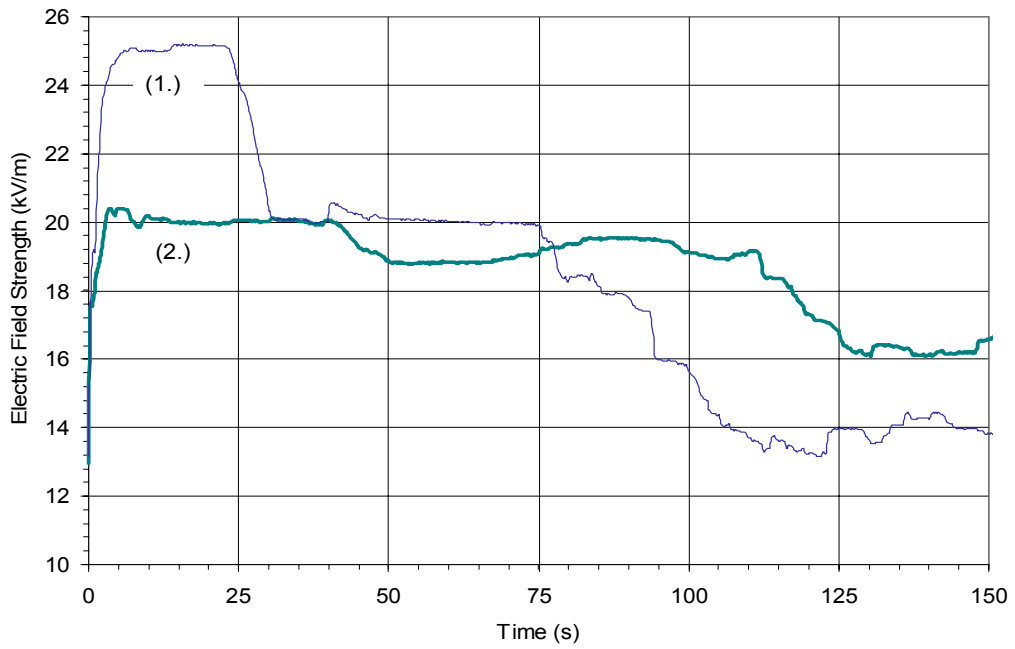


(b)

Figure 4.24: Comparison of electric field (a) and power (b) for the heating of a 3 mm nylon 66 tow to a steady-state temperature of 160°C. (Average of 4 runs; bars indicate measured range)

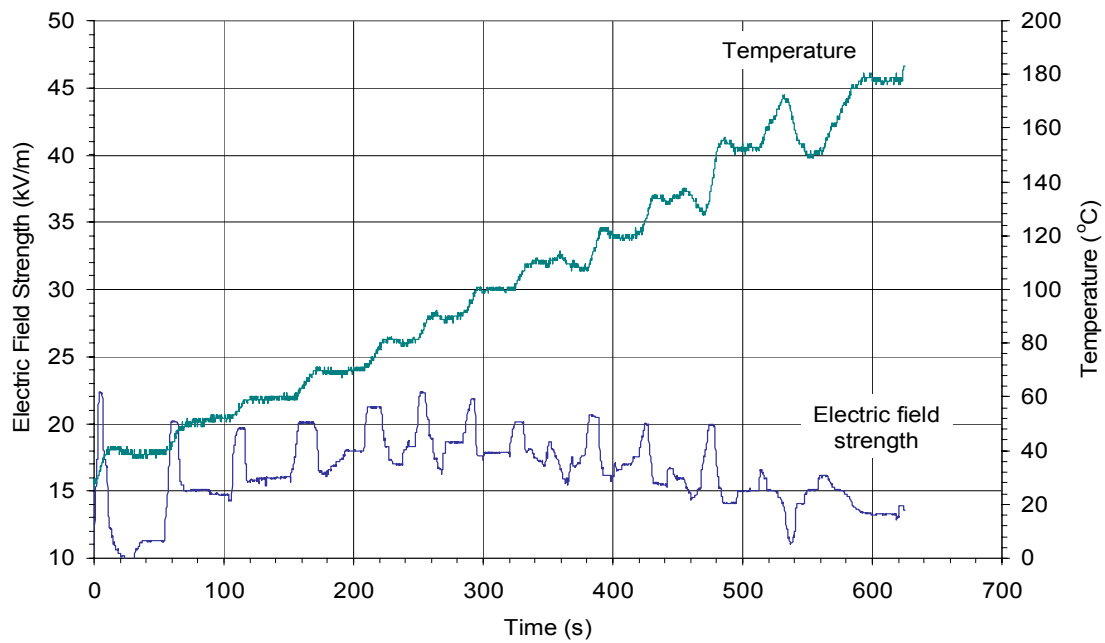


(a)

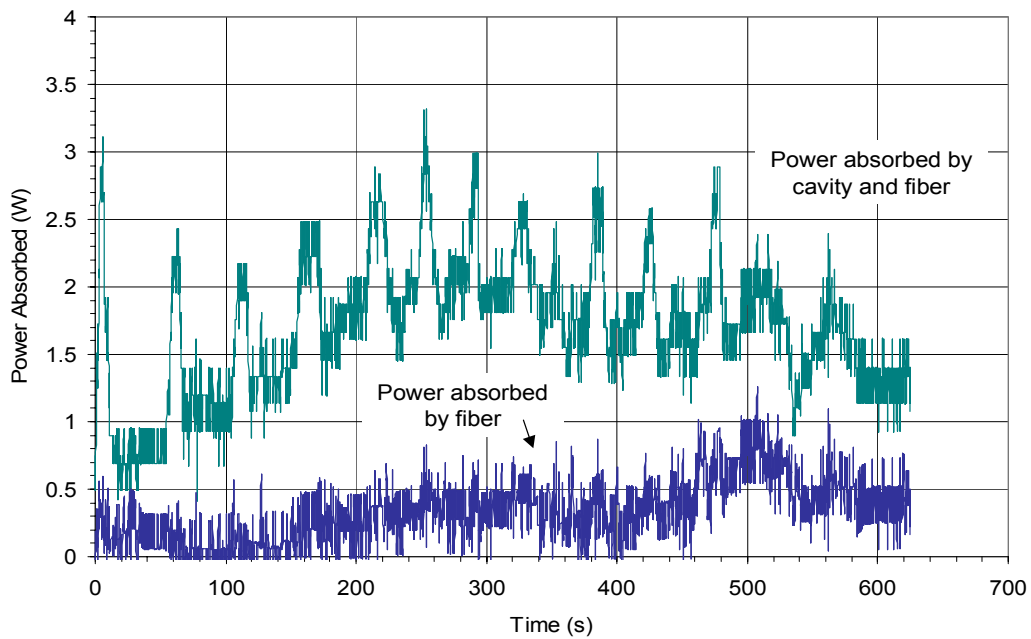


(b)

Figure 4.25: Comparison of temperature (a) and electric field (b) for the heating of a 3 mm nylon 66 tow to steady-state. For run 1, the power absorbed by the tow ~ 0.5 W; for run 2, the power absorbed by the tow is ~ 0.4 W.



(a)



(b)

Figure 4.26: Comparison of temperature (a) and absorbed power (b) for the stepped heating of a 3 mm nylon 66 tow

4.9 Sources of Error

Some of the possible sources of error in the three measured parameters will now be discussed. Most experiments were run four times and averaged. The measured range is indicated by the bars on each plot. The measured range gives an indication of the repeatability of these experiments. The errors discussed next give insight into the temperature, power, and electric field strength variations that were observed in each experiment.

4.9.1 Temperature Measurement

To get an accurate temperature measurement using the pyrometer, there are several constraints that must be met. First, the field of view must be smaller than the sample size, i.e., the target material needs to cover the entire field of view. All of the samples measured in this study were larger than the field of view, which is 2 mm at a distance of 100 mm. To ensure that the object covers the field of view, a large beaker of ice (to provide a cold background) can be placed directly behind the sample. The sample covers the entire field of view once the beaker can be removed with no fluctuation in sample temperature. A pointing device was used to ensure that the pyrometer was focused on the center of the sample. Separate microwave heating experiments were run to steady-state to ensure that the highest sample temperature was measured. Once the pyrometer and the sample were in place, the set of experiments was conducted.

These minor adjustments in pyrometer position could not ensure that the pyrometer was always focused on the hottest spot of the sample. In some cases, the sample temperature varies axially (Goodson, 1997). This variation occurs more frequently for moving samples. Since all heating experiments for this research were conducted on stationary rods, this error is slight.

Since the temperature measurements depend on the emissivity of the surface of the object, inaccurate emissivity data or an inaccurate model of the pyrometer (see Appendix C) could cause an error in the measured temperature. A simple heating procedure was used to calibrate the pyrometer for each material. First, the pyrometer

emissivity is set to a value at a chosen temperature for a given material. For example, the emissivity of mullite at 400°C is 0.76 (Bauer and Steinhardt, 1990). The pyrometer emissivity is set to 0.76 and the rod is heated to 400°C. While maintaining the steady-state temperature at 400°C, the emissivity setting on the pyrometer is manually increased to 1.00 (the emissivity setting at which all the heating experiments were run). The temperature measured by the pyrometer will decrease to some new level. This measurement is then compared to the predicted value from the calibration (see Figure C.3 for the calibration of mullite). The model was accurate up to 500°C, the maximum range of the pyrometer.

4.9.2 Power Measurement

Measurement uncertainties are introduced in each component of the power measurement system, including the dual directional couplers, the power meters and sensors, and the analog to digital conversion of the output signal. Precise knowledge of the coupling value is important in converting the measured power in mW to the actual power in W. A correction procedure was needed because there was some question as to the accuracy of the Cober's factory specifications. The correction procedure for accurately measuring these values is described in Appendix A. In summary, the log of the difference between the attenuation at the forward port and the attenuation at the reflected port is determined. This is done by measuring power at the forward port in the correct forward position. The coupler is then placed in the reverse direction so that the forward power is measured at the reflected port. Assuming the same incident power during the experiments, the measured log difference between the forward and reflected ports is measured. This value was 1.05 db, 0.35 dB higher than the factory specification of 0.7 dB (60.3 dB - 59.6 dB).

Since the couplers are not ideal, some of the reflected power is measured at the forward port and vice-versa. By measuring power into the short as the short is adjusted, the sensitivity of the couplers can be determined. An ideal coupler would measure the exact same signal at all short positions because the power absorbed by the short does not change. The coupling to each port on the directional coupler varies

sinusoidally as the short is adjusted. This fluctuation in power has been measured to be less than 2% of overall power. Also, since slight adjustments in the length of the short are needed to tune the cavity, the error caused by this effect is minimal.

The dual directional couplers are also frequency dependent, meaning the coupling values (amount of attenuation) fluctuates with frequency. This can be seen once again in Figure A.2. The coupling value decreases as the power of the source increases (increasing frequency). The dual directional coupler was calibrated to the source at the expected frequencies used in the heating experiments to ensure that the correct coupling values were used.

The power meters and sensors are rated to $\pm 1\%$ accuracy. For more information on accuracy specifications of the meters and sensors, see (HP Power Meter Manual, 1991) Chapter 1, for more information.

The error in calibration was checked by detuning the cavity and measuring the forward and reflected power. The difference in power should equal zero for an ideal short (the iris acts as a wall when the cavity is untuned). The power absorbed by the iris is not negligible at source powers greater than 200 W (highest power incident on the cavity for this experimental program was 135 W).

The largest source of noise in the power measurement comes from the data acquisition system itself. There is a disturbance between the data acquisition system and the power meters which causes a low frequency signal to propagate through the data. This can be seen in Figures 4.11 a and D.4. The magnitude of the noise is $\pm 1\%$ of the scale of the power meter. Therefore, at larger scales, the magnitude of the noise increases. This is most evident at steady-state, when the power measured fluctuates while the temperature is constant.

4.9.3 Electric Field Strength

The measurement of the electric field strength is founded on the calibration technique described in Appendix B. The procedure combines the equations in section 2.5 with power measurements at the coupler and the probe. The average range of electric field strength has been measured to be within 6% of the steady-state value. Fluctuations

in the electric field strength in the cavity can be attributed to noise in the power meter - data acquisition interface, as well as oscillations that occur due to slight changes in the resonant frequency of the cavity.

Chapter 5

Conclusions

An experimental apparatus for the precise control of thermal runaway materials in a microwave system has been developed. The system was properly configured to obtain an accurate measurement of power into the cavity. This was done by placing the directional coupler at the entrance of the cavity to ensure that losses outside of the cavity were not included. The configuration was further improved by estimating cavity losses in to the walls, iris, and short. This was done by characterizing the cavity without a load and measuring the electric field strength and power into the cavity. Once the wall losses were determined this way, the additional power absorbed by a loaded cavity was attributed to power absorbed by the dielectric.

Several data sets were obtained for three thermal runaway materials (mullite, alumina, and nylon 66). These data will be used to validate future combined heat transfer / electromagnetic field computer models.

Precise control of the electric field in the cavity resulted in precise control of the temperature of the dielectric. Thermal runaway can be avoided by varying the electric field strength to control the power absorbed by the dielectric.

It was found that for the low power heating of 4.67 mm mullite rods, the loss to the cavity walls decreased significantly at steady-state heating. At higher steady-state temperatures (resulting in lower steady-state electric field strengths), the loss to the walls becomes negligible. For smaller diameter rods, the loss to the cavity walls was greater.

Loss to the cavity walls is most significant in the heating of alumina rods. This loss is expected to decrease at sintering temperatures.

Power to the nylon 66 fiber was indirectly controlled by precise control of the electric field strength in the cavity. Temperatures close to melting were reached and thermal runaway was avoided.

The experimental setup and resulting data provide the groundwork for further development of new heating strategies and applicator designs.

5.1 Recommendations

5.1.1 Temperature Measurement System

This experimental program was limited by the temperature range of the pyrometer when heating ceramics. To measure sintering temperatures, another pyrometer should be employed. An Heitronics KTX.D measures temperature from 500 to 2000°C at a spectral range of 2 - 2.7 μm . An L9 lens can provide a target diameter of 4 mm at a distance of 100 mm.

5.1.2 Power Measurement

To increase power measurement speed and accuracy, the power measurement system should be upgraded. A dual channel power meter (HP E4419A) will bring outstanding benefits including fast, accurate and repeatable readings. Compatible with the current power sensors, the system can be used in the digital or analog mode. There are no scale changes which mean the resolution of the meter does not decrease when measuring higher powers. Also, there are no switching delays between scales.

5.1.3 Data Acquisition System

The data acquisition system needs to be overhauled. LabView 5.0 should be incorporated into a new PC to allow the user to create sophisticated data acquisition

programs with little to no prior programming knowledge. The data acquisition system would also be able to take advantage of the RS-232 ports available from the pyrometers. The RS-232 port would provide better resolution of the measured parameters. Using LabView 5.0, the data can be graphed in real time resulting in a more visually friendly interface to work with during heating experiments.

5.1.4 Tuning Devices

Microwave heating will be limited to lab scale work until the microwave energy can be more efficiently coupled to the load. This can be done for this experimental setup by use of a four stub tuner, a tuning shoe, and / or a different aperture. The aperture in use for these experiments was made to couple the applicator to the source at a frequency of 2.93 GHz. An aperture should be designed for coupling at 2.44 GHz.

A four stub tuner or tuning shoe could be incorporated into the setup. This increases losses in the walls before the iris and the stubs themselves. If a tuning shoe is used, there can be significant attenuation of the electromagnetic field by the shoe. However, these tuning devices can increase the efficiency of the system. To accurately measure power to the cavity, the power loss due to these devices must be estimated (despite increased losses to the stubs and walls, more power is concentrated into the cavity itself).

5.1.5 Additional Equipment

A calorimetric load could be added to more accurately calibrate the equipment (such as directional couplers and power meters). Also, a stepping motor should be added to the system for accurate low speed sample throughput to investigate thermal runaway effects on continuous processing.

Bibliography

Bauer, W. and Steinhardt, R., 1990, "Emissivity of Refractories," *Gas Wärme International*, Vol. 39, pp. 388–391.

Bertaud, A. and Badot, J., 1976, "High Temperature Microwave Heating in Refractory Materials," *Journal of Microwave Power*, Vol. 11, No. 4, pp. 315–320.

Chen, M., Sicohi, E., Ward, T., and McGrath, J., 1993, "Basic Ideas of Microwave Processing of Polymers," *Polymer Engineering and Science*, Vol. 33, No. 17, pp. 1092–1109.

Colomban, P. and Badot, J., 1979, "Microwave Heating: Method for Ceramics by 1990," *L'Industrie Ceramique*, Vol. 729, pp. 101–107.

Cross, T., 1994, *Private Communication*.

Duchez, W., 1996, "Role of Electric Field Profiles in Continuous Microwave Processing of Thermal Runaway Materials," M.S. Thesis, Virginia Polytechnic Institute and State University.

Goodson, C., 1997, "Simulation of Microwave Heating of Mullite Rods," M.S. Thesis, Virginia Polytechnic Institute and State University.

Holme, I. and Metaxas, A., 1979, "Microwave Drying of Nylon Tufted Carpets," *Journal of Microwave Power*, Vol. 14, No. 4, pp. 367–382.

HP Power Meter Manual, 1991, *HP 435B Power Meter Operating and Service Manual*, Hewlett-Packard Company.

- Huang, H., 1969, "A Microwave Apparatus for Rapid Heating of Threadlines," *Journal of Microwave Power*, Vol. 4, No. 4, pp. 288–293.
- Huang, H., 1976, "Microwave Heating of Nylon Monofilament," *Journal of Microwave Power*, Vol. 11, No. 4, pp. 296–313.
- Incropera, F. and DeWitt, D., 1996, *Fundamentals of Heat and Mass transfer*, John Wiley and Sons.
- Iskander, M., J.O. Kiggans, J., and Bolomey, J., eds., 1996, *Microwave Processing of Materials V*, Vol. 430, Matls. Res. Soc. Proc.
- Krieger, B., 1992, "Vulcanization of Rubber, A Resounding Success for Microwave Processing," *Proceedings of the American Chemical Society, Div. of Polymeric Materials: Science and Engineering.*, Vol. 66, pp. 339–340.
- Kumar, A., 1982, "Microwave Drying of Polyester Fiber," *INT. Journal of Electronics*, Vol. 52, No. 5, pp. 491–495.
- Lewis, R., 1971, "Method and Apparatus for Regulating Heating in a Microwave Resonant Cavity," *US Patent 3,557,334*.
- Metaxas, A. and Meredith, R., 1983, *Industrial Microwave Heating*, Peter Peregrinus Ltd.
- Roussy, G. and Pearce, J., 1995, *Foundations and Industrial Applications of Microwaves and Radio Frequency Fields*, John Wiley and Sons.
- Stein, D., 1994, *Microwave Processing of Materials*, National Academy Press.
- Terril, N. D., 1998, "Field Simulation for the Microwave Heating of Thin Ceramic Fibers," M.S. Thesis, Virginia Polytechnic Institute and State University.
- Thomas, J. R., Goodson, C. C., Stern, C. H., Jackson, M., and Vogt, G. J., 1998, "Microwave Sintering of Ceramic Rods: Experiments and Models," *Journal of Microwave Power and Electromagnetic Energy*, Vol. 33, No. 2, pp. 113–120.

Touloukian, Y., 1972, "Thermal Radiative Properties for Non Metallic Solids," *Thermal Physical Properties*, Vol. 8, pp. 142.

Vogt, G., Regan, A., Rohlev, A., and Curtin, M., 1995, "Microwave Process Control Through a Traveling Wave Tube Source," in: *Use of a Variable Frequency Source With a Single-Mode Cavity to Process Ceramic Filaments*, pp. F3.1–F3.4.

Vogt, G., Regan, A., Rohlev, A., and Curtin, M., 1996, "Microwave Process Control Through a Traveling Wave Tube Source," in: *Microwave Processing of Materials V*, eds. M. Iskander, J. J.O. Kiggans, and J. Bolomey, Vol. 430, pp. 513–518.

Vogt, G. and Unruh, W., 1993, "Microwave Hybrid Heating of Alumina Filaments," in: *Microwave: Theory and Application in Materials Processing II*, eds. D. Clark, W. Tinga, and J. J.R. Laia, Vol. 36, pp. 297–306.

Vogt, G., Unruh, W., and Plovnick, R., 1994, "Growth and Stabilization of Hot Spots in Microwave Heated Ceramic Fibers," in: *Microwave Processing of Materials IV*, eds. M. Iskander, R. Lauf, and W. Sutton, Vol. 347, pp. 473–478.

Appendix A

Calibration of Coupler

This section outlines the procedure to determine the corrected coupling values for the dual directional coupler. The calibration setup is pictured in Figure A.1.

The absorbing load is used to absorb the forward power, such that no power is reflected back through the system. There are two dual directional couplers in the setup. The first coupler, Coup 1, is used as a control coupler and will be used solely to measure the forward power. The second coupler, Coup 2, is the coupler that will be calibrated. Coup 2 will be placed in the correct forward position between the steel load and Coup 1. The power is measured at the forward port on Coup 1 and on the forward port on Coup 2. Several data sets are taken. The generator is then turned off, and Coup 2 is placed in the reverse direction between the absorbing load and Coup 1. The power is measured at the forward port on Coup 1 and on the reflected port on Coup 2 (the power measured at the reflected port is actually the forward power because the coupler is in the reverse direction). Several data sets are taken for the expected power range that will be used in the microwave heating program.

Measuring forward power by Coup 1 ensures that the powers measured by Coup 2 for both setups are compared at the same source power levels. The log difference between the attenuation at the forward port and at the reflected port is plotted as a function of source power (see Figure A.2).

The average log difference value (1.05 dB) is the coupling difference between the two ports on Coup 2 (the reflected and forward port). The specified rating for

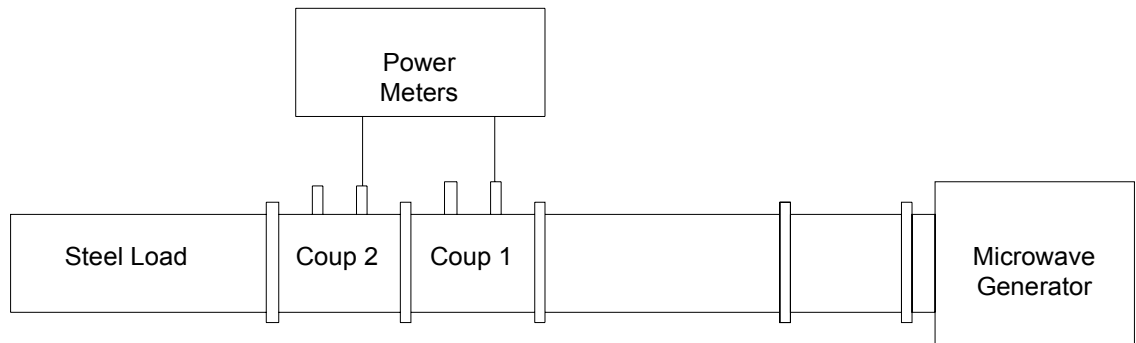


Figure A.1: Setup for calibration of coupler

Coup 2 is 60.3 dB attenuation at the forward port, and 59.6 dB attenuation at the reflected port. Therefore, the specified log difference value is $(60.3 \text{ dB} - 59.6 \text{ dB} = 0.7 \text{ dB})$. The measured log difference value, 1.05 dB, is 0.35 dB higher than the specified value. Figure A.3 shows the error that can result if the specified attenuation value had been used instead of the corrected value. This was an important step in ensuring accuracy of the power measurement system.

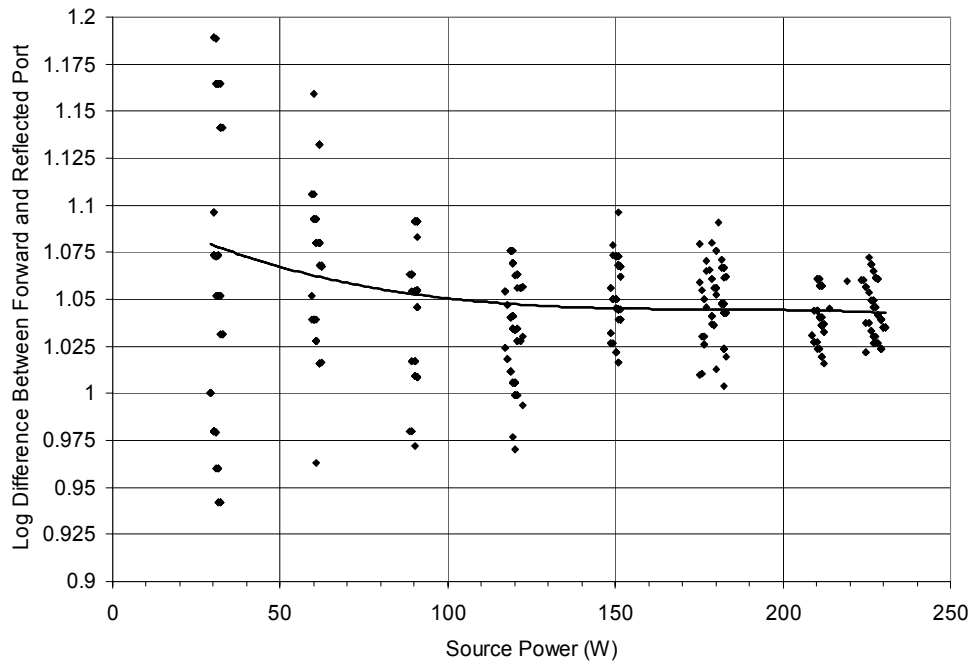
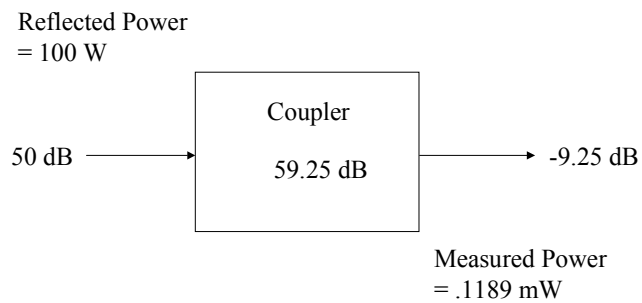


Figure A.2: Characterization of coupler



Convert Measured Power to Actual Power:
 $.1189 \text{ mW} * 10^{(59.6/10)} = 108.4 \text{ W}$
 Error = 8.4 W

Figure A.3: Measurement error for an uncorrected coupler

Appendix B

Calibration of the Cavity Probe

In order to calibrate the cavity probe, the equipment is configured as in Figure B.1. In this setup, there is no iris between the coupler and the cavity. During the calibration,

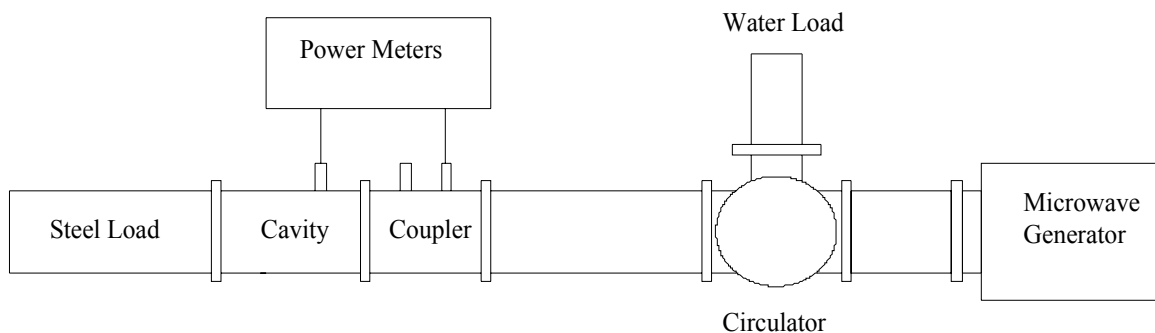


Figure B.1: Equipment setup for electric field calibration

the microwave power is increased over a large range. As this is done, the power is measured at the forward port on the coupler and at the cavity probe. It should be noted that the probe on the cavity is measuring electric field strength (kV/m), but the power meter is converting this signal to watts (Equ. 2.7 applies, with a coupling constant). Figure B.2 is a plot of the power measured at the probe on the cavity against the total power as measured at the forward port on the coupler.

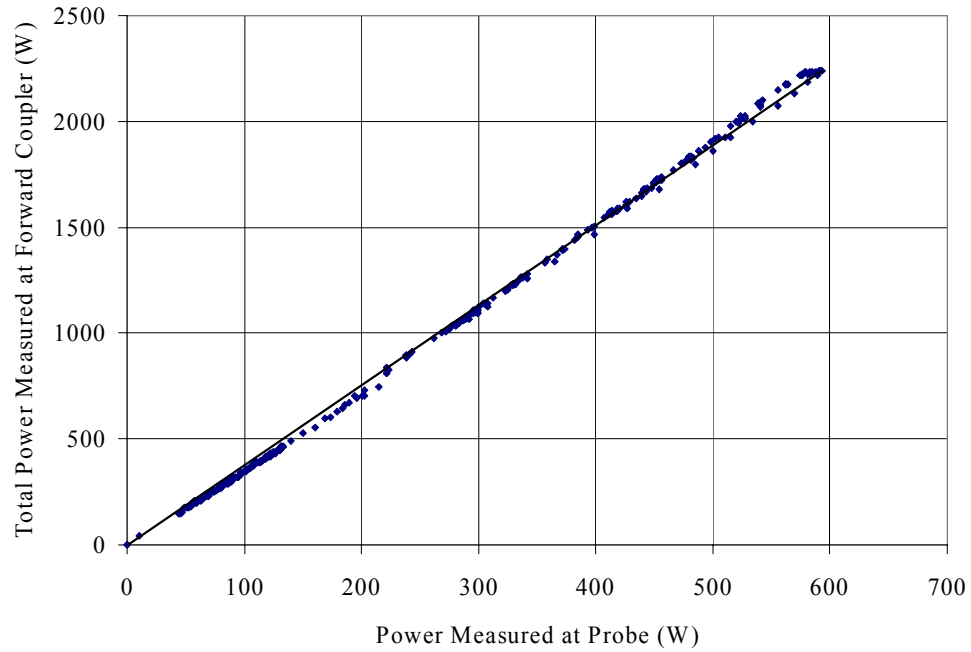


Figure B.2: Coupler / Probe relationship

The absorbing load at the end of the system absorbs all of the forward power, so there is no reflected power back through the system. Therefore, the total power in the cavity consists only of forward power. Given the total power in the waveguide, the waveguide dimensions, and the frequency of the source, the electric field can be calculated (see Section 2.5). The electric field can be plotted against the total power measured at the forward port on the coupler (Figure B.3).

Finally, the probe measurement can be directly related to the electric field strength (Figure B.4) by combining the two relationships from Figure B.2 and Figure B.3. During the heating experiments, the probe measurement will be converted to electric field strength in the data acquisition system. Using Figure B.4, the electric field strength can be determined.

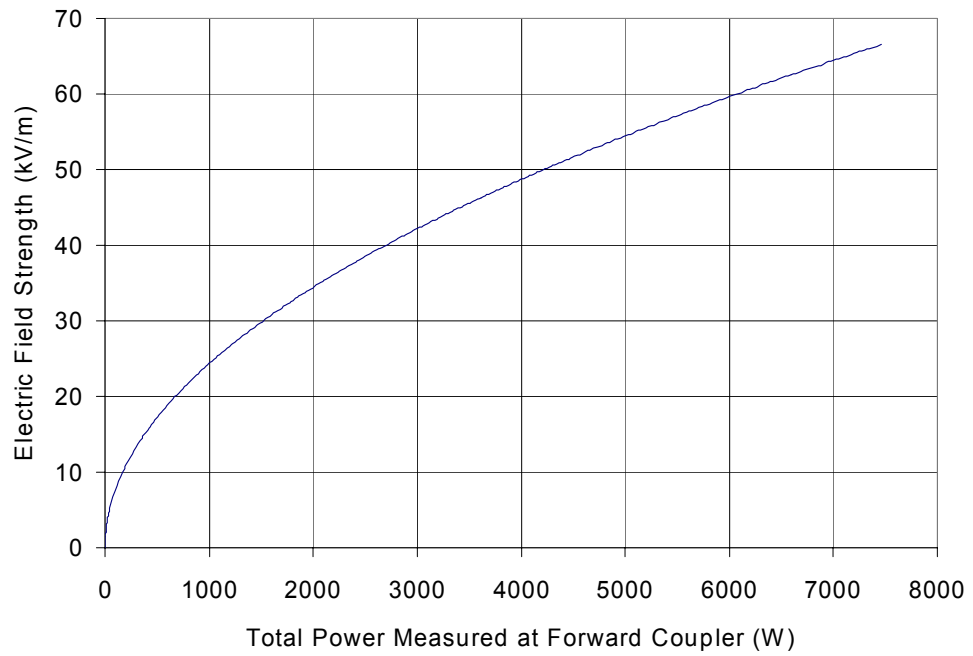


Figure B.3: Total power vs. electric field

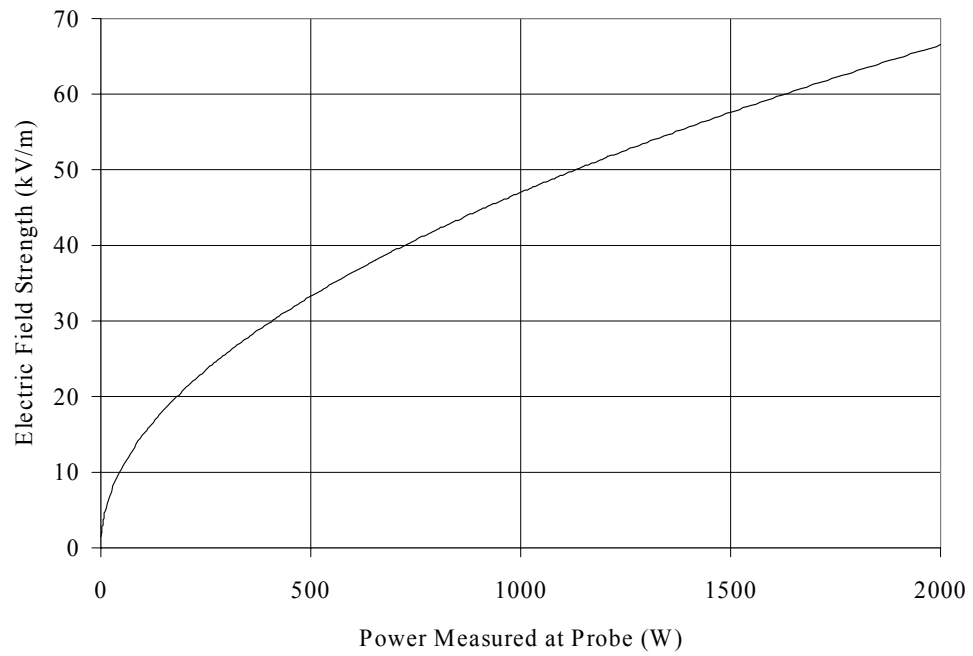


Figure B.4: Power measured by probe vs. electric field

Appendix C

Pyrometer Calibration

Calibration of the pyrometer is required for each material to be heated. This is because each material has a different emissivity-temperature relationship. During the experiments, the pyrometer is set at an emissivity of 1.00. Therefore, the measured temperature needs to be corrected for the actual emissivity of the surface of the object. The pyrometer measures total radiation in the 8-14 μm wavelength range. The total radiation measured by the pyrometer is given by

$$E_{TOTPYRO} = A F_{PYRO8-14\mu m} \sigma \epsilon_{PYRO} T_{PYRO}^4 \quad (C.1)$$

where A is the projected area (m^2) of the target, $F_{PYRO8-14\mu m}$ is the fraction of emissive power of a blackbody emitted in the wavelength band 8 – 14 μm at the measured temperature, σ is the Stefan-Boltzman constant ($5.67 * 10^{-8} \frac{W}{m^2 K^4}$), ϵ_{PYRO} is set at 1.00, and T_{PYRO} is the temperature measured by the pyrometer (K). The actual total radiation from the surface of the object is given by

$$E_{TOTACTUAL} = A F_{ACTUAL8-14\mu m} \sigma \epsilon_{ACTUAL} T_{ACTUAL}^4 + A F_{SURR8-14\mu m} \sigma (1 - \epsilon_{ACTUAL}) T_{SURR}^4 \quad (C.2)$$

where $F_{ACTUAL8-14\mu m}$ is the fraction of emissive power of a blackbody over the wavelength range 8 – 14 μm at the actual temperature, ϵ_{ACTUAL} is the emissivity of the object at the actual temperature, and T_{ACTUAL} is the actual temperature of the object. T_{SURR} is the temperature of the surrounding cavity walls, 30°C.

The temperature measured by the pyrometer, T_{PYRO} is known, so the fraction of emissive power, $F_{PYRO8-14\mu m}$, can be calculated using Figure C.1.

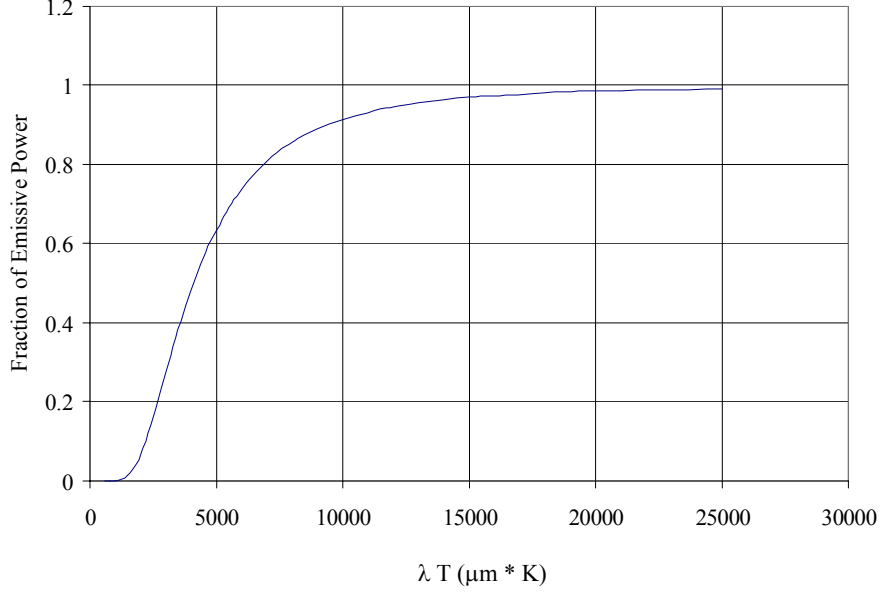


Figure C.1: Fraction of emissive power vs λT for blackbody (Incropera and DeWitt, 1996)

The actual emissivity of the object and the actual fraction of emissive power over the specified wavelength range are both functions of the actual temperature of the object. Since

$$\epsilon_{ACTUAL} = f(T_{ACTUAL}) \quad (C.3)$$

$$F_{ACTUAL_{8-14\mu m}} = f(T_{ACTUAL}) \quad (C.4)$$

$$E_{TOTPYRO} = E_{TOTACTUAL} \quad (C.5)$$

there are three equations and three unknowns. These equations can be solved for each material given emissivity data ¹. Figures C.2 - C.7 show the emissivity data and pyrometer calibration for each material in the experimental program.

¹The emissivity data for nylon 66 fiber was obtained by a simple heating experiment. The nylon 66 fiber was wound around a plate painted flat black. An infrared camera was used to measure the temperature of the black plate at a known emissivity of 0.95. The infrared camera was then focused on the nylon 66 and the emissivity of the camera was adjusted such that the temperature of the nylon was forced to equal the temperature of the black plate

C.1 Calibration for Mullite Rod

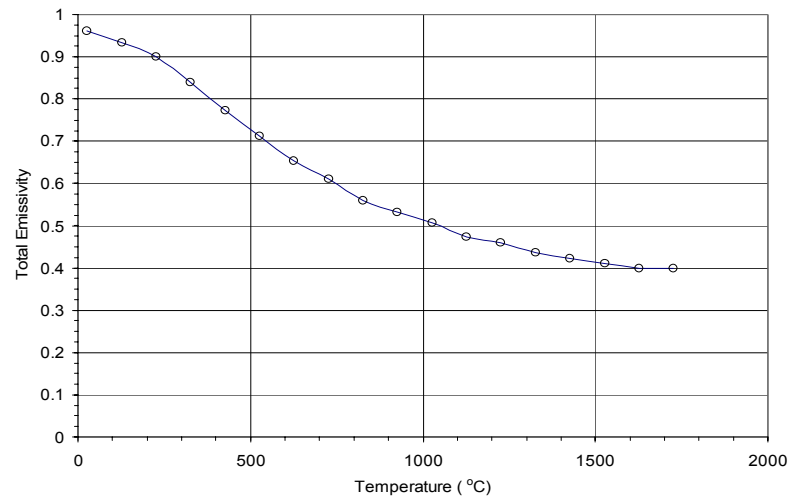


Figure C.2: Emissivity data for mullite (Bauer and Steinhardt, 1990)

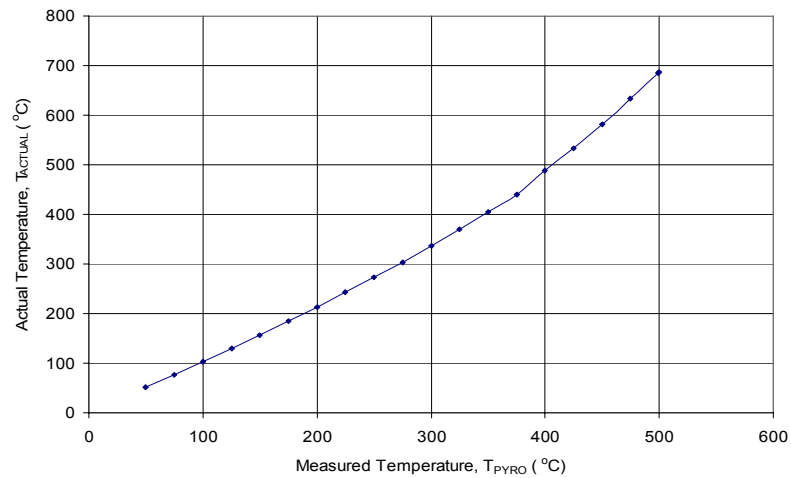


Figure C.3: Temperature calibration of pyrometer for mullite rod

C.2 Calibration for Alumina Rod

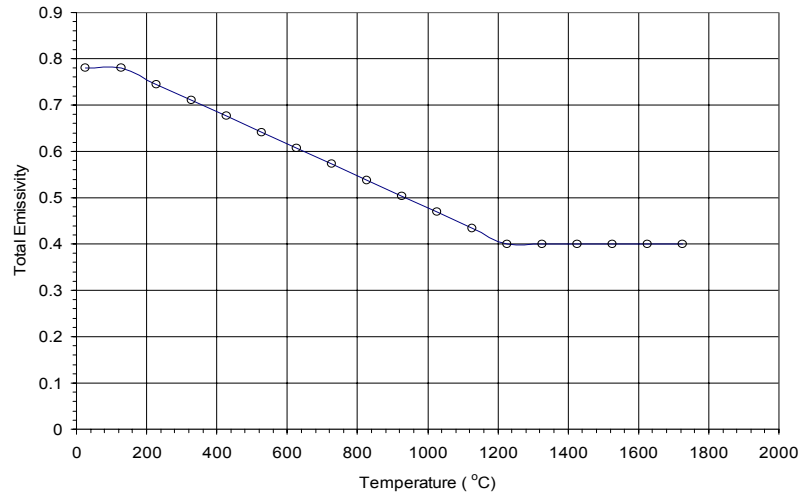


Figure C.4: Emissivity data for alumina rod (Touloukian, 1972)

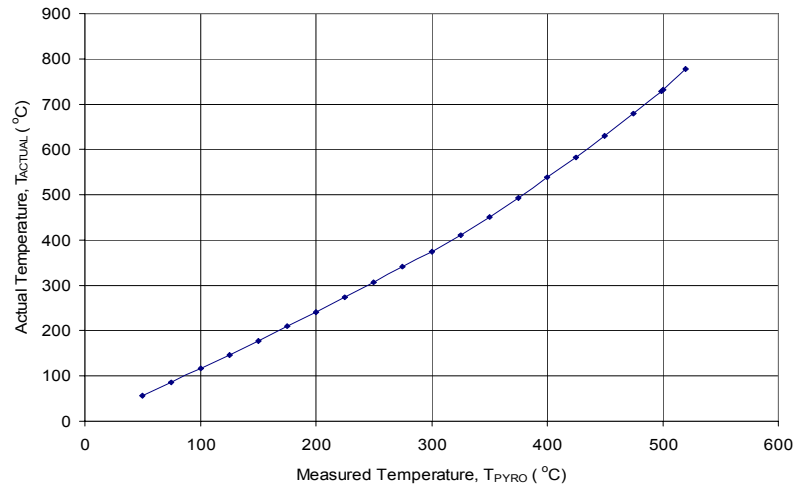


Figure C.5: Temperature calibration of pyrometer for alumina rod

C.3 Calibration for Nylon 66 Fiber

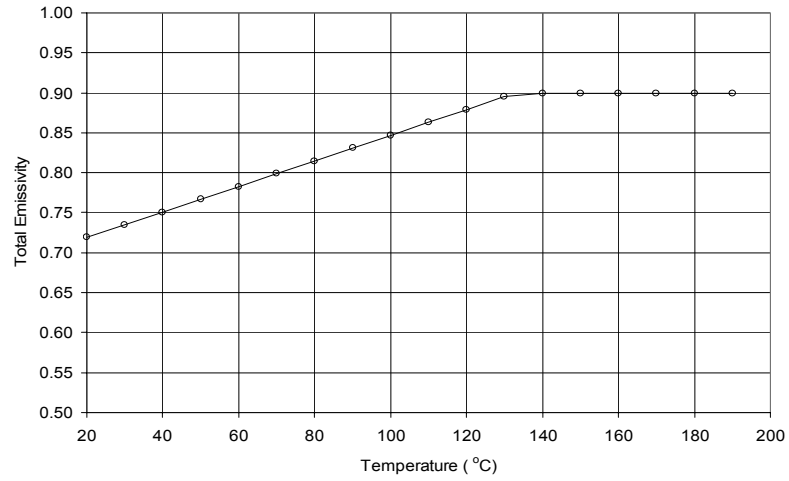


Figure C.6: Emissivity data for nylon 66

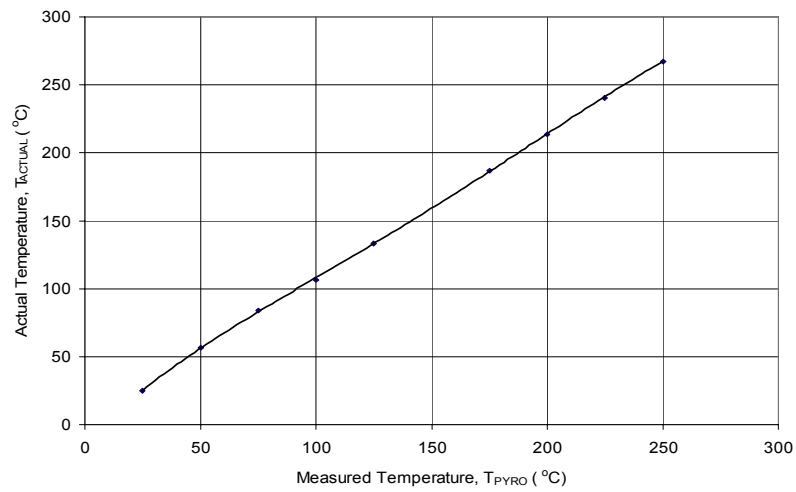


Figure C.7: Temperature calibration of pyrometer for nylon 66

Appendix D

Individual Data Runs

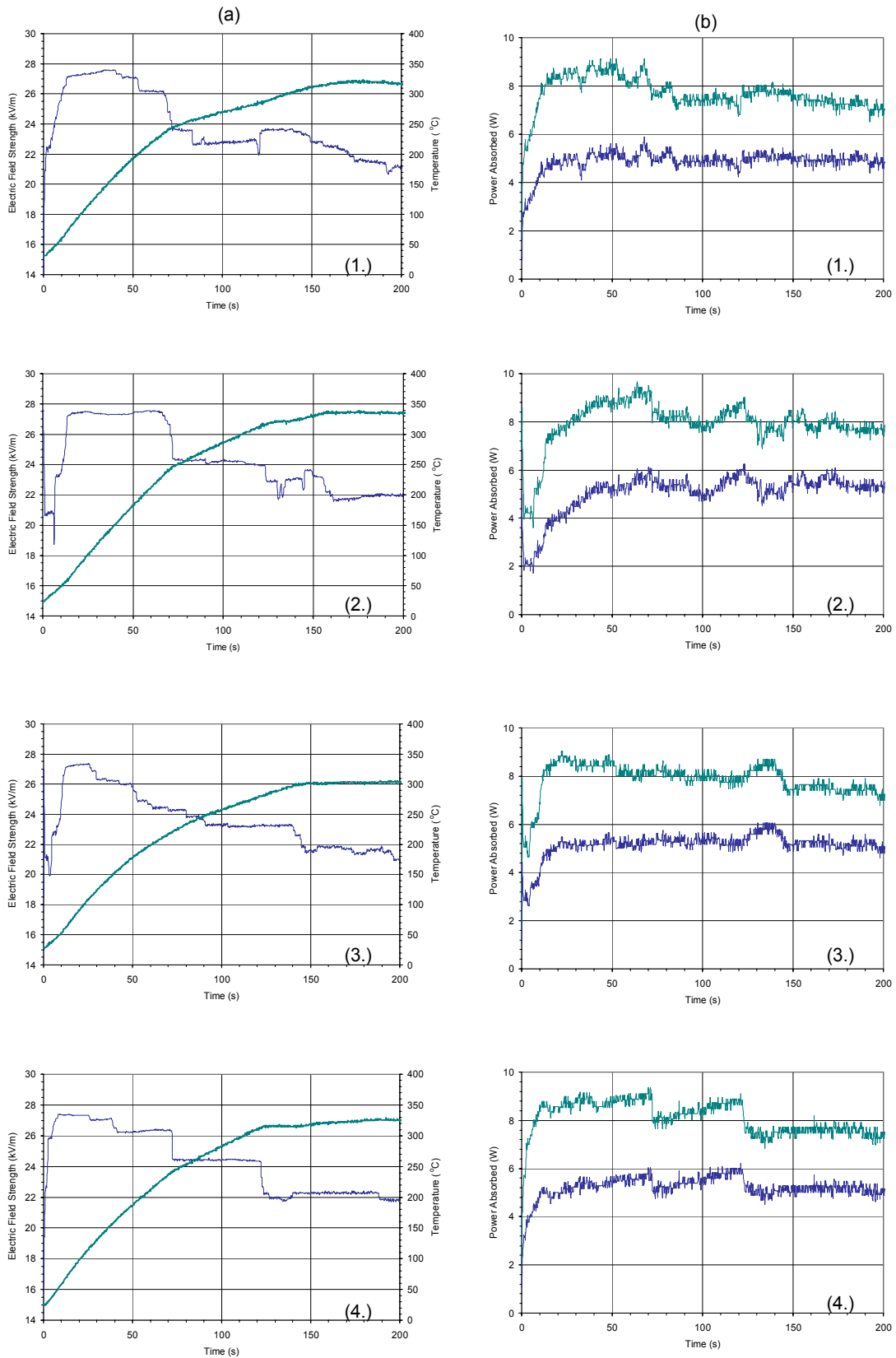


Figure D.1: Individual runs for heating of a 4.67 mm mullite rod, where power absorbed by rod is increased to 5 W and held constant (see Figure 4.3)

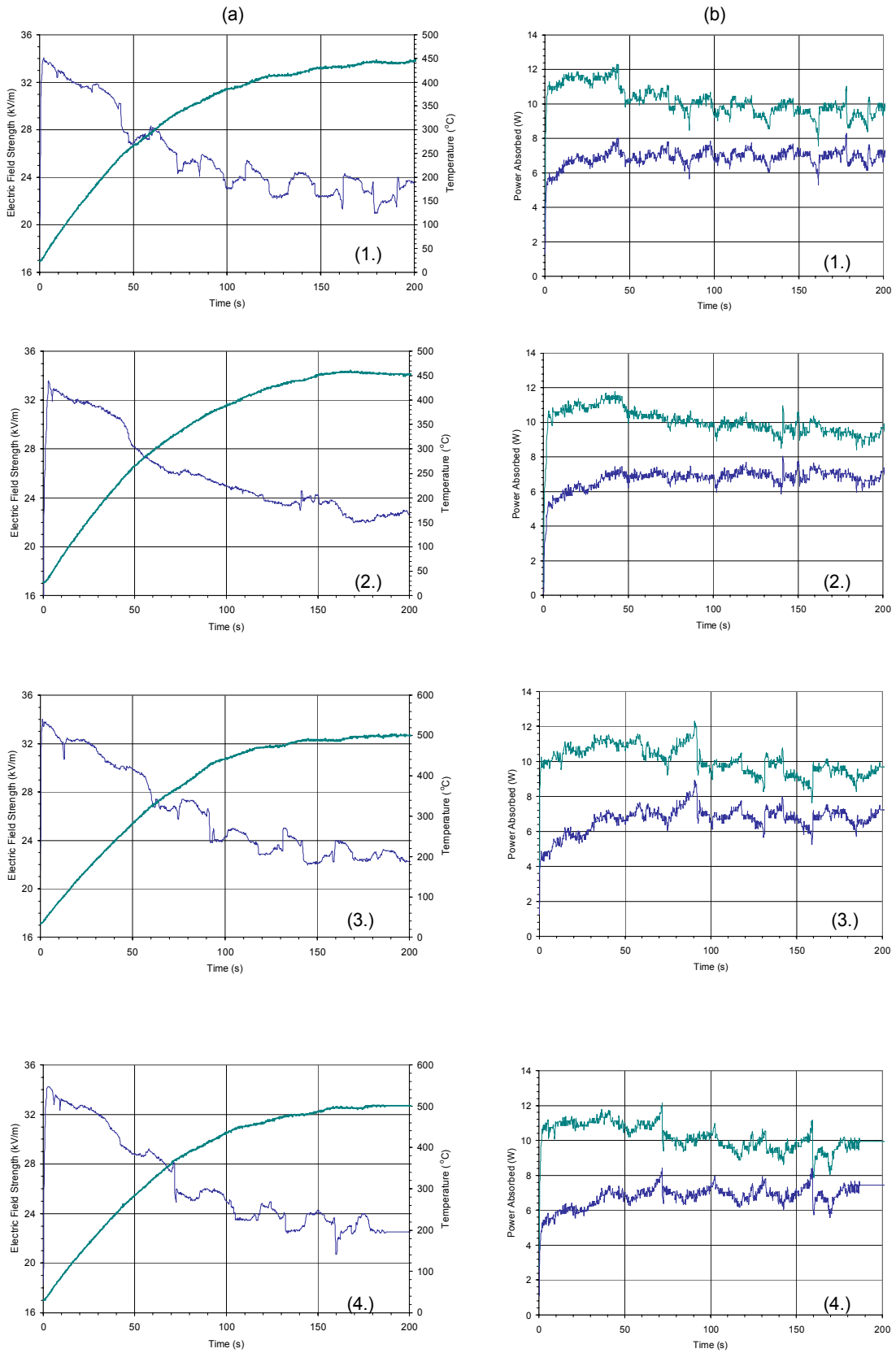


Figure D.2: Individual runs for heating of a 4.67 mm mullite rod, where power absorbed by rod is increased to 7 W and held constant (see Figure 4.4)

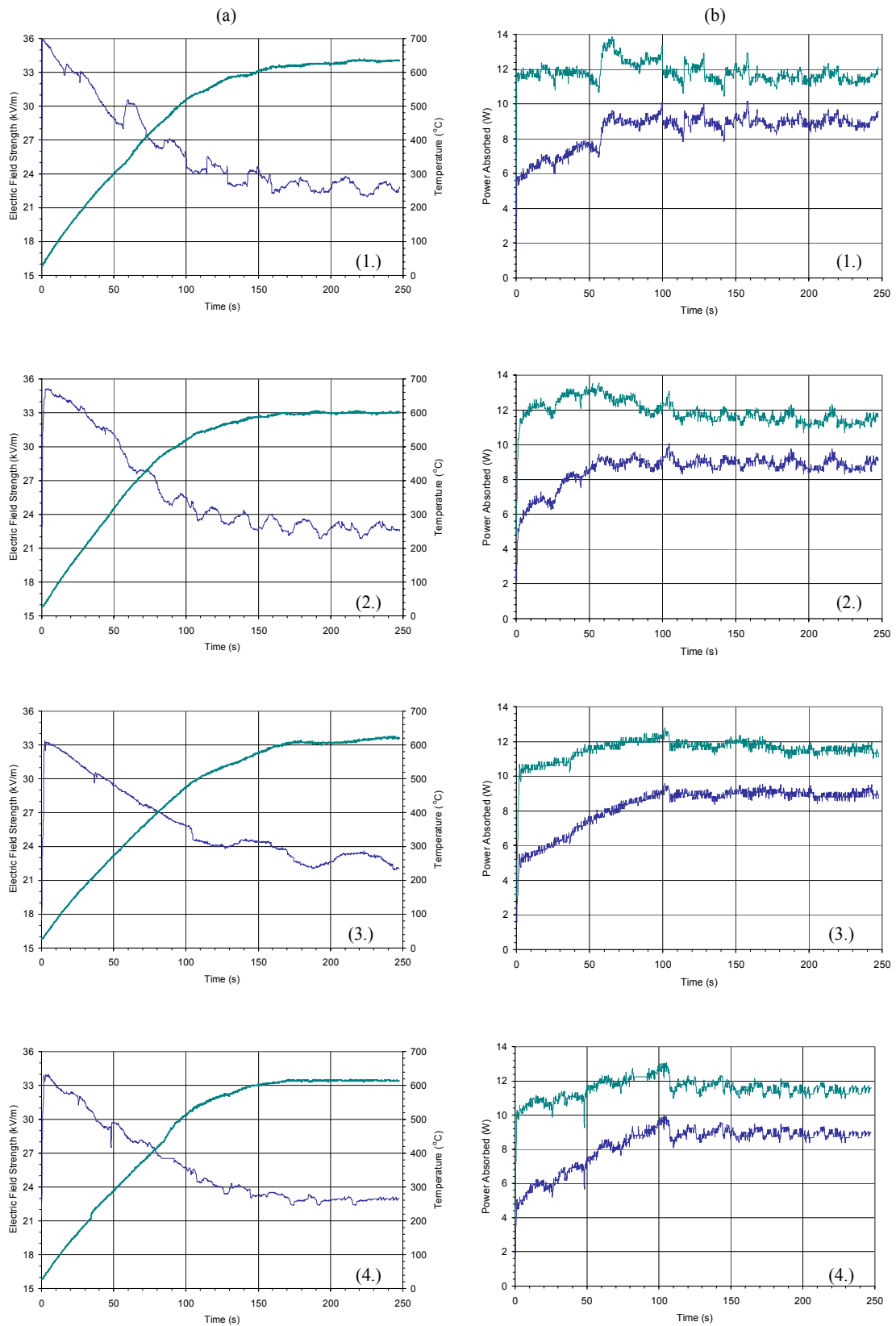


Figure D.3: Individual runs for heating of a 4.67 mm mullite rod, where power absorbed by rod is increased to 9 W and held constant (see Figure 4.5)

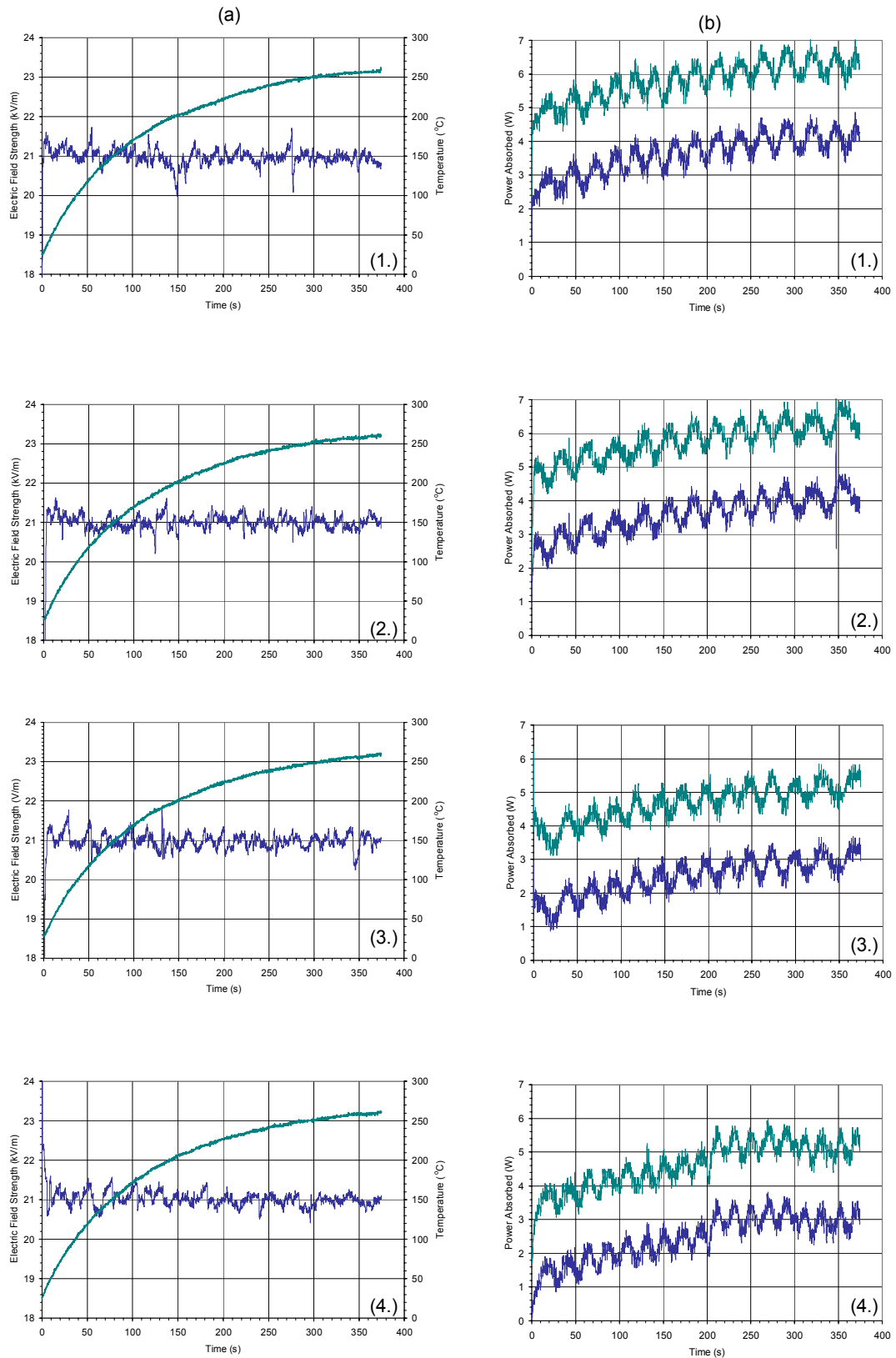


Figure D.4: Individual runs for heating of a 4.67 mm mullite rod, where electric field is held constant at 21 kV/m (see Figure 4.10)

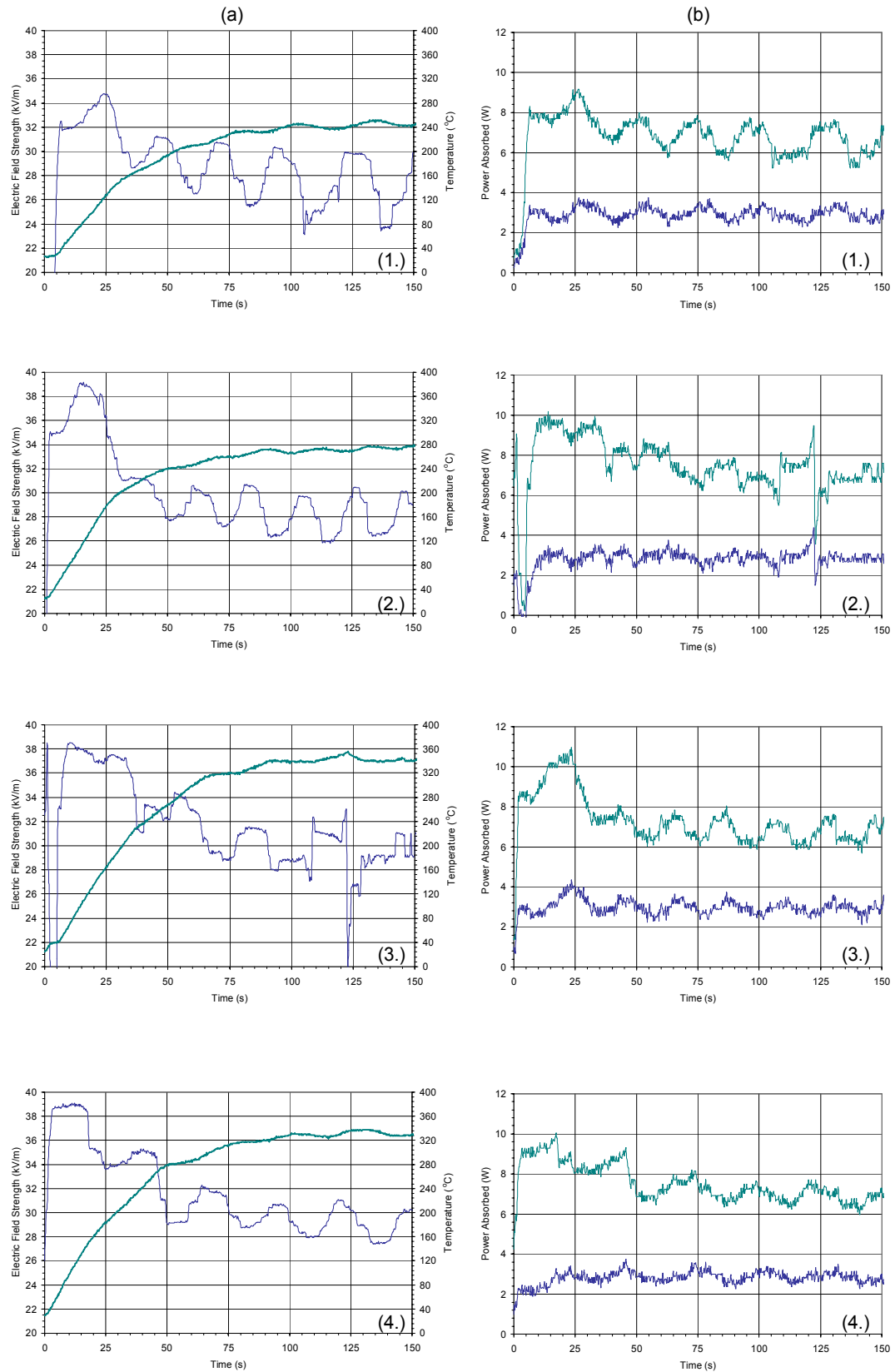


Figure D.5: Individual runs for heating of a 2.75 mm mullite rod, where power absorbed by rod is increased to 3 W and held constant (see Figure 4.12)

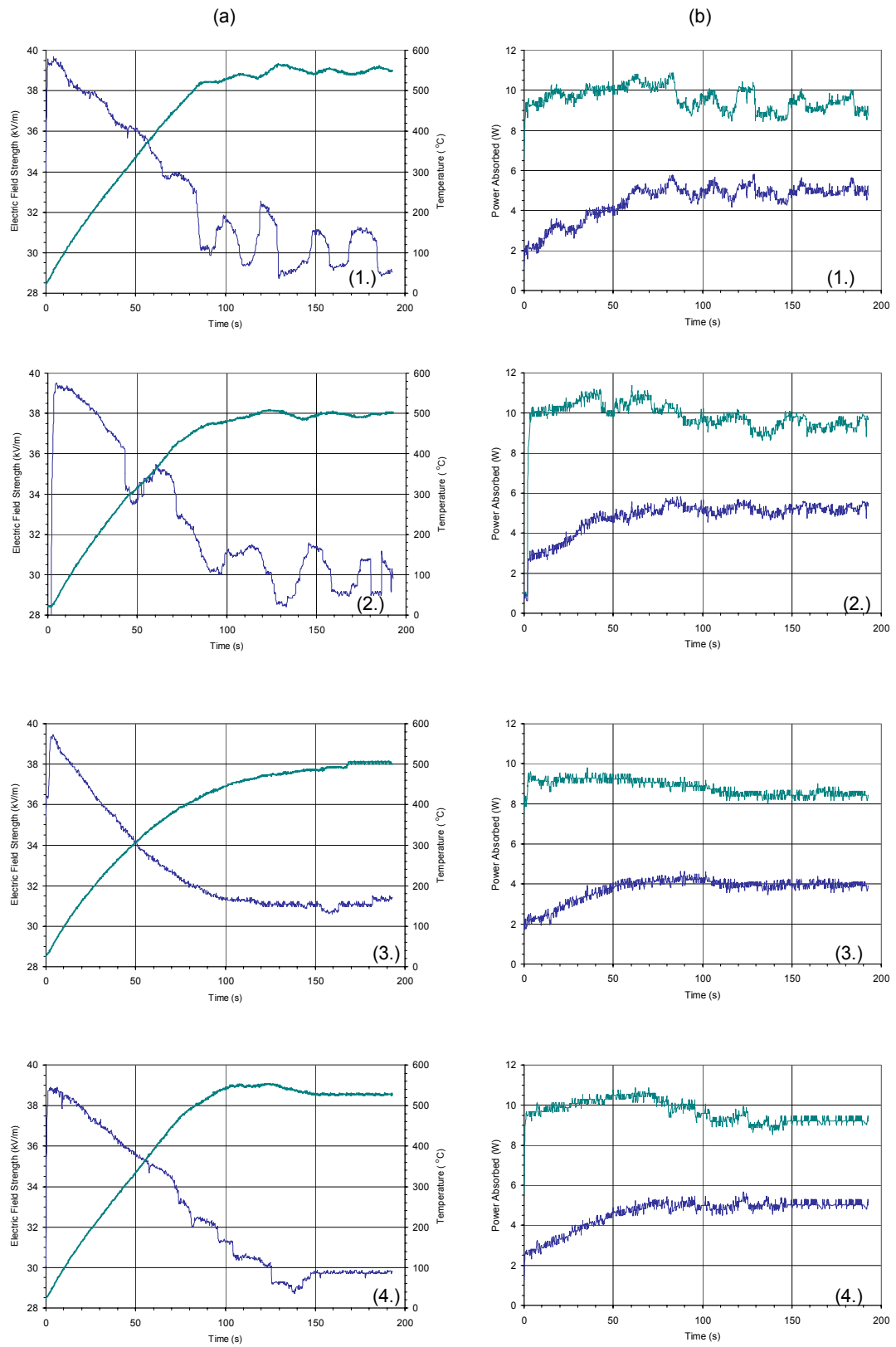


Figure D.6: Individual runs for heating of a 2.75 mm mullite rod, where power absorbed by rod is increased to 5 W and held constant (see Figure 4.13)

that will heat thermal runaway materials.

SOURCE CODE WRITTEN BY: James P. Dolan 7/14/96

MODIFIED BY: John M. Curtis 6/7/99

*****/

```
void error_check (char *, int);
```

```
int warning (int);
```

```
#define offsetChan 0 /* Channel used to measure offset */
#define gain 1 /* Gain for the specified chan
                Valid settings for AT-MIO-16F-5
                -1 (for a gain of 0.5), 1, 2,
                5, 10, 20, 50, 100 */
#define gainAdjust 1 /* Gain multiplying factor */
#define numChans 6 /* Number of MIO channels to scan */
#define numPts (2*numChans) /* TOTAL number of A/D conversions. Must
                             be an integer multiple of numChans */
#define count numChans /* Length of binArray and voltArray */
#define DBmode 1 /* 0: Disables double buffering
                 1: Enables double buffering */
#define port 2 /* Port LPT1 used for RS-232 */

#define mode1 2 /* 0: open file for reading and writing
                1: open file for reading only
                2: open file for writing only */
#define mode2 1 /* 0: truncate file (delete old contents)
                 1: write operations append to end of
file                2: do not truncate file */
#define mode3 1 /* 0: binary 1: ASCII */
```

```

static int      i, C603, C596, C594, C593, CB596,
                CB594, R, S, T, U, err, flag, Month,
                Day, file_handle, num_source, boardCode,
                offset, chanVector[numChans], gainVector[numChans],
                sampTimebase, sampInterval, scanTimebase,
                scanInterval, buffer[numPts],
                daqStopped, halfReady,
                ptsTfr,
                binArray[numChans];

static double   sampleRateDesired,
                scanRateDesired,
                voltArray[numChans],
                time,
                two_hour_time,
                Vreading[16],
                ScaleData;

static char     msg[500],
                buf[50],
                file_name[12];

main()
{

    for (i=0; i < numChans; i++) {
        chanVector[i] = i+1;      /* MIO channels to scan          */
        gainVector[i] = gain;     /* Array containing gains for each chan */
    }
}

```

```

sampleRateDesired = 20000;          /* A/D conversion rate (pts/sec.) */
scanRateDesired   = .2;            /* The amount of delay desired
                                     between acquisitions (scans) (sec/pt) */

cls();

err = SetDir ("C:\\\\VETDATA");
if ( err < 0 ) {
    FmtOut ( "Directory 'C:\\VETDATA' not found\n" );
}
Scan (DateStr(), "%s>%i-%i", &Month, &Day);
Fmt (file_name, "%s<BHI%i[w2p0]%i[w2p0].DAT", Month, Day);
file_handle = OpenFile (file_name, mode1, mode2, mode3);
FmtOut ("%s\n",DateStr());
/*   FmtFile (file_handle,"%s\n\n",DateStr()); DO NOT WRITE DATE TO FILE */
FmtOut ("Data written to: %s\n\n",file_name);

/*****

Init_DA_Brds      required for initializing the data acquisition board
AI_Config        sets the input mode, range and polarity for the board
                  If you are using default settings, this call is optional.
AI_Read          used to obtain a binary reading of the voltage offset on
                  the MIO board, it is subtracted from the acutal reading
SCAN_Setup       initializes circuitry for a scanned data acq operation
DAQ_DB_Config    enables or disables double-buffered data acquisitions
DAQ_Rate         converts a desired data acquisition rate into the require
                  time base and interval
SCAN_Start       initiates a multiple-channel scanned data acq. operation

*****/

```

```

err = Init_DA_Brds (board, &boardCode);
    if (err < 0)
        error_check ("Init_DA_Brds", err);

err = AI_Configure (board,AIchan,inputMode,inputRange,polarity,driveAIS);
    if (err < 0)
        error_check ("AI_Config", err);

err = AI_Read (board, offsetChan, gain, &offset);
    if (err < 0)
        error_check ("AI_Read", err);

err = SCAN_Setup (board, numChans, chanVector, gainVector);
    if (err < 0)
        error_check ("SCAN_Setup", err);

err = DAQ_DB_Config (board,DBmode);
    if (err < 0)
        error_check ("DAQ_DB_Config", err);

err = DAQ_Rate (sampleRateDesired, sampleRateUnits, &sampTimebase,
&sampInterval);    if (err < 0)
        error_check ("Samp_DAQ_Rate", err);

err = DAQ_Rate (scanRateDesired, scanRateUnits, &scanTimebase,
&scanInterval);    if (err < 0)

```

```

        error_check ("Scan_DAQ_Rate", err);

    err = SCAN_Start (board,buffer,numPts,sampTimebase,sampInterval,
scanTimebase,    scanInterval);    if (err < 0)
        error_check ("SCAN_Start", err);

/*****

The data acquisition loop acquires data from the double buffer.

OpenComConfig    Opens COM port and configures defaults
DAQ_DB_HalfReady  checks wether the next half buffer of data is ready
DAQ_DB_Transfer   transfers half the data from the buffer being used for
                  double-buffered data acquisition to another buffer
DAQ_VScale        converts the binary data into actual measured voltages
DAQ_Clear         required if DAQ_Check or DAQ_DB_Transfer is not called

*****/

    two_hour_time = Timer() + 5400.00;
    flag = 0;

    OpenComConfig (port,baud_rate,parity,data_bits,stop_bits,
iq_size,oq_size,port_addr,int_level);
        if (rs232err > 0)
            error_check ("OpenComConfig", rs232err);

    while (keyhit() !=1)
    {
        err = DAQ_DB_HalfReady (board, &halfReady, &daqStopped);
        if (err < 0)
            error_check ("DAQ_DB_HalfReady", err);

```

```

if (halfReady == 1){

    ComWrt (port,"SI\15\12",4);

    Scan (buf, "%s>%s[dt#]%.f", &ScaleData);

    err = DAQ_DB_Transfer (board, binArray,&ptsTfr,&daqStopped);
        if (err < 0)
            error_check ("DAQ_VScale", err);

    err = DAQ_VScale (board,0,gain,gainAdjust,offset,
count,binArray, voltArray);  if (err < 0)
error_check ("DAQ_VScale", err);

    time = Timer();
    FmtOut ("%s<%.f[w9p2]", time);
    FmtFile (file_handle,"%s<%.f[w9p2]", time);
    R = 10; /* 100 micro watt scale */
    S = 0.1; /* 10 mW scale */
    T = .01; /* 100 mW scale */
    U = 100; /* 10 micro watt scale */
    C603 = 1071.51/1;
    C596 = 870.96/R; /* 59.400 */
    C594 = 808.16493/1; /* 59.075 */
    C593 = 803.526122/R; /* 59.050 */

    CB596 = 841.396; /* 59.525 3 kw Source */
    CB594 = 822.243; /* 59.15 3 KW Source */

    for (i=0; i < numChans; i++) {

```

```

Vreading[0] = 500*voltArray[0];

Vreading[0]= .00000000182645*pow(Vreading[0],4)+.000000879979*pow
(Vreading[0],3)-.000333593*pow(Vreading[0],2)+1.10336*Vreading[0]
- 4.11551; /*MULLITE TEMP CALIBRATION*/

Vreading[1] = .1*CB596 * voltArray[1];
/* HP B Power Meter: First Number refers to scale.
If scale is set at 100uW, the constant is 0.1. If the scale is set
at 300uW, the constant is .31623.
If the scale is set at 3mW, the constant is 3.1623*/
Vreading[2] = .1*C603 * voltArray[2]; /*HP A Power Meter */
Vreading[3] = 2210627.856*691.831*1*voltArray[3]; /*HP D Power Meter */
/* Vreading[3] = pow(Vreading[3],.5); /* Calculation of electric field */
Vreading[4] = Vreading[2] - Vreading[1]; /* Power absorbed by cavity
(including rod) */
Vreading[5] = Vreading[4] - (.0000000041731*pow(Vreading[3],2)
+.000016304 * Vreading[3]); /* Calculation of power absorbed by rod */}
    FmtFile (file_handle,"%s< %f[w7p2]", Vreading[0]);
    FmtFile (file_handle,"%s< %f[w7p2]", Vreading[1]);
    FmtFile (file_handle,"%s< %f[w7p2]", Vreading[2]);
    FmtFile (file_handle,"%s< %f[w8p2]", Vreading[3]);
    FmtFile (file_handle,"%s< %f[w7p2]", Vreading[4]);
    FmtFile (file_handle,"%s< %f[w7p2]", Vreading[5]);
/*    FmtFile (file_handle,"%s< %f[w7p2]", Vreading[6]); */

    FmtOut ("%s< %f[w7p2]", Vreading[0]);
    FmtOut ("%s< %f[w7p2]", Vreading[1]);
    FmtOut ("%s< %f[w7p2]", Vreading[2]);
    FmtOut ("%s< %f[w8p2]", Vreading[3]);
    FmtOut ("%s< %f[w7p2]", Vreading[4]);

```

```

        FmtOut ("%s< %f[w7p2]", Vreading[5]);
/*    FmtOut ("%s< %f[w7p2]", Vreading[6]);    */
    FmtOut ("\n");
    FmtFile (file_handle, "\n");
    if ( (time > two_hour_time) && (flag < 3) )
        { flag = warning (flag); }
    }
}

DAQ_Clear (board);
CloseCom (1);
CloseFile (file_handle);
}

void error_check (func, err)
char func[];
int err;
{
    Fmt(msg, "%s<Function %s returned error %i", func, err);
    MessagePopup (msg);
    exit(1);
}

int warning (int flag)
{
    Beep();
    Beep();
    Beep();
    flag = flag + 1;
    return (flag);}

```

Appendix F

Characterization of Cavity

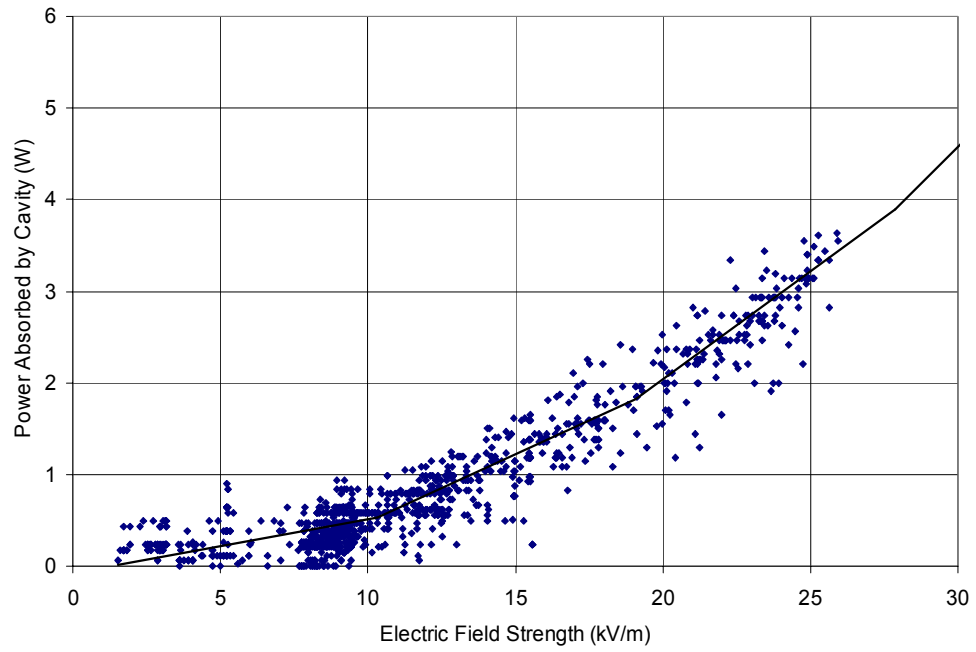


Figure F.1: Characterization of cavity at an incident power of 65 W

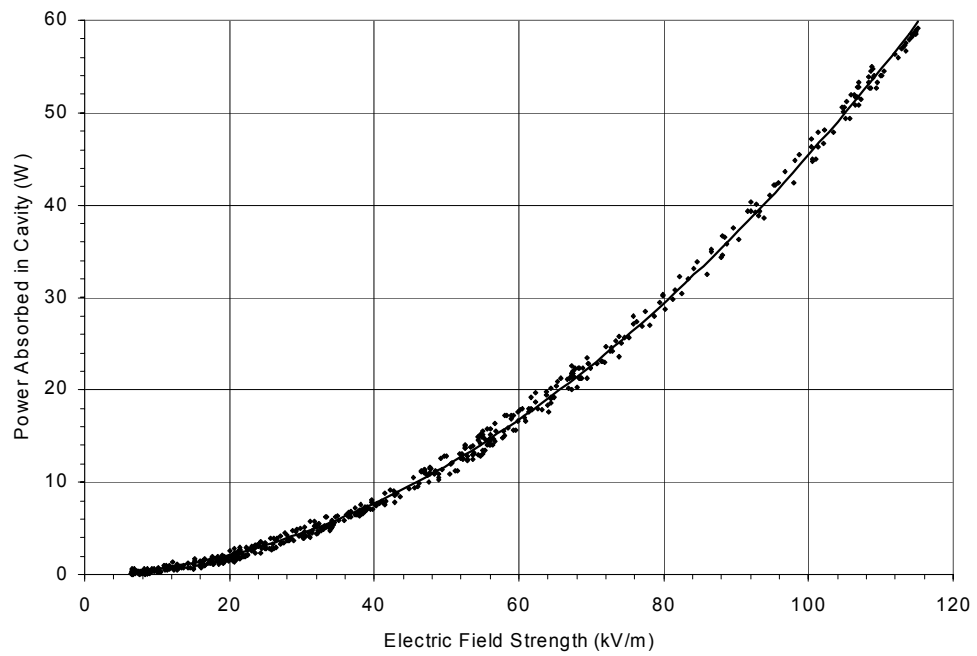


Figure F.2: Characterization of cavity at an incident power of 135 W

Vita

The author, John M. Curtis Jr., son of John M. Curtis and Marcia L. Curtis, was born on May 25, 1976, in Jacksonville, Florida. He obtained his high school diploma from Kempsville High School, in Virginia Beach, Virginia, in 1994. He then went on to Virginia Polytechnic Institute and State University, in Blacksburg, Virginia, where he earned a Bachelor of Science in Mechanical Engineering in 1998. Pursuing his interest in mechanical engineering and heat transfer, he earned his Master of Science in Mechanical Engineering the next year.

Permanent Address: 1200 Worthington Ln.

Virginia Beach, Virginia 23464

This thesis was typeset with $\text{\LaTeX} 2_{\epsilon}$ ¹ by the author.

¹ $\text{\LaTeX} 2_{\epsilon}$ is an extension of \LaTeX . \LaTeX is a collection of macros for \TeX . \TeX is a trademark of the American Mathematical Society. The macros used in formatting this thesis were written by Greg Walker, Department of Mechanical Engineering, Virginia Tech.